Synthesis and Evaluation of Nuclear and Optical Tetrazine-6-Hydrazinopyridine-3-Carboxylic Acid Probes for Molecular Imaging using Pretargeting and Bioorthogonal Chemistry

by

Zoya Naperstkow, BSc.

A Thesis Submitted to the School of Graduate Studies

In Partial Fulfillment of the Requirements

For the Degree

Master of Science

McMaster University

MASTER OF SCIENCE (2017) McMaster University

(Chemistry and Chemical Biology Department) Hamilton, Ontario

TITLE: Synthesis and Evaluation of Nuclear and Optical Tetrazine-6-Hydrazinopyridine-3-Carboxylic Acid Probes for Molecular Imaging using Pretargeting and Bioorthogonal Chemistry

AUTHOR: Zoya Naperstkow, B.Sc. (Carleton University)

SUPERVISOR: Dr. John F. Valliant

NUMBER OF PAGES: XXI, 100

Abstract

The aim of this thesis was to develop a new platform for the creation of targeted nuclear and optical molecular imaging probes. Current probes suffer from low target-to-background ratios, which can hinder diagnosis and monitoring of disease treatments due to poor image acquisition. To overcome this limitation, the approach taken involved coupling 6-hydrazinopyridine-3-carboxylic acid (HYNIC) to a tetrazine, where the product could be used to create targeted ^{99m}Tc and near-infrared dye probes. Targeting could then be accomplished using bioorthogonal chemistry with *trans*-cyclooctene (TCO) functionalized biomolecules, through an inverse electron demand Diels-Alder cycloaddition.

The assessment for the clinical translation of ^{99m}Tc-HYNIC based nuclear probes was evaluated to determine the feasibility of using a 'kit-like' formulation system. A limitation associated with the development of HYNIC-based radiopharmaceuticals is the need for HPLC purification. The investigation into the need for HPLC purification was performed, where it was determined that there was no significant difference in target uptake between the HPLC-purified and non-purified ^{99m}Tc-HYNIC probe **6** when used with bone-seeking TCO-derived bisphosphonate (4.73 ± 0.47 versus 4.15 ± 0.27%ID/g in shoulder, 6.32 ± 0.21 versus 5.94 ± 0.59%ID/g in knee, respectively). This suggests that a kit-like system would be practical; thus streamlining the chemistry required for radiopharmaceutical development. Efforts to reduce non-target organ uptake observed with using **6** was accomplished through the synthesis of a more polar construct **12**. While the compound rapidly cleared from non-target organs, it also displayed lower target uptake compared to **6** (1.62 ± 0.22 versus 4.15 ± 0.27%ID/g in shoulder, 2.39 ± 0.22

versus 5.94 ± 0.59%ID/g in knee, respectively), demonstrating the need for further pharmacokinetic optimization.

The synthesis and evaluation of optical imaging probes was also completed, where the HYNIC-tetrazine core was linked to a commercially-available near-infrared dye through a hydrazone linkage. The bacterial binding capabilities of fluorescent compounds **22** and **24** (analogous to the ^{99m}Tc-labelled **6** and **12**) were investigated *in vitro* using Gram-positive *Staphylococcus aureus* with TCO-modified vancomycin. The targeted samples exhibited a 3.8-fold (**22**) and 8.6-fold (**24**) increase in fluorescent intensity when compared to the blocking control used to account for binding specificity. Fluorescent microscopy images were also obtained, however only bacterial aggregates were observed, indicating the need for optimization of microscopy procedures. As such, a HYNIC-tetrazine platform was successfully developed as a means synthesize various targeting probes for molecular imaging applications using pretargeted, bioorthogonal chemistry.

Acknowledgements

I would like to start by acknowledging my supervisor Dr. John Valliant for the amazing opportunity to work in such an interdisciplinary field. The experience, wisdom and expertise you imparted on me is immeasurable. Your professionalism and dedication to research are valuable traits I aspire to have. Thank you for giving me independence, while still providing guidance throughout my degree. The skills and hands-on experience I have gained from working in your group will forever be instilled in me, along with many other life-lessons I have gathered along the way. I would also like to thank my committee members, Dr. Capretta and Dr. Sheardown for their feedback, constructive criticisms and support during this time. For lack of better words, thank you for helping me become a better scientist.

I would like to thank all past and previous members of the Valliant Research Group that I had the pleasure to work with. Each of you provided me with support and knowledge in fields and techniques I was lacking – and I will forever be thankful for your teachings. A special thank you to Nancy Janzen and Shannon Czorny, for all their help with biological studies and for always allowing me to work alongside them. For amazing support, guidance and unconditional friendship I thank Aimen, Holly, Sam, Steph and Zainab. I had an amazing two years, and have you all to thank (for coffee, softball, conferences, beers, and life-chats); I could not have succeeded with you.

Lastly, I give many thanks to my family and friends. You have always supported me, helped me and pushed me towards pursuing my goals. Thank you, Mom and Dad, for leading through example. You are both hard-workers, and I would not be here today without you. Thank you to my sister for always listening to me, and for a never-ending

source of entertainment in times of need. Special thanks to Taryn, Nicole, Kaylyn and Chelsea – I am forever grateful for our friendships (and love of wine). I could not have done this without you all.

Table of Contents

List of Tables

List of Figures

List of Schemes

List of Abbreviations and Symbols

%ID/g	Percent injected dose per gram
%ID/O	Percent injected dose per organ
^{111}In	Indium-111
^{11}C	Carbon-11
^{123}I	Iodine-123
^{124}I	Iodine-124
^{188}Re	Rhenium-188
^{18}F	Fluorine-18
^{18}F-FBA	^{18}F-fluorobenzaldehyde
^{18}F-FDG	2-Deoxy-2-[^{18}F]fluoroglucose

^{1}H NMR	Proton NMR
^{13}C NMR	Carbon-13 NMR
^{235}U	Uranium-235
^{64}Cu	Copper-64
^{99}Mo	Molybdenum-99
^{99m}Tc	Technetium-99m
Å	Angstrom
β	Beta emission
β^{+}	Positron
Boc	*tert*-butyloxycarbonyl
BODIPY	Boron-dipyrromethene
BPTz	Bispyridyl tetrazine
Bq	Becquerel
CFU	Colony forming units
Ci	Curie
cm^3	Cubic centimeters
$COCF_3$	Trifluoroacetamide
CT	Computed tomography
Cy5	Cyanine
DCC	*N*,*N*'-Dicyclohexylcarbodiimide
DCM	Dichloromethane
DIPEA	*N*,*N*-Diisopropylethylamine
DMF	Dimethylformamide
DMSO	Dimethyl sulfoxide
EDDA	Ethylenediamine-*N*,*N*′-diacetic acid
Et_3N	Triethylamine
EtOAc	Ethyl acetate
EtOH	Ethanol
f	Fission
γ-ray	Gamma ray
H_2O	Water
HCl	Hydrochloric acid
HOMO	Highest occupied molecular orbital
HPLC	High performance liquid chromatography
HRMS	High resolution mass spectroscopy
HYNIC	Hydrazinonicotinic acid/6-Hydrazinopyridine-3-carboxylic acid
Hz	Hertz
IEDDA	Inverse electron demand Diels-Alder
IR	Infrared
J	Coupling constants

keV	Kilo electron-volts
kg	Kilogram
LC	Liquid chromatography
logP	Distribution coefficient
LUMO	Lowest unoccupied molecular orbital
M	Molar
MeOH	Methanol
mg	Milligram
MI	Molecular imaging
ml	Milliliter
mM	Millimolar
mmol	Millimole
mol	Mole
MRI	Magnetic resonance imaging
MS	Mass spectroscopy
n	Neutron
N_2	Nitrogen gas
NHS	*N*-Hydroxysuccinimide
NIR	Near-infrared
nM	nanomolar
NMR	Nuclear Magnetic Resonance spectroscopy
p	Probability value
PBS	Phosphate-buffered saline
PBS-F	Phosphate-buffered saline with fetal bovine serum (FBS) and bovine serum albumin (BSA)
PEG	Polyethylene glycol
PIDA	Phenyliodine(III) diacetate
PET	Positron emission tomography
PMT	Photomultiplier tubes
PPh_3	Triphenylphosphine
PyBOP	(Benzotriazol-1-yloxy)tripyrrolidinophosphonium hexafluorophosphate
RCP	Radiochemical purity
RCY	Radiochemical yield
R_t	Retention time
S-4FB	N-succinimidyl-4-formylbenzamide
$SnCl_2$	Tin(II) chloride/stannous chloride
SPECT	Single photon emission tomography
SUV	Standard uptake value
TCO	*trans*-cyclooctene
TCO-BP	TCO-bisphosphonate

TCO-OH	*trans*-cyclooctenol
TCO-vanc.	TCO-vancomycin
TcO_4^-	Pertechnetate
TFA	Trifluoroacetic acid
THF	Tetrahydrofuran
TLC	Thin-layer chromatography
TSB	Tryptic soy broth
Tz	Tetrazine
US	Ultrasound
UV/Vis	Ultraviolet-visible
λ	Wavelength
µ	Micro
µg	Microgram
µl	Microliter
µM	Micromolar

1 Introduction

1.1 Molecular Imaging

Molecular imaging (MI) can be defined as a technique used for non-invasive, real-time visualization of biological processes and targets.[1] MI has benefited from advances in specialized instrumentation and new targeted imaging agents, enabling the detection of biochemical markers, as well as identification of abnormal morphological and physiochemical changes. MI is routinely used in diagnostic medicine, including the assessment of response to new therapeutics.[1] MI is important because it can look at processes in real time (in their natural environment), amalgamate pharmacokinetic data, and allow for repeat and longitudinal studies.[1]

Nuclear medicine based MI involves administering small quantities of compounds labelled with radioisotopes to visualize specific biochemical processes and targets. Other commonly known clinical imaging modalities such as ultrasound, MRI, and CT are more typically used to image anatomical features of diseases (Table 1). Nuclear imaging has superior sensitivity compared to most other diagnostic methods, providing the means to detect disease biomarkers that are present in low concentrations; allowing for earlier diagnosis and treatment.[1] One of the main challenges in the MI field is the development of imaging probes that can achieve highly selective target uptake *in vivo*, which to overcome requires new chemistry.

Table 1: Overview of non-nuclear imaging modalities[1]

	Computed Tomography (CT)	Magnetic Resonance Imaging (MRI)	Ultrasound (US)	Optical Imaging
Source for Imaging	X-ray attenuation	Magnets and radiofrequencies	High frequency soundwaves	Emitted light from excited fluorophores
Advantages	Limitless depth of penetration, high spatial resolution and fast acquisition	Limitless depth of penetration, high spatial resolution and quantifiable data	Great sensitivity, inexpensive and quantifiable data	Inexpensive, able to multiplex and has high sensitivity
Disadvantages	Poor sensitivity, only for anatomical imaging and limited resolution	Poor sensitivity, slow acquisition and expensive	Limited depth of penetration, only for soft tissue imaging	Limited depth of penetration, poor resolution and *in vivo* autofluorescence

1.1.1 Nuclear Imaging Methods

Nuclear imaging methods exploit the radiation emitted from radioactive elements to generate images of fluids, tissues and organs using specialized cameras. Positron Emission Tomography (PET) uses isotopes that contain excess protons in the nucleus, which to attain stability, decay through the emission of positrons (β^+) that are ejected from the nucleus (Figure 1). The positrons ultimately collide with electrons and annihilate, creating two photons (511 keV each) travelling approximately 180˚ apart. For PET, the gamma rays are detected in coincidence by a detector ring which surrounds the patient, allowing the point of emission to be localized (line of response).[1] PET detectors are composed of scintillation crystals and photomultiplier tubes (or avalanche photodiodes),[2] where the former emit light upon interaction with the emitted photon, ultimately resulting in transmitted electrical pulses which are used to generate a 3-D image.[3]

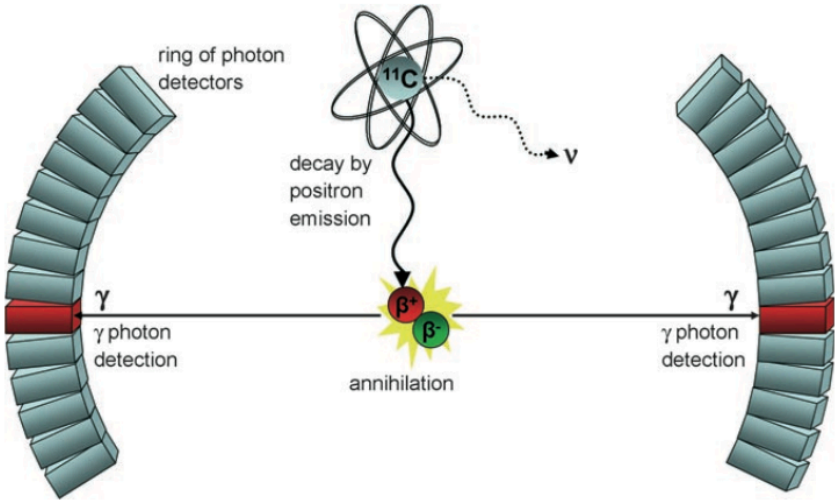

Figure 1: Schematic of positron decay and detection of the gamma rays in coincidence; a process that is used to generate PET images. [4]

^{11}C, ^{18}F, ^{64}Cu, and ^{124}I are examples of PET isotopes that can be used with a wide variety of molecular targeting vectors to create PET radiopharmaceuticals. By determining the standard uptake value (SUV) of these radiopharmaceuticals from a PET scan, semi-quantitative data (ratio of specific activity in region of interest (kBq/cm^3) to the amount of activity per body mass (MBq/kg)) can be obtained.[2] However, the limitations of PET include lack of multiplexing (imaging multiple targets/probes in one session), high radiation burden, and the need to access a nearby cyclotron or isotope generator due to the short half-life of common PET isotopes.

A second nuclear imaging technique is Single Photon Emission Computed Tomography (SPECT), which employs radionuclides that decay via emission of γ-rays (e.g. ^{99m}Tc, ^{111}In, ^{123}I). SPECT scanners consist of one or more detectors that rotate around the subject to collect the emitted gamma rays (Figure 2). As such, localization of the point of emission is done by the addition of a collimator in front of the detectors to

exclude photons outside of the field of view. This lowers the sensitivity of the instrument (compared to PET), as the gamma rays are emitted in all directions and only a fraction reach the detector.[1]

SPECT instrumentation is more widely available and typically less expensive than PET, and SPECT radiopharmaceuticals generally deliver lower radiation doses to patients.[5] An added advantage of SPECT is the ability to multiplex, because different SPECT radioisotopes emit gamma rays with different energies, allowing for imaging of multiple agents concurrently.[1]

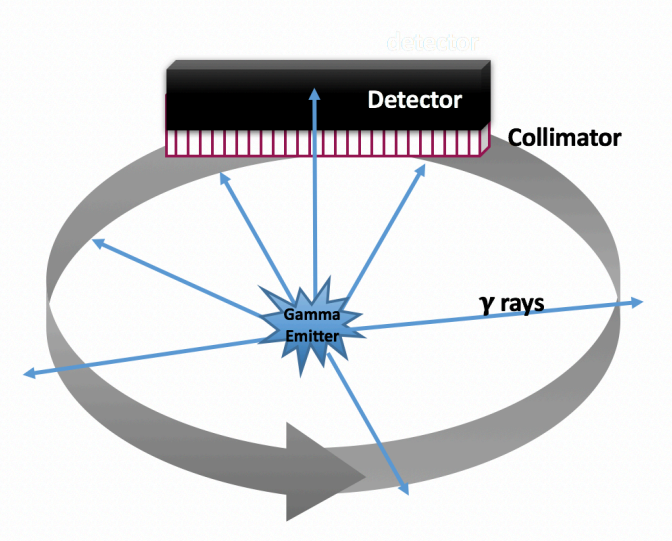

Figure 2: Schematic of gamma ray detection and localization, used to generate SPECT images.

1.2 Technetium-99m

Technetium-99m is the most widely used radionuclide in diagnostic medicine, comprising over 80% of all doses used in nuclear imaging.[6] Tc-based agents are used to image various organs, tissues, and biomarkers of disease, including those associated with infection and cancer. Its widespread use is due to its attractive nuclear properties, which includes a half-life of 6 hours, 140 keV photon energy (which is near optimal for

imaging), and minimal corpuscular radiation.[7] Furthermore, it is readily accessible through a $^{99}Mo/^{99m}Tc$ generator at a low cost.

With respect to the chemistry of the $^{99}Mo/^{99m}Tc$ generator, fission produced ^{99}Mo [$^{235}U(n, f)^{99}Mo$)] is loaded onto an alumina column as $^{99}MoO_4^{2-}$. The parent isotope decays via β-emission to ^{99m}Tc (Figure 3) as pertechnetate (TcO_4^-) which can be eluted in saline due to the higher binding affinity of molybdate to the matrix. TcO_4^- is therefore the starting material for all technetium radiopharmaceuticals. The various oxidation states of technetium (+VII to –I) allows for the synthesis of a diverse range of radiopharmaceuticals. Most compounds incorporating technetium exist in the +I, +III, +IV and +V oxidation states, and are prepared by treating TcO_4^- with a reducing agent in the presence of a complexing ligand.[7]

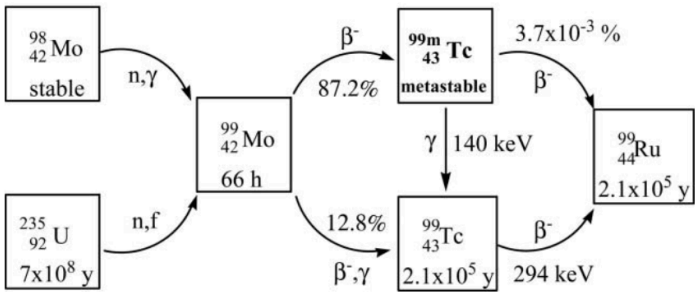

Figure 3: Production and decay pathways of ^{99m}Tc. [8]

1.2.1 Direct Labelling of Biomolecules with ^{99m}Tc

There is a growing need for targeted radiopharmaceuticals, particularly with the advent of targeted drug therapies - which are only effective when a specific biomarker is present. Incorporating ^{99m}Tc into biomolecules to localize the radionuclide to a specific target *in vivo* has proven to be challenging, largely because of the impact of the radiometal on pharmacokinetics.[6] Ideally, methods for labelling should be fast, efficient,

and produce products that are easy to purify, while retaining the parent vectors' target affinity. While much progress has been made to overcome the limitations associated with direct labelling, challenges are still evident.

Technetium labelling of biomolecules is typically accomplished through formation of coordination complexes with bifunctional ligands.[6] In the case of proteins (which includes antibodies) a chelating agent is typically ligated via lysine residues, which often results in enhanced non-specific binding.[9] Furthermore, antibodies have long circulation time (upwards of days), which can increase systemic radiation to patients, along with obtaining poor images because ^{99m}Tc ($t_{½}$ = 6h) decays prior to optimal target accumulation.

There are also issues with direct labelling of small molecular targeting vectors with ^{99m}Tc. The ligation of large metal complexes to small molecules can reduce or eliminate binding to the desired target. For example, direct labelling has been reported with antibiotics such as vancomycin and ciprofloxacin, where the products (influenced by the presence of the radiometal) can no longer differentiate sterile inflammation from bacterial infection.[10] One additional concern for all ^{99m}Tc complexes is *in vivo* degradation, which can occur via enzymatic degradation or radiolysis. With all these challenges in mind, there is a need for better methods to create targeted ^{99m}Tc-radiopharmaceuticals.

1.2.2 6-Hydrazinopyridine-3-carboxylic acid (HYNIC)

6-Hydrazinopyridine-3-carboxylic acid (HYNIC) was first reported by Abrams *et al*. in 1990 as a new class of ligands for labelling biomolecules with ^{99m}Tc.[11] HYNIC compounds have two donor groups (pyridine and hydrazine nitrogen atoms) which form a

coordination complex with ^{99m}Tc. For Tc(V), the HYNIC ligand does not saturate the coordination sphere of the metal. As a result co-ligands are used to fill the coordination sphere, which in turn allows for a large versatility with respect to altering the pharmacokinetics and *in vivo* stability of the labeled product (Figure 4)[12].

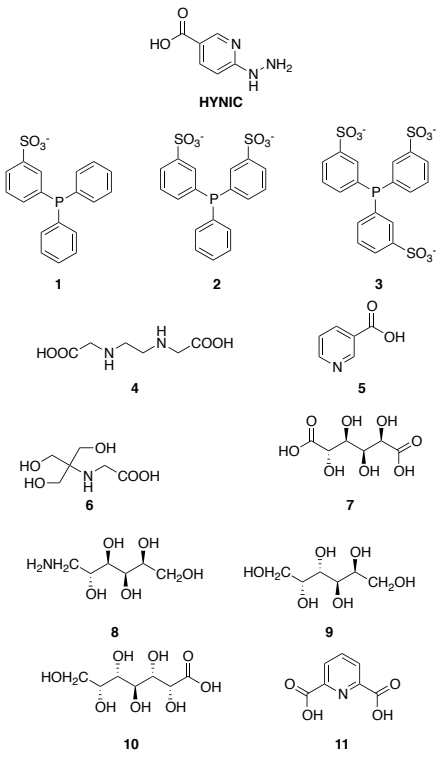

Figure 4: Examples of common co-ligands employed in ^{99m}Tc-HYNIC labelling: TPPMS **1**, TPPDS **2**, TPPTS **3**, EDDA **4**, nicotinic acid **5**, tricine **6**, glucaric acid **7**, glucamine **8**, mannitol **9**, glucoheptonic acid **10**, PDA **11**.[12]

^{99m}Tc-labelling of HYNIC is accomplished by reducing TcO_4^- with stannous chloride in the presence of the ligand and the desired co-ligand.[12] Tricine is one of the most commonly used co-ligands because of its effectiveness at forming an intermediate Tc(V) oxo-complex upon reduction of the metal, which in turn reacts readily with HYNIC.[12] HYNIC has been used successfully to label ^{99m}Tc-label biomolecules such as

annexin V (for detection of apoptosis), image somatostatin receptors (using ^{99m}Tc-HYNIC-TOC), infections, and specific growth factors expressed by tumors.[13–17]

HYNIC can also be adapted for use in PET imaging by using a ^{18}F-labeled aromatic aldehyde to form a hydrazone linkage with the hydrazine functional group.[12] Rennen *et al*. reported the synthesis of ^{18}F-fluorobenzaldehyde (^{18}F-FBA) and its conjugation to HYNIC derived peptides, demonstrating that HYNIC can be used for labelling of multiple isotopes, either through prosthetic groups or chelation. (Figure 5).[18] ^{18}F-HYNIC has been successfully used for labelling of Human Serum Albumin, $\alpha_v\beta_3$-integrin antagonists for ischemia models, and most recently with polypeptides using 2-Deoxy-2-[^{18}F]fluoroglucose (^{18}F-FDG) in place of ^{18}F-FBA.[19–21] HYNIC can also be labelled with the beta-emitting therapeutic isotope ^{188}Re, which was most recently assessed as a treatment for breast cancer and melanoma in mice.[22,23]

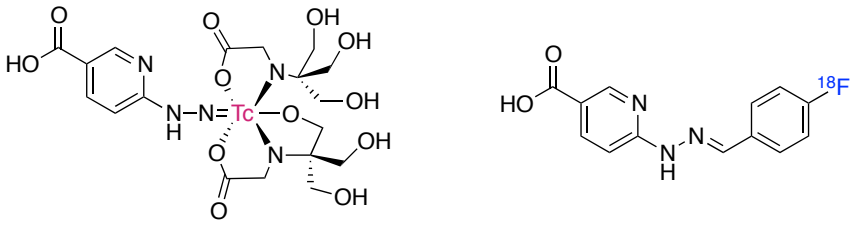

Figure 5: ^{99m}Tc-HYNIC (with tricine co-ligand) and ^{18}F-HYNIC (through a hydrazone linkage with ^{18}F-FBA)

1.3 Multimodal Probes

Conventional targeted MI probes typically consist of three parts: a source of a signal (radioisotope, fluorophore, etc.), a targeting moiety, and a linker to minimize self-interactions between the groups and to optimize pharmacokinetics. [24] There is an active search to create MI probes that can be used with different imaging modalities

(multimodal probes). The goal is to exploit the strengths of each modality and overcome the limitations, or to expand the utility of a single class of probes (e.g. whole body imaging and surgical guidance).

Multimodal instruments exist in clinical settings, with the most common being SPECT/CT, PET/CT and PET/MRI. SPECT or PET can be used to image a specific biochemical process while CT and MRI provide high resolution images for anatomical referencing. Multimodal images of this nature provide additional information and can reduce the need for high resolution CT scans, thus saving time and lowering the radiation burden. Other imaging modalities are increasingly being used in a complementary manner, including optical imaging and PET/SPECT for image guided surgery and lymph node mapping.[25] In this case a whole-body nuclear scan can be performed to localize tumors and lesions, with tumor margins identified using subsequent intraoperative optical imaging.[25]

In an ideal setting, one single probe would be administered (e.g. containing a radioisotope and an optical imaging/MRI contrast agent). However, modality sensitivities can vary by >3 orders of magnitude, and it may not be feasible to include all imaging agents (radioisotopes, fluorophores, contrast agents, etc.) within a single probe.[26] An alternative is to develop a common core which can be labelled with different radioisotopes, contrast agents or fluorophores. This approach would mitigate the need to synthesize and optimize new probes for each modality, ultimately saving time and money.

1.4 Objectives

The goal of this thesis was to develop tetrazine derived hydrazinonicotinic acid ligands (TzHYNIC) and to demonstrate that they can be labelled with radioisotopes and fluorophores, and to show that the products could be targeted using bioorthogonal chemistry (*vide infra*). To this end, a research strategy was developed, where modifications to an existing ^{99m}Tc-TzHYNIC derivative was prepared in order to optimize pharmacokinetic properties. The radiochemistry and bioconjugate chemistry of the resulting products developed were assessed to create nuclear (Chapter 2) and optical (Chapter 3) probes.

1.5 Bioorthogonal and Pretargeting Chemistry

Bioorthogonal chemistry refers to reactions that occur without interfering with biological processes.[27] Specifically, highly selective biocompatible reactions can be performed under physiological conditions to study, target, and manipulate biological systems. One of the earliest examples utilized a Staudinger ligation between an azide and a PPh_3-fluorophore conjugate (Figure 6-i). The platform was evolved by using Cu(I) catalyzed "click" reactions (Figure 6-iv), however the toxicity of copper and complexity of using a catalyst hindered the effectiveness of the approach *in vivo*. Copper-free versions of this reaction were subsequently explored using strain-promoted azide-alkyne systems (Figure 6-ii). Following on from this work, one of the most promising bioorthogonal reactions reported to date is the strain-promoted, [4+2] inverse electron demand Diels-Alder (IEDDA) reaction (Figure 6-iii); which was shown to have superior reaction rates and bioorthogonality compared to other ligation pairs.[27]

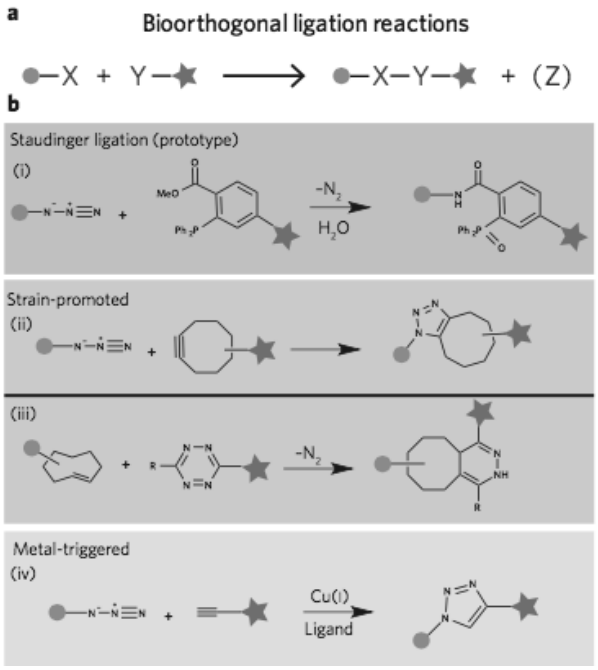

Figure 6: Figure obtained from Li *et al*., showing examples of bioorthogonal reactions including the IEDDA reaction between TCO and Tz (iii). [27]

The tetrazine (Tz) – *trans*-cyclooctene (TCO) IEDDA reaction, with its fast reaction kinetics, is a promising bioorthogonal ligation reaction for creating MI probes. The reactivity of tetrazines with unsaturated dienophiles was reported in 1959 by Carboni *et al*., which yielded pyridazines upon expulsion of N_2. Also noted was the immediate color change, which allowed for a simple means of visualizing when a reaction was complete.[28] The synthesis of various tetrazines have been reported in literature, where Karver *et al*., reported an extensive reaction kinetic screen on various tetrazines. Reactivity with TCO derivatives were noted as high as 10^6 $M^{-1}s^{-1}$, however some of the fastest tetrazines evaluated were not soluble or stable in water, rendering them ineffective for biological applications.[29] It was also noted that functionalizing tetrazines with electron withdrawing groups at 3- or 6-positions increased the reactivity by lowering the LUMO of the diene.[30]

Trans-cyclooctene is a strained dienophile partner for bioorthogonal reactions with tetrazines. Seminal work by Sauer in 1990 reported various rate constants with tetrazines and over 40 dienophiles including cyclopropane, norbornene and TCO. It was ultimately demonstrated that the ring strained *trans*-conformation of TCO exhibited faster reactivities than the *cis*-isomer.[31] Since then, the use of TCO has been widely reported, with various TCO-derivatives being employed for bioorthogonal ligations. It is important to note that the light-sensitive *trans*-cyclooctene can convert to the more stable and less strained *cis*-isomer (however through photochemical flow protocols it can be converted back to the *trans*-isomer).[32]

As mentioned, directly radiolabelled biomolecules, particularly those derived from radiometal complexes, often suffer low target-to-background ratios, resulting in poor image quality and higher doses of systemic radiation to healthy tissue.[33] Pretargeting, coupled with bioorthogonal chemistry can be used as an alternative approach to direct labelling; where a TCO-labelled, non-radioactive targeting molecule can be injected and allowed adequate time to circulate, bind to the target and clear from non-target tissue. A radiolabelled tetrazine is then injected, which undergoes ligation at the site of uptake, ultimately achieving a higher signal-to-background ratio with an overall lower radiation burden.

Methods for radiolabelling tetrazines with ^{11}C, ^{18}F, ^{64}Cu, ^{68}Ga. ^{111}In, and ^{125}I have been previously reported for use in SPECT and PET imaging. [34–39] Recently, ^{99m}Tc-labelled tetrazines have been published, all in 2016 (with three originating from our research group).[40–42] Preliminary assessment of ^{99m}Tc-labelled tetrazines were first presented in 2015, whereafter García *et al.,* published the first ^{99m}Tc-TzHYNIC construct;

using a methylated-tetrazine to increase serum stability.[40,43–46] In the reported *in vivo* studies using LS174T tumor bearing mice, the biodistribution showed 1.39 ± 0.42%ID/g tumor uptake using a TCO-labelled CC49-antibody, with the majority of the activity accumulating in the liver, GI tract and kidneys at 2 hours post-injection (8.96 ± 0.55%ID/g, 8.07 ± 0.21%ID/g, 6.44 ± 1.11%ID/g, respectively).[40] Yazdani *et al*., reported the use of a ^{99m}Tc-Tz for imaging sites of active bone turnover using TCO-bisphosphonate (TCO-BP) and a Tc(I) tridentate tetrazine complex. The biodistribution data at 1 hour post-injection showed high bone target uptake (20.07 ± 4.91%ID/g in the knee and 16.16 ± 4.84%ID/g in the shoulder) along with high non-target uptake in the gall bladder (91.46 ±17.09%ID/g) and intestines (8.26 ± 0.58%ID/g).[41]

Vito *et al*. reported using a ^{99m}Tc-TzHYNIC construct for imaging infection and bone turnover using a TCO-vancomycin conjugate and TCO-BP, respectively. Using TCO-vancomycin in an infection study, the infected calf muscle had a modest uptake (1.96 ± 0.13%ID/g) compared to the control (0.93 ± 0.13%ID/g) at 1 hour post-injection, along with moderate non-target uptake in the blood, liver/gall bladder and small intestine (4.29 ± 0.25%ID/g, 7.03 ± 0.22%ID/g, and 13.82 ± 0.87%ID/g, respectively). With TCO-BP, and the same tetrazine, there was appreciable uptake in the knee and shoulder (9.57 ± 0.39%ID/g and 7.03 ± 1.04%ID/g) at the 6 hour mark, however there was also similar uptake in non-target organs such as the blood, gall bladder and stomach (7.00 ± 0.08%ID/g, 9.65 ± 1.08%ID/g and 8.48 ± 0.91%ID/g).[42] These values indicate that existing ^{99m}Tc-tetrazine compounds are not optimal in terms of high non-specific uptake and low target uptake. As a result, there is a need for better ^{99m}Tc-tetrazines.

1.6 TCO-Derivatives Used in this Work

Two different derivatives of TCO were used during the course of this research to evaluate tetrazine complexes (Figure 7). TCO-bisphosphonate (TCO-BP) accumulates at sites of high bone turnover, and is useful for imaging skeletal diseases.[41] The ability of TCO-BP to target regions of high Ca^{2+} turnover has the added benefit of being a fast and cost effective method, in that it can be performed in normal mice. The reagent is much less expensive than the more commonly used TCO-derived antibodies.[41] The second derivative is TCO-functionalized vancomycin, which was previously developed and used to label gram-positive bacteria by binding to the D-alanyl-D-alanine residues in peptides constituting the bacterial cell wall.[47,48]

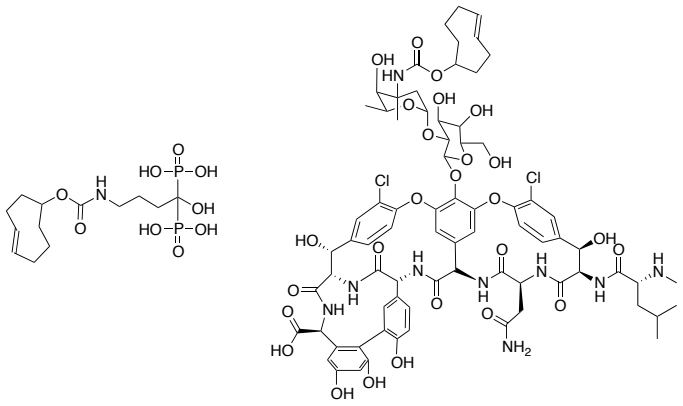

Figure 7: Pretargeting vectors used in this thesis. TCO-Bisphosphonate (**1**) and TCO-Vancomycin (**2**)

2 Synthesis of Tetrazine-HYNIC Derivatives and Radiolabelling with ^{99m}Tc

2.1 Design Strategy

The approach taken towards creating a platform for generating optical and nuclear probes that can be targeted using Tz and TCO chemistry involved the previously reported tetrazine-HYNIC derivative prepared by Vito *et al*. (**6**).[42] Here the hydrazine of the HYNIC ligand can be labelled with ^{99m}Tc or conjugated to fluorescent aldehydes, while the tetrazine can be linked to TCO-derived targeting molecules.

Ideally, imaging probes should have high target uptake with fast clearance from non-target tissues and fluids, thereby achieving high target-to-background ratios. To accomplish this, optimization of target binding and general pharmacokinetic properties are necessary. For the latter, blood half-life, bioavailability, protein binding, metabolism and clearance route are vital components that must be optimized in order for radiopharmaceuticals to be successful *in vivo*. [49] To this end, following the preparation and optimization of the labelling of **6**, the impact of introducing a PEG spacer into a previously reported TzHYNIC derivative (Scheme 3) was assessed.

2.2 Synthesis and Characterization of TzHYNIC

The synthesis of HYNIC, which has been widely used to radiolabel biomolecules with ^{99m}Tc, was first reported by Abrams *et al*. in 1990.[11] Following that procedure, the first step towards the desired product involved nucleophilic displacement of the chlorine atom in 6-chloronicotinic acid with hydrazine at reflux (Scheme 1). The desired product **1** was obtained in 65% yield by precipitation following acidic workup using concentrated

HCl. The characterization data, which included ^{1}H NMR, was consistent with the literature data for **1**.[11]

Compound **1**, with its free hydrazine group, is nucleophilic and can undergo polymerization.[12] Consequently it was promptly protected with a *tert*-butoxycarbonyl (Boc) group. The Boc-protection reaction afforded **2** in 70% yield following silica-gel column chromatography. The free acid was subsequently converted into the active ester using *N*-hydroxysuccinimide (NHS) and dicyclohexylcarbodiimide (DCC), and the desired product was isolated by silica-gel column chromatography and recrystallized in DCM to afford **3** in a 50% yield.[11] The ^{1}H NMR of the isolated product showed a singlet in the alkyl region associated with the methylene protons on the succinimide, supporting the assertion the ester had been synthesized, consistent with literature data.[11]

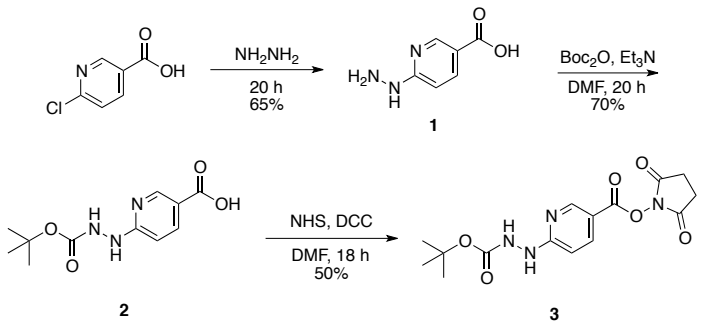

Scheme 1: Synthesis of HYNIC **1** and its derivatives

The synthesis of TzHYNIC **6** was previously reported by our group by coupling Boc-protected HYNIC (**2**) with (4-(1,2,4,5-tetrazin-3-yl)phenyl)methanamine hydrochloride (benzylamino tetrazine) using benzotriazol-1-yl-oxytripyrrolidinophosphonium hexafluorophosphate (PyBOP) (Scheme 2).[42] The Boc-protected ligand (**4**) was resynthesized following the same method and purified via column chromatography in 72% yield. Prior to radiolabelling, compound **4** was deprotected in a 1:2 v/v TFA/DCM mixture to afford compound **5**, with both the free

hydrazine and trifluroacetamide derivative present. The presence of the trifluoroacetamide was not a concern for radiolabelling, as it was reported by Surfraz *et al*. that the reaction conditions with ^{99m}Tc cleave the trifluroacetamide group prior to coordination. According to this publication, the trifluoroacetamide group also allows for protection from unwanted side reactions with electrophiles, increasing the labelling yield.[50]

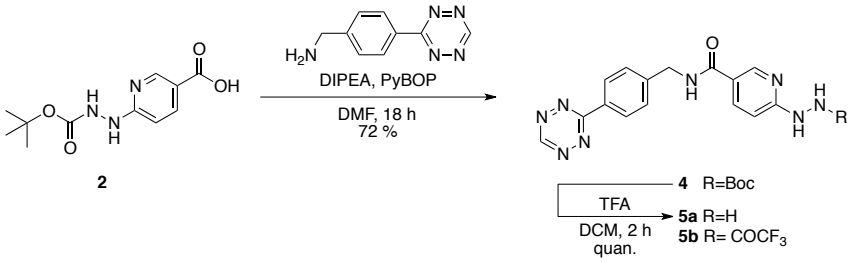

Scheme 2: Synthesis of TzHYNIC **5a/b**

2.2.1 Radiolabelling of TzHYNIC with ^{99m}Tc

The radiolabelling of TzHYNIC with ^{99m}Tc was repeated using a previously optimized experimental procedure with tricine as the co-ligand and stannous chloride as the reducing agent (Scheme 3).[42] The formation of **6** was monitored by gamma-HPLC (Figure 8, right), and the product isolated thereafter in 28% radiochemical yield (RCY) and 91% radiochemical purity (RCP) (Figure 8, left). The reactivity of the compound was also tested *in vitro* by incubating the HPLC-purified product with TCO-vancomycin (Figure 9). The reduction in the size of the peak associated with **6** and the appearance of a new peak indicated that ligation had occurred, demonstrating that the tetrazine reactivity was not hindered. While the conversion was not 100%, this could have been attributed to premature degradation of the tetrazine *in situ*.

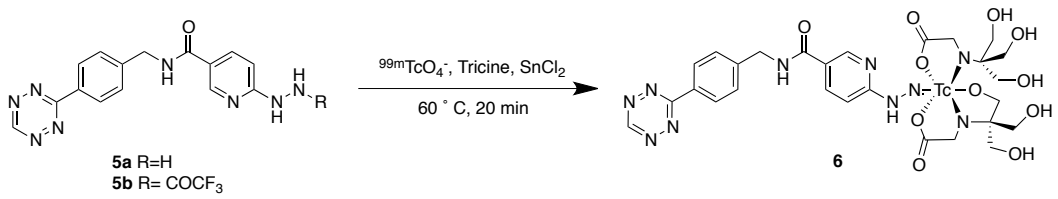

Scheme 3: ^{99m}Tc Radiolabelling of TzHYNIC **5a/b**

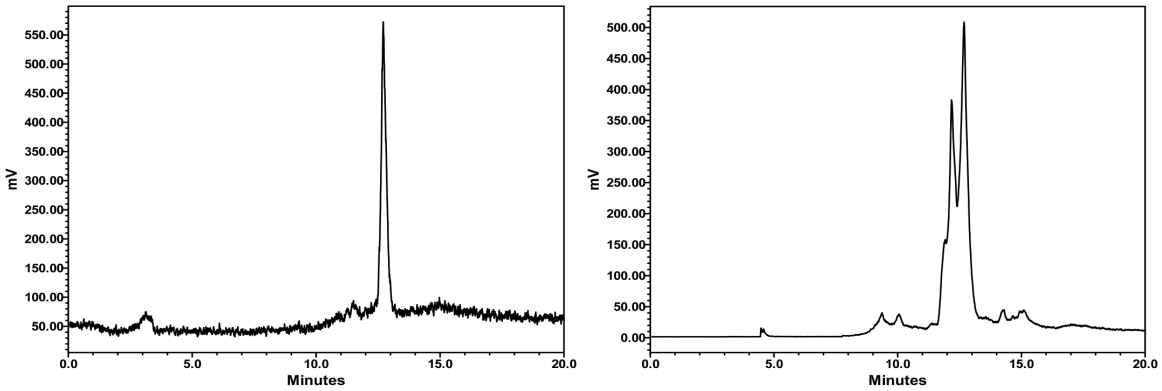

Figure 8: Gamma HPLC chromatograms of purified **6** (left) and the reaction mixture prior to purification (right) using Method A on a Waters 1525 Binary HPLC with a 2998 UV/Vis (λ = 254 nm) detector and Bioscan Glow count gamma detector with Empower 2 software. A semi-preparative Gemini 5 µM NX-C18 110 Å LC Column 250 x 10 mm was used, where Method A used HPLC grade water (solvent A) and acetonitrile (solvent B) as eluents using a gradient mobile phase from 95% 5% A over 30 minutes at a flow rate of 4 ml/min.

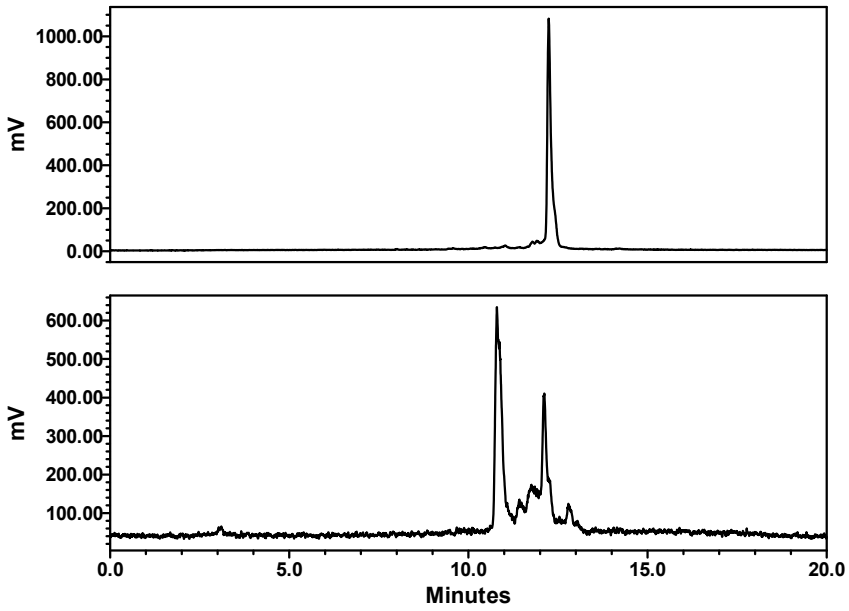

Figure 9: Gamma HPLC chromatograms of HPLC-purified **6** (top) before and after incubation with TCO-vancomycin (bottom) using Method A on a Waters 1525 Binary HPLC with a 2998 UV/Vis (λ = 254 nm) detector and Bioscan Glow count gamma detector with Empower 2 software. A semi-preparative Gemini 5 µM NX-C18 110 Å LC Column 250 x 10 mm was used, where Method A used HPLC grade water (solvent A) and acetonitrile (solvent B) as eluents using a gradient mobile phase from 95% 5% A over 30 minutes at a flow rate of 4 ml/min.

2.3 ^{99m}Tc-TzHYNIC – Biodistribution Studies; A comparison of HPLC purified and kit formulated products

The biodistribution of HPLC purified ^{99m}Tc-HYNIC was reported by Vito *et al*., in the presence and absence of TCO-bisphosphonate and TCO-vancomycin.[42] The reported procedure employed HPLC purification to isolate the radiolabelled tetrazine, which involved extensive handling and processing of the radioactive material; and would therefore not be suitable for clinical translation. HPLC purification would also hinder future studies around assessing the impact of new co-ligands, since each preparation would require development of new separation methods. Furthermore, it was noted that the repeated use of HPLC for isolation and reformulation of the material resulted in

product degradation and the formation of pertechnetate. Pertechnetate accumulates in non-target organs including the gallbladder, stomach and thyroid, lowering the signal-to-noise ratio.[6] The processing may also explain the lack of complete reactivity seen between TCO-vancomycin and **6** in Figure 9.

The gamma-HPLC chromatogram of the reaction mixture when compound **6** is formed (Figure 8, right) shows two main peaks that are likely due to different isomers. ^{99m}Tc-complexes of HYNIC with select co-ligands have been shown to exist as multiple isomers. For example, tricine can coordinate to Tc through binding of the carboxyl or hydroxyl group (Figure 10, A and C), which can occur on either or both sides of the distorted octahedral complex (Figure 10, A/B and A/C and D). Furthermore, the HYNIC moiety may coordinate to Tc in a hydrazido or diazenido fashion – producing numerous structural and stereoisomers with respect to the multiple binding modes of tricine (Figure 10, E).[51]

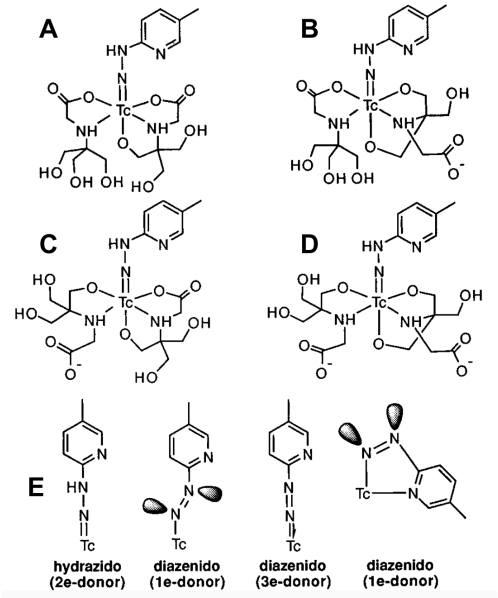

Figure 10: Various structures of Tc-HYNIC complexes with tricine as the co-ligand (reprinted from Liu *et al.*) [51]

To determine if HPLC purification was in fact necessary, the biodistribution of the reaction mixture, as opposed to HPLC purified material, was evaluated. If it were possible to eliminate HPLC purification, the resulting 'kit-like' production would simplify optimization and have the added benefit of reducing non-target uptake by avoiding the formation of pertechnetate associated with reformulation.

The biodistribution of the non-HPLC purified product and HPLC purified ^{99m}Tc-TzHYNIC (**6**) were evaluated in parallel using healthy CD1 mice that were administered TCO-BP (Figure 9). The experiments involved administration of TCO-BP (5 mg/kg) followed by the labelled tetrazines (formulated in 0.9% saline at 200 μCi/ml) 1 hour later. Tissue and fluids were collected and the activity counted at 6 h post administration of the tracer (Table 2). Uptake in bone was comparable between the purified and non-purified products (4.73 ± 0.47 versus 4.15 ± 0.27%ID/g in shoulder, 6.32 ± 0.21 versus 5.94 ± 0.59%ID/g in knee, respectively), suggesting that the multiple peaks in the HPLC of the reaction mixture do not alter the extent of the reaction with the TCO-derived target. The HPLC purified material did however show significant uptake in the stomach and thyroid, which is consistent with the presence of pertechnetate. The non-HPLC purified product showed similar uptake in blood (5.89 ± 0.18%ID/g compared to 7.77 ± 1.38%ID/g in the HPLC purified) and most non-target organs including the intestines, lungs, kidneys and heart, based on the data being compared to the HPLC purified product using Student's t-test and a two-tail hypothesis where $p < 0.5$. The higher activity accumulating in the liver (16.23 ± 0.74%ID/g) and spleen (14.39 ± 0.60%ID/g) may be associated with the presence of additional co-ligand and lack of decomposition to pertechnetate, where the thyroid and stomach showed low activity concentrations of 2.32 ± 0.21 and 1.14 ±

0.09%ID/g respectively. These levels also could be attributed to colloidal technetium, which has also been reported to accumulate in those organs.[52] The data does show that it is feasible to avoid HPLC purification and prepare compound **6** in a single step.

Table 2: Biodistribution data for HPLC purified and non-HPLC purified ^{99m}Tc-TzHYNIC **6** at 6 h post-administration in CD1 mice administered TCO-BP (5 mg/kg). The data is reported as %ID/g and statistical analysis was done using a Student's t-test and a two-tailed hypothesis where * is $p < 0.5$, and n.s. is an abbreviation of "not significant".

	Timepoint (h)		
Organs	HPLC-Purified	Reaction Mixture	Data Comparison
Blood	7.77 ± 1.38	5.89 ± 0.18	n.s.
Adipose	0.70 ± 0.17	1.18 ± 0.37	n.s.
Adrenals	6.85 ± 0.71	9.19 ± 0.40	*
Bone (arm + shoulder)	4.73 ± 0.47	4.15 ± 0.27	n.s.
Bone (leg + knee)	6.32 ± 0.21	5.94 ± 0.59	n.s.
Brain	0.13 ± 0.02	0.11 ± 0.02	n.s.
Gall Bladder	40.0 ± 35.2	6.64 ± 1.26	n.s.
Heart	2.20 ± 0.40	1.66 ± 0.06	n.s.
Kidneys	15.2 ± 9.64	4.37 ± 0.36	n.s.
Lg Intestine + Caecum	6.92 ± 1.70	3.80 ± 0.45	n.s.
Liver	11.0 ± 1.55	16.2 ± 0.74	*
Lungs	4.78 ± 1.23	4.48 ± 0.09	n.s.
Pancreas	0.92 ± 0.30	0.64 ± 0.05	n.s.
Skeletal Muscle	0.59 ± 0.27	0.56 ± 0.19	n.s.
Sm Intestine	1.71 ± 0.28	1.11 ± 0.08	n.s.
Spleen	9.49 ± 1.16	14.4 ± 0.60	*
Stomach	7.29 ± 0.88	1.14 ± 0.09	*
Thyroid/Trachea	15.7 ± 2.45	2.32 ± 0.21	*
Urine + Bladder	8.16 ± 4.98	18.1 ± 8.40	n.s.

Data are expressed as %ID/g ± SEM

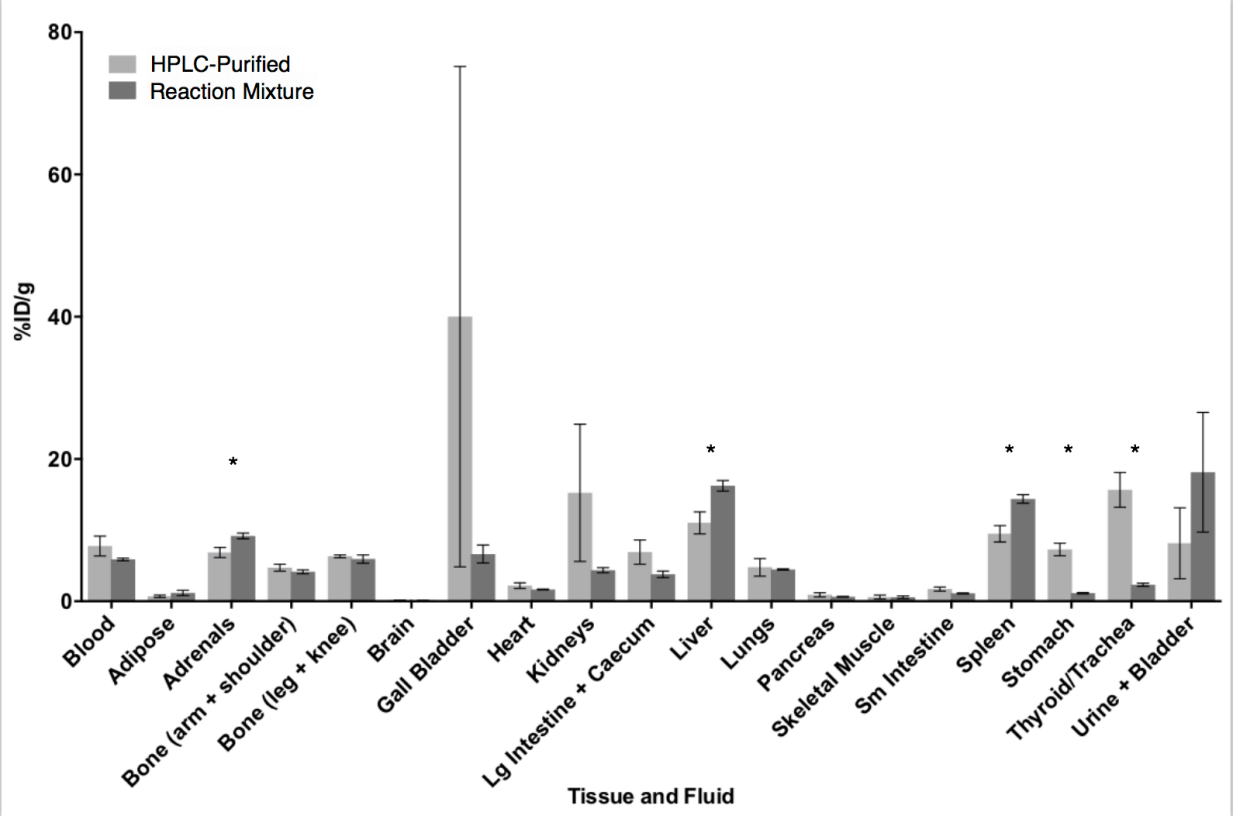

Figure 11: Plot of the percent injected dose per gram (%ID/g), per tissue and fluid harvested 6 h post-injection of ^{99m}Tc-TzHYNIC **6** (HPLC purified and the non-purified reaction mixture 20 µCi/100µl) in healthy CD1 mice that had been administered with TCO-BP (5 mg /kg) 1 hour prior to injection of **6.** * indicates significance where $p < 0.5$ using a Student's t-test and a two-tailed hypothesis.

2.4 Synthesis and Characterization of TzPEG$_{11}$HYNIC

The first generation TzHYNIC derivative (whether HPLC purified or not) demonstrated less than optimal uptake in non-target organs such as the liver and gall bladder, along with retention in the blood up to 6 h post-injection (Table 2). To improve the clearance from non-target organs, a polar linker group was introduced. The commercially available benzylamino tetrazine was coupled to HYNIC using a PEG$_{11}$ spacer, which was selected to increase the overall polarity and clearance from blood and other tissues. The choice of PEG spacer length was based on previous work with a similar

tetrazine which showed optimal biodistribution data when the chelator was labeled with ^{111}In. [34]

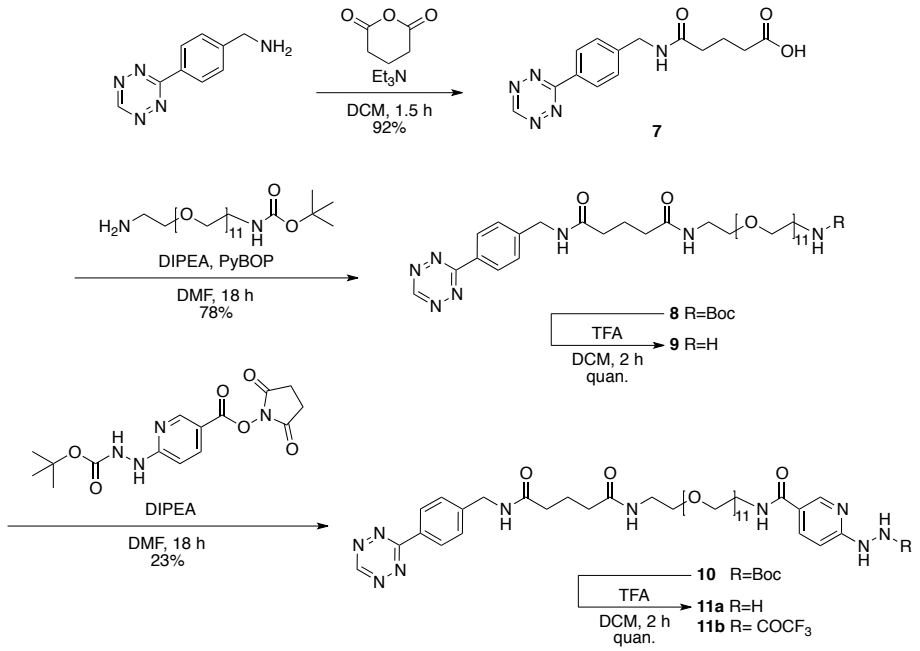

Scheme 4: Synthesis of $TzPEG_{11}HYNIC$ **11a/b**

The synthesis of ligand **11a/b** was adapted from Rossin *et al*., which involved derivatization of benzylamino tetrazine with glutaric anhydride to afford the carboxyl-terminated tetrazine **7** (Scheme 4).[34] It was ultimately determined that the addition of triethylamine to the reaction solvent at room temperature was key and enabled the reaction to proceed to completion, and a liquid-liquid extraction was used to afford **7** in a high yield without need for elevated temperatures (contrary to what was reported in literature).[39,53–55] Compound **7** was conjugated to a commercially available protected polyethylene glycol (PEG) derivative using a PyBOP-mediated coupling procedure. The product **8** was isolated in 78% yield as a pink oil via silica gel chromatography. The ^{1}H NMR showed a broad peak at 3.63 ppm, which was indicative of the incorporation of the PEG spacer, along with a singlet at 1.43 ppm that integrated for 9H of the Boc-protecting

group. The Boc group was removed with TFA to afford intermediate **9**, which was passed through a Sep-Pak to remove excess acid by washing with water until the pH of the eluent was between 5-6. The compound was eluted off the Sep-Pak cartridge in methanol, dried, and immediately combined with a solution of NHS-HYNIC-Boc (**3)** in DMF to afford **10** as a pink oil in 23% yield, where the desired product was isolated by silica-gel chromatography. The ^{1}H NMR had three new peaks in the aromatic region corresponding to the HYNIC pyridyl hydrogen atoms (8.55, 8.00 and 8.70 ppm), along with a singlet at 1.49 ppm associated with the Boc-protecting group, verifying that the compound was successfully synthesized for ^{99m}Tc-labelling.

2.4.1 Radiolabelling of TzPEG$_{11}$HYNIC with ^{99m}Tc

Prior to radiolabelling, **10** was deprotected in 1:2 v/v TFA/DCM to afford **11a** and the trifluoroacetamide derivative **11b,** which was confirmed by positive mode electrospray mass spectroscopy (m/z 963 **11a**) and ^{1}H NMR, where the absence of the Boc-group at 1.49 ppm was observed. The radiolabelling of ligand **11a/b** was adapted from the TzHYNIC labelling protocol, and included the use of tricine as the coligand.[42] The labelling however was performed in saline (as opposed to water), allowing for direct use of the reaction mixture for subsequent *in vivo* studies without having to reformulate (Scheme 5). Compound **11** (0.103 μmol) was treated with pertechnetate and stannous chloride in the presence of tricine to obtain compound **12** (Figure 12, middle). Radio-iTLC was done to in order to assess the extent of free pertechnetate using acetone as the eluent. Under these conditions, pertechnetate migrates to the solvent front; where there was minimal activity observed (<3%) (Figure 13). The reactivity of **12** was also assessed by HPLC following incubating the reaction mixture with excess TCO-vancomycin

(Figure 12, bottom). The appearance of a new peak indicated that ligation had occurred with the tetrazine moiety. The gamma-HPLC showed multiple peaks, which as previously noted, is likely due to the isomers present, and are associated with the use of tricine and the different binding modes of HYNIC.[39]

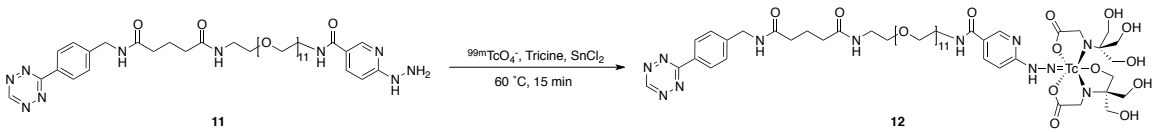

Scheme 5: ^{99m}Tc Radiolabelling of TzPEG$_{11}$HYNIC **11**

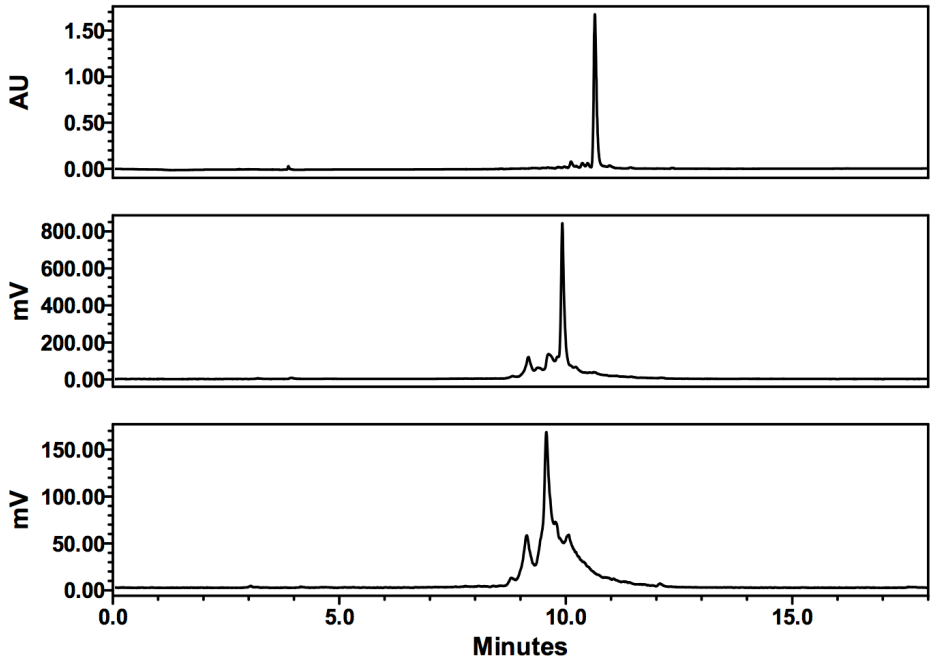

Figure 12: UV-HPLC chromatogram of **11** (top), gamma HPLC chromatogram of ^{99m}Tc-TzPEG$_{11}$HYNIC **12** (middle) and gamma-HPLC chromatogram of **12** after incubation with TCO-vancomycin (bottom) using Method B on a Waters 1525 Binary HPLC with a 2998 UV/Vis (λ = 254 nm) detector and Bioscan Glow count gamma detector with Empower 2 software. An analytical Gemini 5 µM NX-C18 110 Å LC Column 250 x 4.6 mm was used, where Method B used HPLC grade water (solvent A) and acetonitrile (solvent B) as eluents using a gradient mobile phase from 95% to 40% A from 0-10 min, followed by 40% to 20 %A from 10-16 min, followed by 20% A to 95% from 16-18 min at a flow rate of 1 ml/min.

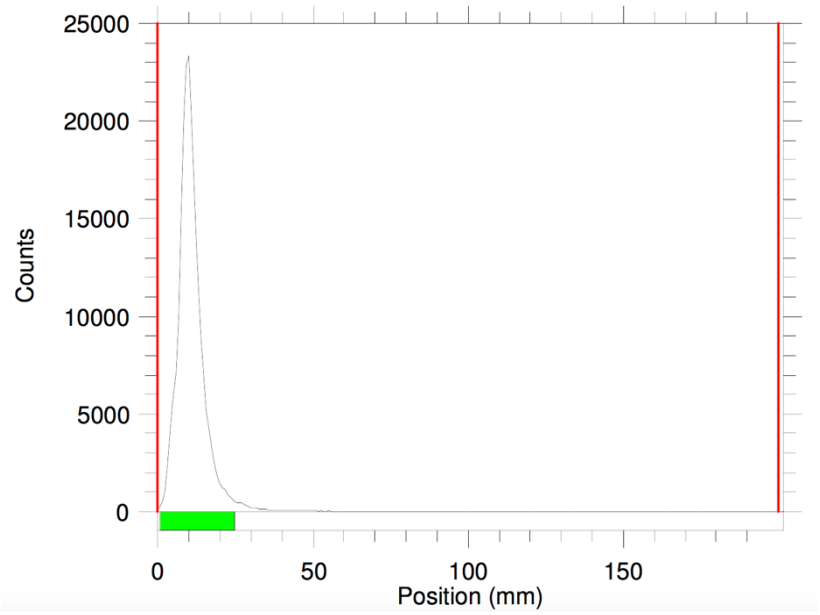

Figure 13: Radio-iTLC of ^{99m}Tc-TzPEG$_{11}$HYNIC **12** eluted using acetone

2.4.2 Stability Studies

In order to test the stability of compound **12**, a solution of the product (12.5 mCi/mL) in saline was left at room temperature and analyzed by HPLC and radio-iTLC as a function of time. Stability studies were carried out for 6 hours, with particular focus on the amount of pertechnetate present. Interestingly, the HPLCs show that the various isomers, which can interconvert, result in different profiles as a function of time. Nevertheless, radio-iTLC analysis at 4 hours reported less than 1% pertechnetate, indicating that the direct labelling mixture was stable.

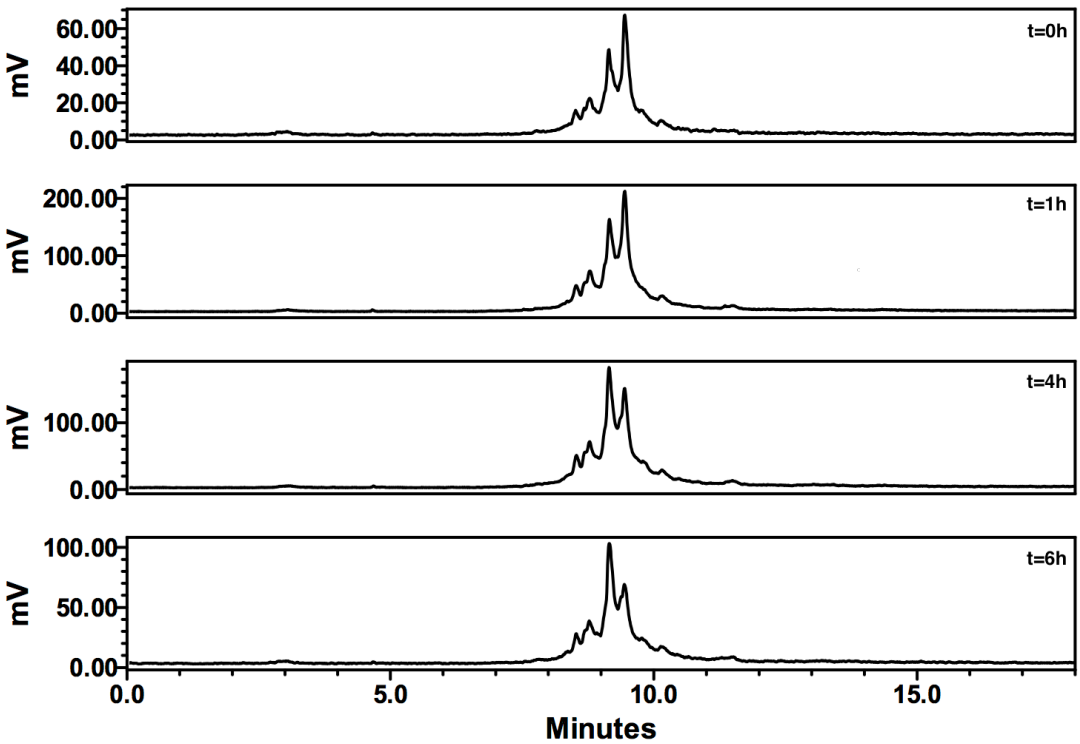

Figure 14: Gamma HPLC chromatograms of ^{99m}Tc-TzPEG$_{11}$HYNIC **12** in saline at various time points. using Method B on a Waters 1525 Binary HPLC with a 2998 UV/Vis (λ = 254 nm) detector and Bioscan Glow count gamma detector with Empower 2 software. A semi-preparative Gemini 5 µM NX-C18 110 Å LC Column 250 x 10 mm was used, where Method B used HPLC grade water (solvent A) and acetonitrile (solvent B) as eluents using a gradient mobile phase from 95% to 40% A from 0-10 min, followed by 40% to 20 %A from 10-16 min, followed by 20% A to 95% from 16-18 min at a flow rate of 4 ml/min.

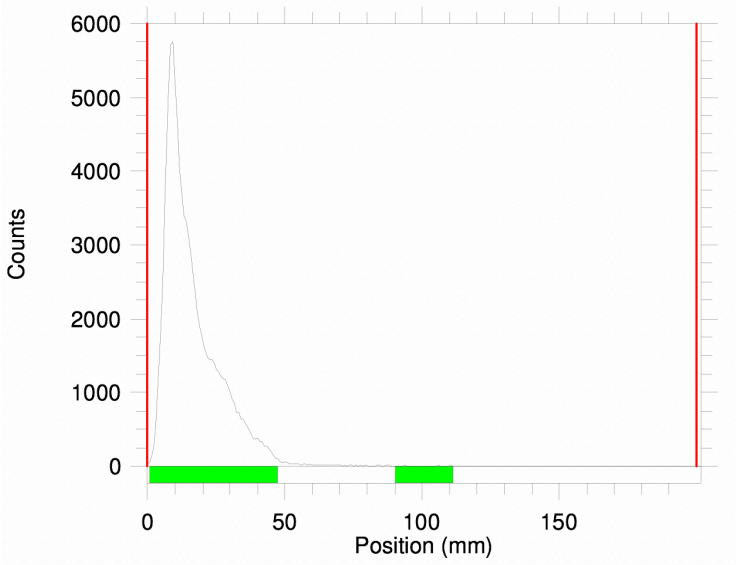

Figure 15: Radio-iTLC of ^{99m}Tc-TzPEG$_{11}$HYNIC **12** eluted in acetone after 4 h in saline at room temperature

2.5 Biodistribution of ^{99m}Tc-TzPEG$_{11}$HYNIC

A biodistribution study was performed on **12** using TCO-BP as the targeting vector (Figure 16). The uptake in the bone was significantly less in the shoulder and knee compared to the non-pegylated derivative **6** (1.62 ± 0.22 versus 4.15 ± 0.27%ID/g in shoulder, 2.39 ± 0.22 versus 5.94 ± 0.59%ID/g in knee, respectively). In contrast to **6**, **12** showed a marked decrease in non-target uptake, especially in the blood, adrenals, kidneys, liver, lung and spleen (Table 3). However, there was higher uptake in the large intestine (19.48 ± 0.24 versus 3.80 ± 0.45%ID/g).

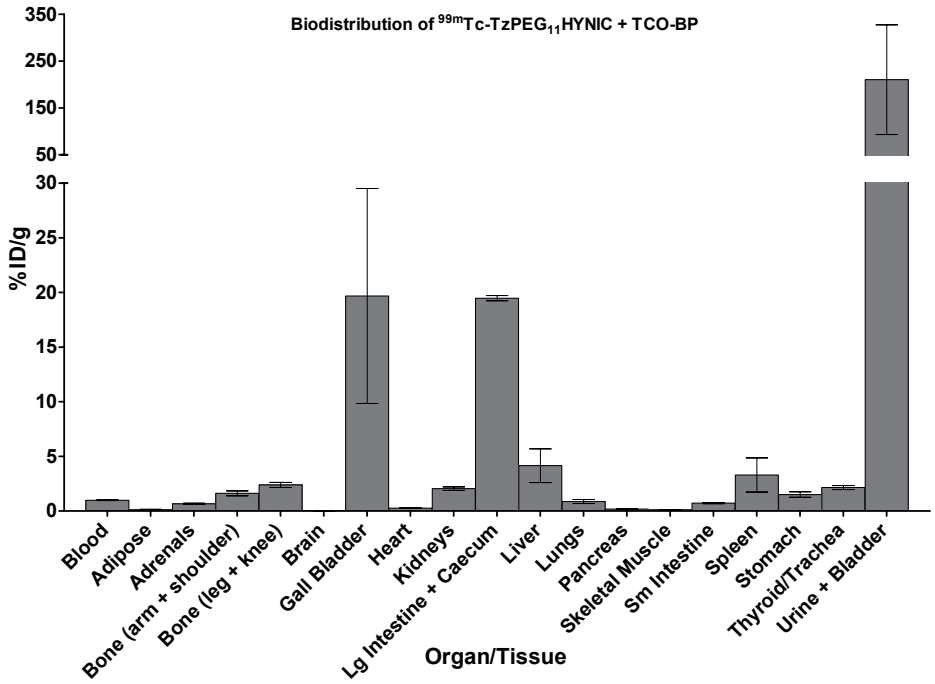

Figure 16: Plot of the percent injected dose per gram of tissues and fluids (%ID/g) harvested 6 h post-injection of ^{99m}Tc-TzPEG$_{11}$HYNIC **12** (20 μCi/100μl) in healthy CD1 mice that had been administered with TCO-BP (5 mg/ml) 1 hour prior to the injection of **12.**

Both **6** and **12** showed high gall bladder uptake, which could be due to organic anion transporters found in the hepatobiliary clearance pathway. While the ^{99m}Tc-complex would have an overall neutral charge, we hypothesize that interaction between **6** or **12** and residual TCO-BP in the blood would form an anionic complex and result in gall bladder and intestinal uptake.[56] Furthermore, it has been reported that compounds containing PEG chains can exhibit significant absorption in the large intestines (up to 10 %ID/g with PEG chains between 350-1000g/mol).[57] However, with only one time point for this study, it cannot be conclusively said whether this is active uptake or simply a matter of ongoing clearance. LogP measurements indicated that this compound is not particularly lipophilic (0.927) when compared to the methylated ^{99m}Tc-TzHYNIC

reported by García *et al*. (-0.54), which is consistent with the 210.52±117.10 %ID/g found in the urine and bladder of **12**.[40] The latter demonstrates that the primary method of elimination is through the renal system.

Table 3: Biodistribution data for ^{99m}Tc-TzHYNIC **6** and ^{99m}Tc-TzPEG$_{11}$HYNIC **12** reported as %ID/g. Statistical analysis was done via Student's t-test using a two-tailed hypothesis where * is $p < 0.5$ and n.s. is an abbreviation of "not significant".

	Timepoint (h)		
Organs	TzHYNIC	TzPEG$_{11}$HYNIC	Data Comparison
Blood	5.89 ± 0.18	0.99 ± 0.03	*
Adipose	1.18 ± 0.37	0.12 ± 0.03	*
Adrenals	9.19 ± 0.40	0.66 ± 0.06	*
Bone (arm + shoulder)	4.15 ± 0.27	1.62 ± 0.22	*
Bone (leg + knee)	5.94 ± 0.59	2.39 ± 0.22	*
Brain	0.11 ± 0.02	0.03 ± 0.01	*
Gall Bladder	6.64 ± 1.26	19.7 ± 9.84	n.s.
Heart	1.66 ± 0.06	0.27 ± 0.02	*
Kidneys	4.37 ± 0.36	2.05 ± 0.16	*
Lg Intestine + Caecum	3.80 ± 0.45	19.5 ± 0.24	*
Liver	16.2 ± 0.74	4.15 ± 1.55	*
Lungs	4.48 ± 0.09	0.87 ± 0.18	*
Pancreas	0.64 ± 0.05	0.19 ± 0.04	*
Skeletal Muscle	0.56 ± 0.19	0.10 ± 0.02	n.s.
Sm Intestine	1.11 ± 0.08	0.73 ± 0.05	*
Spleen	14.4 ± 0.60	3.30 ± 1.57	*
Stomach	1.14 ± 0.09	1.51 ± 0.25	n.s.
Thyroid/Trachea	2.32 ± 0.21	2.15 ± 0.19	n.s.
Urine + Bladder	18.1 ± 8.40	211 ± 117	n.s.

Data are expressed as %ID/g ± SEM

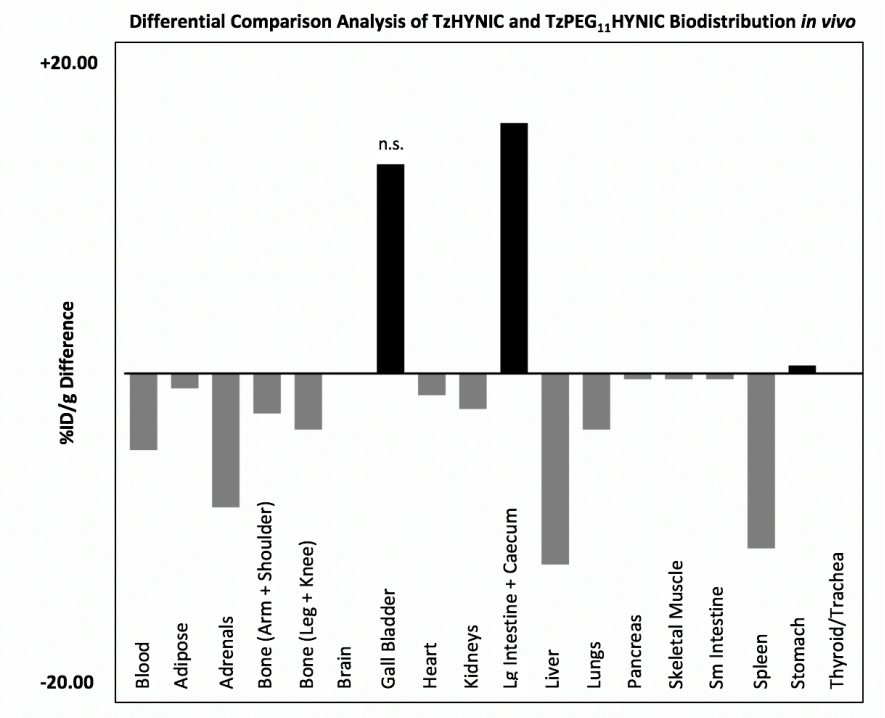

Figure 17: Waterfall plot comparing %ID/g in various tissues and fluids for ^{99m}Tc-TzHYNIC **6** and ^{99m}Tc-TzPEG$_{11}$HYNIC **12**. Positive values (black bars) indicate higher tissue and fluid uptake after administering **12**, with negative (grey bars) indicating decreased tissue and fluid uptake comparing **12** to **6**.

While a decrease in most non-target organs was observed, there was also a decrease in the uptake at the target site. At less than 5% ID/g in the knee and shoulder, it was hypothesized that the new polar complex may clear the body too quickly, which limits the extent of coupling to TCO-BP *in vivo*. To test this, a blood clearance study was performed, and based on literature data, a blood half-life of 10-15 minutes is optimal.[34,35] The results indicated that the half-life for **12** was only 2.6 minutes, which may explain the low target uptake (Figure 18).

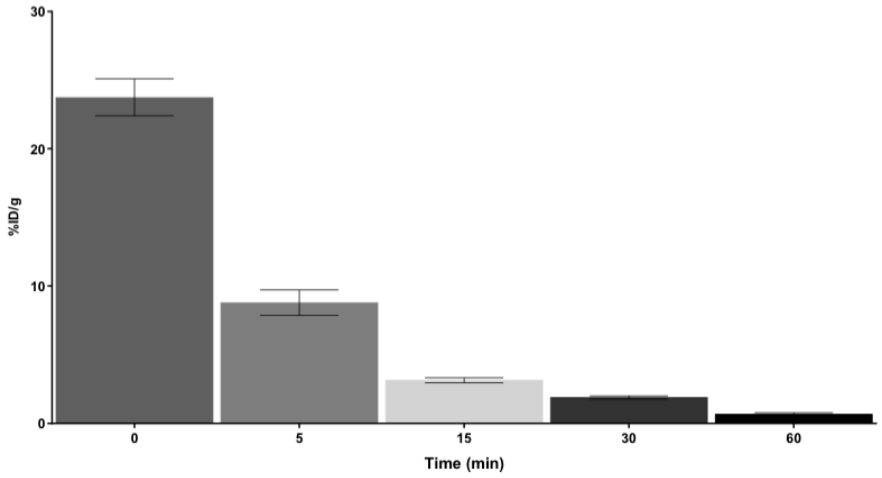

Figure 18: Blood clearance and half-life of ^{99m}Tc-TzPEGHYNIC **12**, presented as %ID/g using healthy CD1 mice administered with 200µl of **12** formulated at 1.75mCi/ml. At selected time points, the mice were placed under anesthesia and blood removed via cardiac puncture followed by cervical dislocation. Pre-weighed gamma tubes with ~500µl of blood were left to decay overnight and counted to determine %ID/g in the blood.

2.6 Synthesis and Attempted Radiolabelling of a Bispyridyl Tetrazine-HYNIC Ligand

In tandem with developing a more hydrophilic construct, the synthesis of a HYNIC derivative with a different tetrazine moiety was investigated. Rossin *et al*. reported the use of a bispyridyl tetrazine linked to a DOTA chelate to image colon cancer using ^{111}In.[34] This particular derivative demonstrated faster reaction kinetics, and may have decreased non-specific binding compared to the benzylamino tetrazine.[29]

The synthesis of **19** was adapted from literature methods, which included preparing the initial bispyridyl tetrazine substrate **13** (Scheme 6).[34,58] The acid-derivatization of **13** to afford **15** reported by Rossin *et al*. was not successfully reproduced. As a solution, triethylamine was added to the reduced form of the bispyridyl tetrazine with glutaric anhydride to ultimately afforded **14** in 40% yield. The product was

oxidized using phenyliodonium diacetate to generate **15** in 80% yield. The ^{1}H NMR agreed with literature, where the singlet at 6.36 ppm (which corresponded to the primary amine of the tetrazine, 2H) was no longer apparent, and the appearance of a new peak for one proton of the now secondary amine was seen. Furthermore, new peaks in the alkyl region where observed, which corresponded to the methylene protons of the 5-carbon spacer linker.

The addition of the PEG_{11} spacer to form **16** was accomplished by treating **15** with $NH_2CH_2CH_2$-PEG_{11}-NHBOC using PyBOP-mediated amine coupling procedures. The product was isolated in 50% yield by silica chromatography as a purple oil. The ^{1}H NMR was in agreement with the literature, where a large peak at 3.64 ppm was indicative of the PEG group, along with the broad singlet at 1.43 ppm for 9H for the Boc-protecting group. Following isolation, **16** was deprotected in TFA/DCM, and loaded onto a Sep-Pak cartridge to remove excess acid (following same method to synthesize **10**) and immediately combined with NHS-HYNIC-Boc (**3**) in DMF to afford the penultimate product **18** as a purple oil in a 30% yield. New peaks, which corresponded to the HYNIC pyridyl hydrogen atoms were observed in the aromatic region, along with the Boc-protecting group at 1.49 ppm, where formation of the compound was further supported by HRMS.

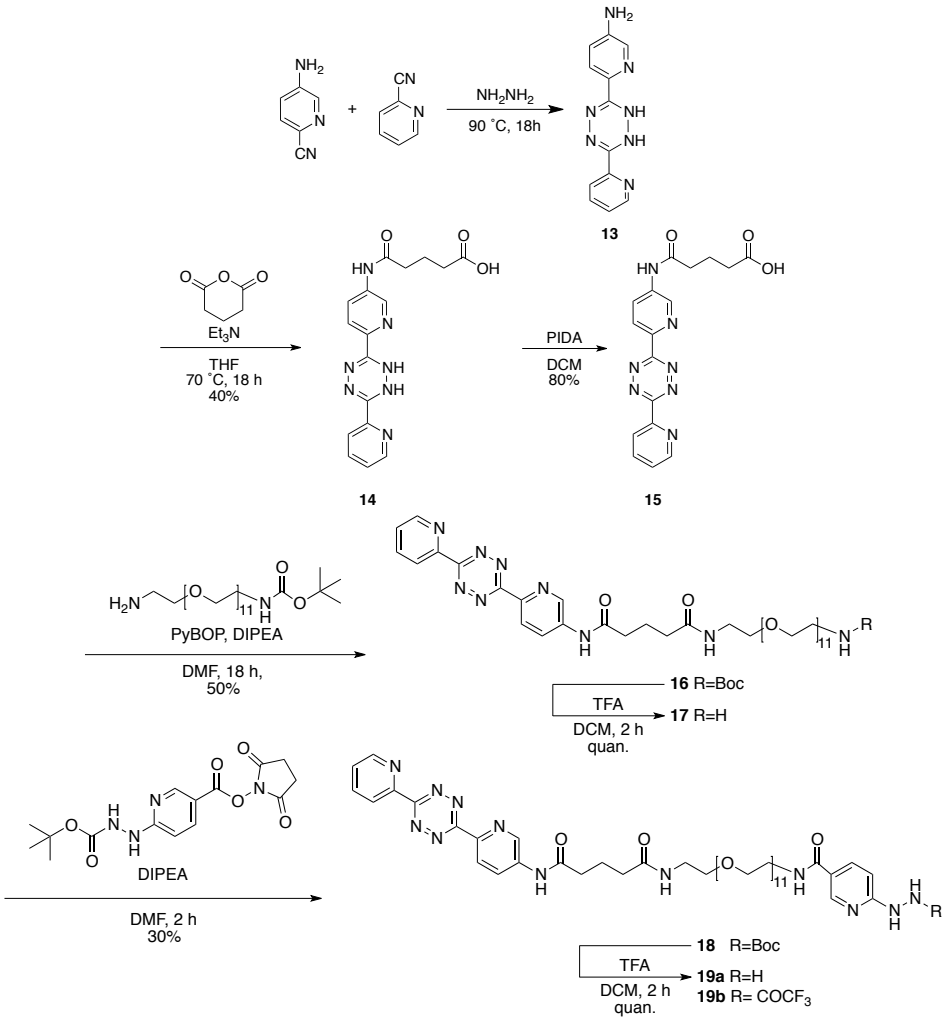

Scheme 6: Synthesis of the bispyridyl tetrazine ligand **19a/b**

Prior to radiolabelling, **18** was deprotected with 1:2 v/v TFA/DCM to generate the desired product **19**. Unfortunately, radiolabelling of **19** was not successful. The resulting gamma-HPLC trace showed only a complex mixture of ^{99m}Tc-labelled compounds that were unable to be separated and isolated. Additional products (outside of the tricine isomers) formed as a possible result of the coordination of technetium to the bispyridyl tetrazine.[59] While compound **19** cannot be used to produce Tc-labelled tetrazines, it does

have the potential to be used with other signaling agents, specifically conjugation to fluorophores for optical imaging applications.

2.7 Conclusions

A new tetrazine-HYNIC ligand was synthesized for bioorthogonal chemistry and development of new MI probes using pretargeting approaches. Initially, and for comparison, the synthesis and ^{99m}Tc-radiolabelling of the first generation TzHYNIC **6** was completed. Furthermore, it was discovered that HPLC purification was not needed to generate the product and that a kit-like formulation could be used to prepare the desired complex while eliminating unwanted by-products. The synthesis, radiolabelling and biodistribution of a derivative with a PEG spacer was also completed, and showed better clearance from most non-target fluid and organs, but also reduced uptake in the target when TCO-BP was used. This is likely due to its fast blood clearance. A second PEG-HYNIC tetrazine construct was synthesized, however the radiolabelling was ultimately unsuccessful due to formation of unwanted ^{99m}Tc-complexes.

2.7.1 Future Work

Compound **12** is a promising candidate for bioorthogonal chemistry applications. With the preliminary biodistribution data in hand, the next step is to vary the co-ligands to further refine the pharmacokinetics. Figure 4 shows various co-ligands that are currently used in HYNIC labellings. The choice of co-ligand can vastly influence the labelling conditions, the radiochemical yield, and the distribution *in vivo*. Several studies have assessed the effect of various co-ligands on LogP and pharmacokinetics. García *et al*. for example reported the use of tricine and EDDA (two of the most common co-ligands used) on a TzHYNIC in which the tetrazine used was a methylated derivative.

The LogP values reported with tricine, EDDA and tricine/EDDA were -0.54, -0.40, and -0.51 respectively (with tricine being the most hydrophilic complex).[40] With respect to our lead compound (LogP of 0.927), the use of more lipophilic co-ligands could promote longer blood residence, which would allow for greater target uptake while still rapidly clearing from non-target organs and tissues. Furthermore, the use of neutral or non-charged co-ligands should be investigated to assess how the overall charge affects distribution through anion transporters in the hepatobiliary organs. Examples of prospective co-ligands include alkylated derivatives of EDDA (Me_2EDDA, Et_2EDDA etc.) or potentially a new class of lipophilic compounds.[60] Once the complexes have been prepared, they can be tested *in vivo* to assess their biodistribution and reactivity with TCO-derivitized biomolecules.

3 HYNIC-Tetrazine Derived Fluorescent Probes and Optical Imaging

3.1 Introduction to Fluorescent and Optical Imaging

In tandem with developing nuclear imaging probes, the ability to use HYNIC-tetrazine derivatives to create complementary fluorescent probes for optical imaging was investigated. Optical imaging agents impart vastly reduced radiation burden to patients when compared to nuclear probes, and are valued as an emerging resource in the clinic for diagnostic applications as well as for surgical guidance.[1] They can also be used to assess target binding on a cellular level using fluorescence microscopy.

Luminescence, or the emission of light in response to absorption of electromagnetic radiation, can be categorized as fluorescence or phosphorescence.[61] As seen in Figure 19, following light absorption - fluorophores are excited to a higher energy

singlet state (S_1, and occasionally S_2). Relaxation to the ground singlet state emits a photon, generating fluorescence (average fluorescence lifetime of 10 nanoseconds). In contrast, excited compounds in the S_1 state may undergo conversion to the triplet state T_1 through intersystem crossing. Because the transition from T_1 to ground state is forbidden, the process to return to ground state, referred to as phosphorescence, takes much longer (minutes to hours) than the corresponding process associated with fluoresence.[61]

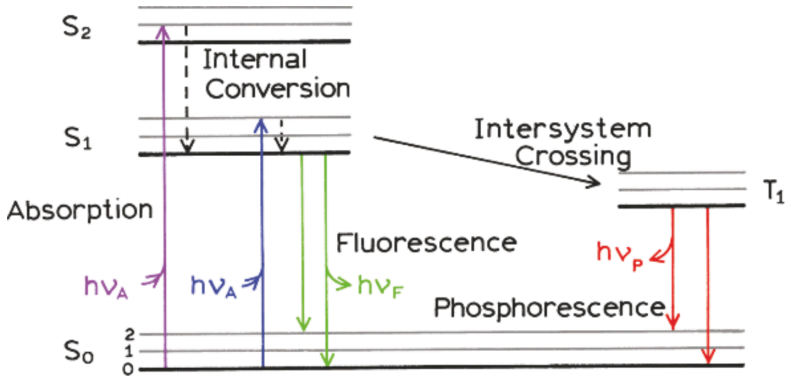

Figure 19: Jablonski diagram demonstrating absorption and emission processes associated with fluorescence and phosphorescence [61]

Optical imaging utilizes luminescent molecules to visualize specific targets, which can include cells and tissues. It is a relatively inexpensive and widely accessible method, which rivals SPECT and PET with regards to sensitivity. It also has a better safety profile since it does not involve the use of ionizing radiation; however more contrast agent must be administered (upwards of milligrams), which can pose toxicity concerns at higher levels. Similar to SPECT, optical imaging can be used for multiplexing due to the different excitation and emission wavelengths of various fluorophores. In contrast to nuclear imaging, the major limitation of optical imaging

methods is the depth of penetration, which is only a few centimeters due to attenuation/scattering (however it can be increased through the use of near-infrared (NIR) dyes).[1,62] The optical absorbance window between 600 to 1000 nm allows for little absorbance and optimal transparency (from water, lipids, and biological chromophores such as hemoglobin), which increases imaging depth while also reducing light scattering and autofluorescence.[63] While whole body optical imaging is not yet practical for human subjects, optical imaging has been reported for image guided surgery, along with lymph node mapping, and solitary tumor detection and monitoring.[64] Fluorophores currently approved by the FDA for clinical applications include fluorescein and indocyanine green, which are used as ophthalmologic agents to obtain retinal angiograms.[62] Optical imaging is more commonly used in preclinical studies, where the limited depth of penetration is less of an issue (Figure 20).

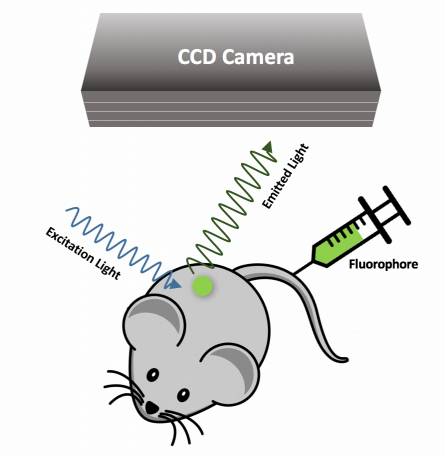

Figure 20: Schematic for preclinical optical imaging using an exogenous fluorophore. [1]

For *in vivo* applications, there are a number of desired features for an optical probe. Preferably, the excitation and emission wavelength are in the range of 650-900 nm, to allow for optimal tissue penetration and to minimize the influence of tissue

autofluorescence. Secondly, the brightness of the probe is an important factor as it influences the depth of penetration and the maximum achievable signal-to-background ratios. The brightness depends on the quantum yield (photons emitted/photons absorbed), and the higher the yield, the less excitation light is needed; reducing the amount of tissue heating and damage that can occur, which is particularly important for near-infrared probes. The stability of the probe *in vivo* must also be considered, especially if a longitudinal study is required, as most fluorophores decompose and/or lose fluorescent activity over the span of several days. Finally, optimal pharmacokinetics are important, as the addition of a large fluorophore to a targeting molecule may alter the distribution *in vivo*, leading to accumulation in non-target tissues.[62]

Targeting fluorophores suffer from many of the same challenges as radionuclide containing prosthetic groups (non-target uptake, poor signal-to-background ratios, etc.). To address the impact of fluorophores on targeting molecules, the use of pretargeting and bioorthogonal chemistry have been explored. Here, a targeting vector functionalized with TCO is injected and allowed adequate time to circulate, accumulate at the target site and clear from non-target tissues and fluids. Afterwards, a fluorescent tetrazine is injected, where it undergoes the IEDDA cycloaddition with TCO, localizing the signaling agent to the site of interest.

Turn-on type luminescent probes have been reported, where the emission is quenched by an appended tetrazine. Reactions with various dienophiles (such as TCO and cyclopropane) "turn-on" the fluorescence, thereby minimizing background signals. Devaraj *et al*. in 2010 demonstrated this with various tetrazine-modified fluorophores including coumarin, BODIPY and Oregon Green, where they reported a 3.3-fold to 20.6-

fold increase in fluorescence when the associated tetrazines derivatives were combined with TCO. Live cell imaging of microtubules using a TCO-taxol derivative with a tetrazine-BODIPY probe was reported using this approach, demonstrating the potential of using bioorthogonal chemical probes for optical imaging.[65] Wu *et al*. also reported fluorescein, tetramethylrhodamine and BODIPY functionalized alkenyl-tetrazines, which had a 400-fold, 76-fold and 200-fold turn-on in fluorescence intensity respectively when ligated with a TCO derivative.[66]

Optical imaging of A33 antigens on LS174T human carcinoma cells was demonstrated using a pretargeted approach with TCO-derived monoclonal antibodies. Cells without TCO incubation had negligible background staining with a tetrazine-BODIPY derivative, while cells labeled with the TCO-antibody conjugate showed highly fluorogenic regions of antigen expression.[66] This work has been extended to imaging cellular organelles such as the Golgi apparatus using a silicon-rhodamine tetrazine and a ceramide-TCO derivative for super-resolution microscopy. The bioorthogonal approach allowed for better visualization of dynamic processes in live cells without extensive photobleaching seen in conventional fluorescent imaging methods.[67] Lastly, Agarwal *et al*. reported in 2015 the fluorescence imaging of zebrafish glycoproteins. This was accomplished in live embryos using a cyclooctyne-sialic acid derivative and an Oregon Green tetrazine derivative. The metabolic incorporation of the acid allowed for imaging of sialylated glycoconjugates during embryonic development.[68]

While the utility of TCO-tetrazine chemistry for targeting fluorophores has been demonstrated, there are limited examples that employ tetrazine-NIR dyes. Some examples include a silicon-rhodamine tetrazine that were used to image *E. coli* cells

genetically encoded with *trans*-cyclooctene lysine amino acids; a VivoTag680-tetrazine that was ligated with Cetuximab-norbornene to image A549 lung cancer cells; and various pentamethine-core based tetrazines (which varied in charge and lipophilicity) to image TCO-modified B16F10 murine melanoma cells and assess their pharmacokinetic properties *in vivo*.[69–71] As previously mentioned, the advantage of using NIR dyes is that they have attractive photophysical properties and their clinical utility for surgical guidance has been well demonstrated.[25] However, there is a lack of general, accessible chemistry to allow for preparing tetrazine-derived NIR dyes, which can be used for various imaging applications.

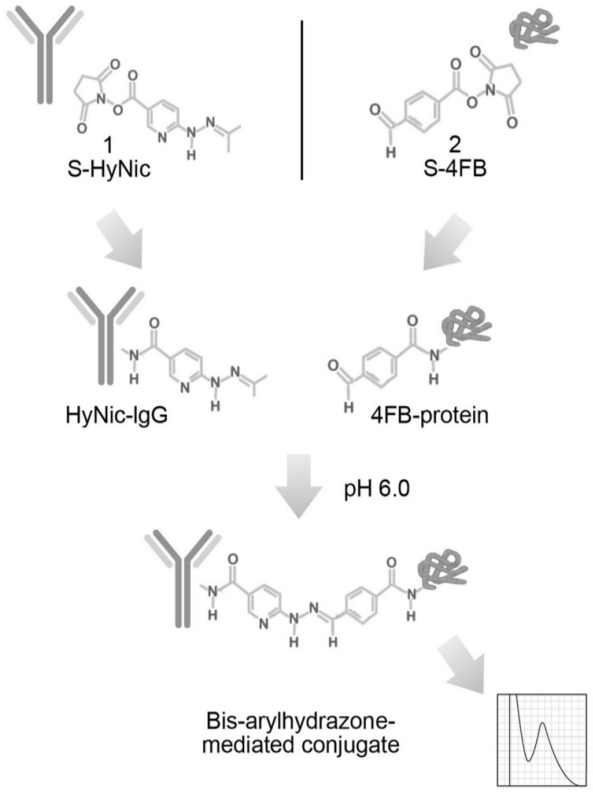

Figure 21: Schematic for creating probes for optical imaging using HYNIC and two convergent syntheses. In this example an antibody conjugated with HYNIC and protein functionalized with an aromatic aldehyde are ligated together via a biasrylhydrazone linkage[74]

3.2 Objectives

As a complement to the ^{99m}Tc probes reported in Chapter 2, a parallel goal was to develop fluorescent probes using the same TzHYNIC core. To accomplish this, the exploitation of the highly efficient coupling of hydrazines and aromatic aldehydes was performed. Hydrazone ligations are fast, selective, and proceed under mild reaction conditions, allowing for preparation of fluorophore conjugates.[72] The ligation is stoichiometrically efficient, avoiding the need to use a large excess of one reactant and is reported to proceed at concentrations as low as 10 μM. The use of aniline as a

nucleophilic catalyst increases the reaction rates, where ligations have been reported to be complete in a few hours at room temperature, making this chemistry attractive for time-sensitive biological applications.[72,73] This conjugation chemistry can be applied to a variety of systems, including antibodies, small proteins, peptides and oligonucleotides. [74]

3.3 Synthesis of Fluorescent Probes

The approach to synthesizing fluorescent probes involved utilizing TzHYNIC **5** reported in Chapter 2 and developing the means to couple it to fluorescent aldehydes. This required convergent synthesis of two moieties; the HYNIC core and the aldehyde functionalized fluorophore. The hydrazine **5**, which was generated by treatment of **4** with TFA to remove the Boc-protecting group, was found to decompose if not used immediately after synthesis, even when stored at low temperatures. An alternative protecting group for HYNIC was therefore explored. The goal was to be able to form the hydrazine under mild conditions in conjunction with ligating it to the desired aldehyde. HYNIC-hydrazones are known to be stable, however the free hydrazines can be liberated in aqueous solution. The 'pseudo-protecting group' does not need to be removed prior to conjugation, as the hydrazone exists in equilibrium with the free hydrazine group under conditions that do not degrade aldehydes.[74]

Unfortunately, the synthesis of TzHYNIC-hydrazone **20** (Scheme 7) was problematic. Multiple solvent and substrate screens were undertaken, using various combinations of HYNIC cores and tetrazine derivatives. Initially, the synthesis of NHS-HYNIC-hydrazone (analogous to NHS-HYNIC-Boc) was completed and then coupled to the commercially available benzylamino tetrazine. Solubility and reactivity issues prevented the amine coupling reaction from proceeding, and while the product was

visible by TLC and MS, isolating **20** was not achieved. Reactions using the free base of the tetrazine (which is typically purchased as the HCl salt) with the HYNIC-hydrazone using various coupling agents also had limited success. It was eventually determined that the most straightforward route to **20** was to synthesize TzHYNIC-Boc **4** and deprotect the compound in a mixture of TFA, DCM and acetone.[75] This resulted in the formation of the desired hydrazone in a quantitative yield. The ^{1}H NMR of **20** was similar to that of the precursor **4**, however the peak corresponding to the Boc-group was no longer observed, and 2 singlets corresponding to the methyl protons of the hydrazone protecting group were seen at 2.08 and 1.96 ppm. HRMS was also used to confirm the identity of the compound, where the observed m/z of 363.1674 corresponded to the calculated value of 363.1676, indicating that **20** was synthesized.

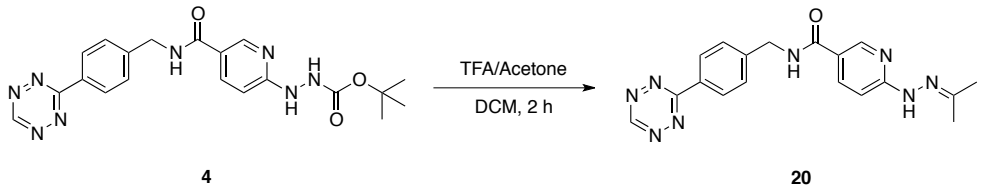

4 20

Scheme 7: Synthesis of TzHYNIC-Hydrazone **20**

In tandem with the preparation of **20**, the functionalization of a commercially available fluorescent dye as a model reagent was undertaken. Initial attempts involved the use of commercially available dansylcadaverine (a blue-green dye; excitation 335 nm/emission 518 nm). This product was combined with N-succinimidyl-4-formylbenzamide (S-4FB) (Scheme 8) and the product isolated via column chromatography as a pale yellow oil. However, **21** was not stable and shortly decomposed when stored in the freezer, and consequently the focus shifted to an aldehyde derivative of a near-IR dye.

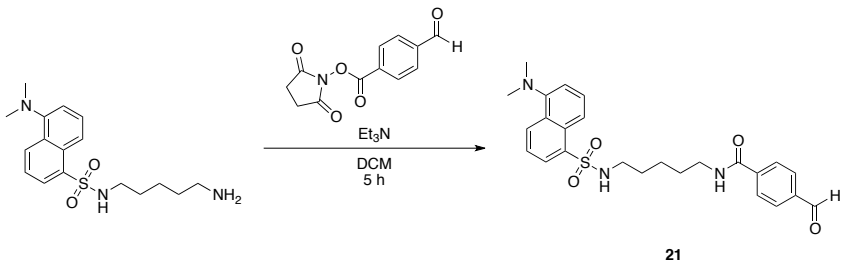

Scheme 8: Attempted synthesis of dansylcadaverine-4FB **21**

Recently, our group reported a method to functionalize the near-IR dye IR783, with an aromatic aldehyde (Scheme 9).[76] This was achieved by functionalizing IR783, which is commercially available, through a Suzuki coupling using p-formylphenylboronic acid to afford IR783-BA (synthesized, isolated and characterized by Samantha Slikboer). This provided access to a near-IR dye with an aromatic aldehyde that could be coupled to **20** to form IR783-TzHYNIC **22**.

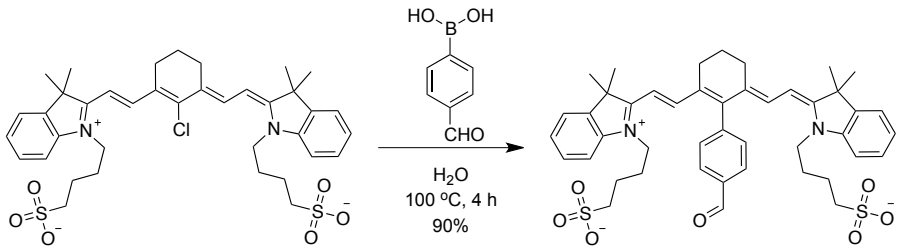

Scheme 9: Synthesis of IR783-Benzaldehyde (IR783-BA) developed and provided by Samantha Slikboer

Compounds **20** and IR783-BA were initially reacted in methanol and water with a catalytic amount of aniline, which resulted in the desired product **22** (Scheme 10) albeit in low (9%) yield. Various parameters were explored to improve the yield including longer reaction times, elevated temperatures and varying the pH.[72] Ultimately, the most successful conditions involved running the reaction with an excess of aniline in ethanol at room temperature, where the product was purified using polar reversed phase HPLC column (Synergi 4 μM Polar-RP 80 Å LC Column 250 x 10 mm) to afford **23** as a green oil in a 35% yield (Scheme 10, Figure 22). The ^{1}H NMR showed the presence of the

tetrazine aromatic proton at 10.33 ppm, multiple aromatic protons associated with the cyanine-dye, benzyl tetrazine and pyridyl-groups, along with peaks associated with the sulfonate chains centered around 1.85 ppm. Along with observing the corresponding m/z for 1099.4290 in HRMS (calculated m/z of 1099.4328), it was concluded that **22** was successfully synthesized.

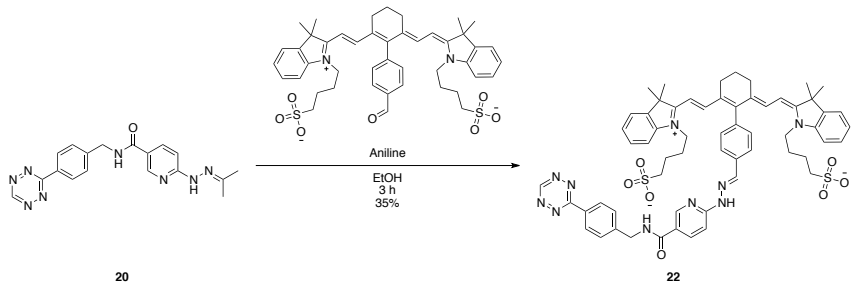

Scheme 10: Synthesis of IR783-TzHYNIC **22**

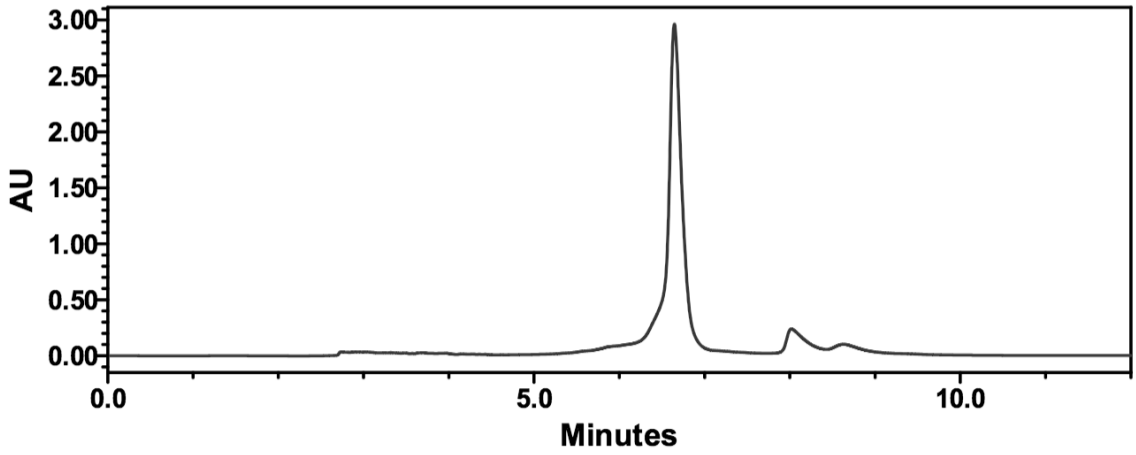

Figure 22: UV-HPLC chromatogram of the reaction mix of **22** using Method C on a Waters 1525 Binary HPLC with a 2998 UV/Vis (λ = 350 nm) detector with Empower 2 software. A semi-preparative Synergi 4 µM Polar-RP 80 Å LC Column 250 x 10 mm was used, where Method C used HPLC grade water with 0.1% TFA (solvent A) and acetonitrile with 0.1% TFA (solvent B) as eluents using a gradient mobile phase from 10% to 90% A from 0-20 min, followed by 90% to 10%A from 20-21 min at a flow rate of 4 ml/min.

The absorbance and emission of **22** in 10% EtOH/H_2O at 50 µM was recorded at room temperature. The maximum absorbance was at 764 nm, with the associated emission maxima at 786 nm (Figure 23). The absorbance and emission data were similar

to IR783 (abs. 778, ex. 800 nm) and IR783-BA (abs. 762, ex. 798 nm) in the same solvent and concentration (50 μM, 10% EtOH/H_2O), demonstrating that the addition of the tetrazine did not drastically change the near-IR photophysical properties of the parent dye.

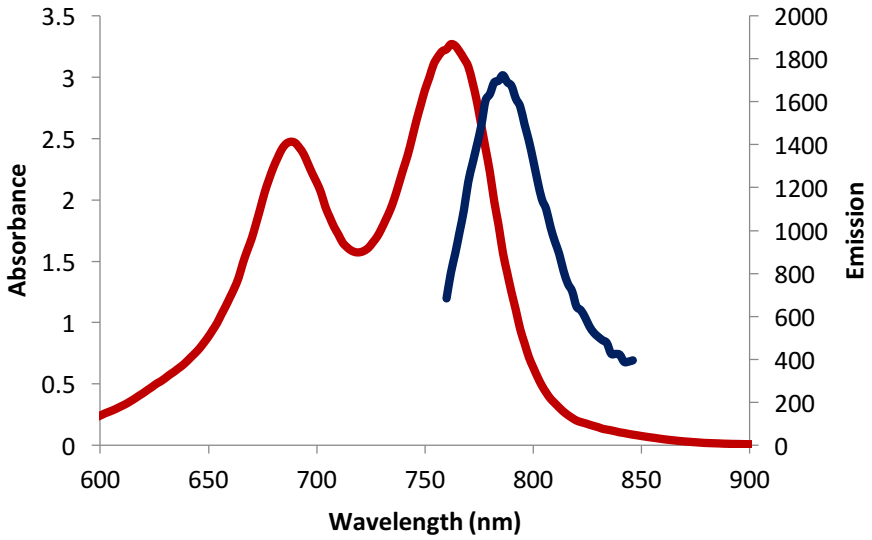

Figure 23: Absorbance (red) and emission (blue) of **23** measured at room temperature in 10% EtOH/H_2O (50μM) using a TECAN 96-well plate reader (study performed by Samantha Slikboer)

The stability of the hydrazone bond was assessed in PBS at 37˚C over 48h (Figure 24). According to HPLC analysis of the solution (2 mg/ml, 910 μM) at select time points, **23** remained stable and showed no sign of hydrolysis to **20** and IR783-BA. It should be noted that the chromatographic method was not ideal and requires further optimization to minimize peak broadening. The reactivity of **22** towards TCO was also assessed *in vitro* by combining the tetrazine with TCO-vancomycin (Figure 25). The dye in 10%EtOH/PBS (100 μL) was incubated with an excess of TCO-vancomycin for 10 min, whereafter the solution was subjected to HPLC analysis. The rapid disappearance of the

peak at 7 and the formation of a new peak in the solvent front suggested successful coupling occurred.

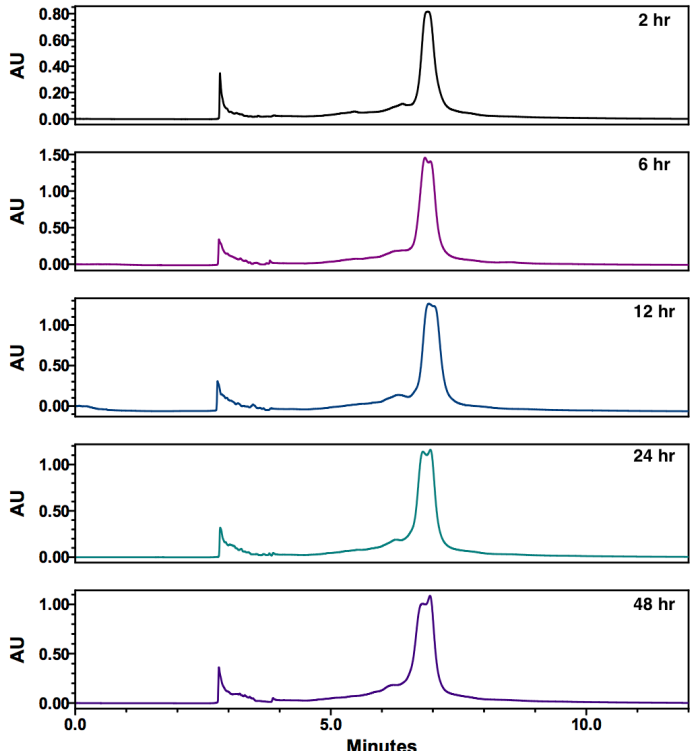

Figure 24: Stability of **22** in 10% EtOH/PBS at 37˚C as determined by UV HPLC using Method C on a Waters 1525 Binary HPLC with a 2998 UV/Vis (λ = 350 nm) detector with Empower 2 software. A semi-preparative Synergi 4 µM Polar-RP 80 Å LC Column 250 x 10 mm was used, where Method C used HPLC grade water with 0.1% TFA (solvent A) and acetonitrile with 0.1% TFA (solvent B) as eluents using a gradient mobile phase from 10% to 90% A from 0-20 min, followed by 90% to 10%A from 20-21 min at a flow rate of 4 ml/min.

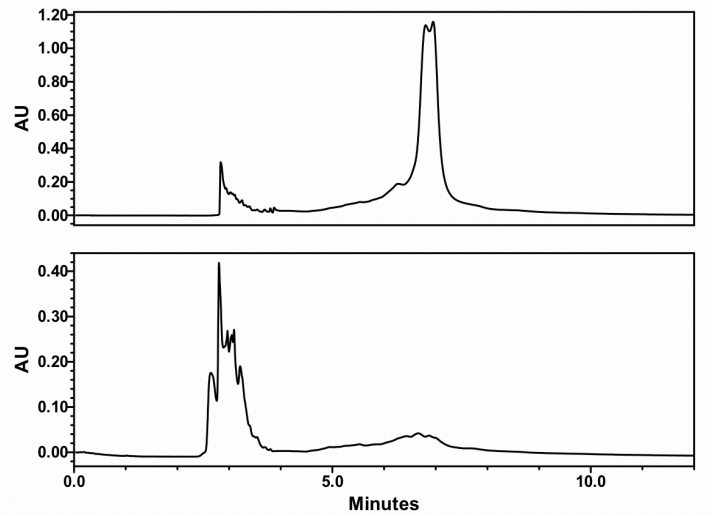

Figure 25: UV-HPLC traces of **22** before (top) and after (bottom) incubation with a molar excess of TCO-vancomycin for 10 min (bottom) using Method C on a Waters 1525 Binary HPLC with a 2998 UV/Vis (λ = 350 nm) detector with Empower 2 software. A semi-preparative Synergi 4 µM Polar-RP 80 Å LC Column 250 x 10 mm was used, where Method C used HPLC grade water with 0.1% TFA (solvent A) and acetonitrile with 0.1% TFA (solvent B) as eluents using a gradient mobile phase from 10% to 90% A from 0-20 min, followed by 90% to 10%A from 20-21 min at a flow rate of 4 ml/min

Building on this approach, the same reactions were performed using $TzPEG_{11}HYNIC$ **11** in place of TzHYNIC **5**. Deprotection of **10** with TFA, DCM and acetone afforded the hydrazone derivative **23** in a quantitative yield. The signals associated with the Boc-group seen in the ^{1}H NMR of **10** were no longer observed, leaving 2 sharp singlets that integrated to 3H, each at 2.18 and 2.12 ppm, which were associated with the desired hydrazone. The product was combined with IR783-BA overnight in ethanol containing excess aniline and the product (**24**) was isolated via reverse phase HPLC using a polar RP column as a green oil in a 21% yield (Scheme 11, Figure 26). HPLC confirmed the presence of a single product, and HRMS showed the expected m/z value of 1740.8145 (calculated m/z/ of 1740.8189). Insufficient material was produced to collect NMR of adequate quality.

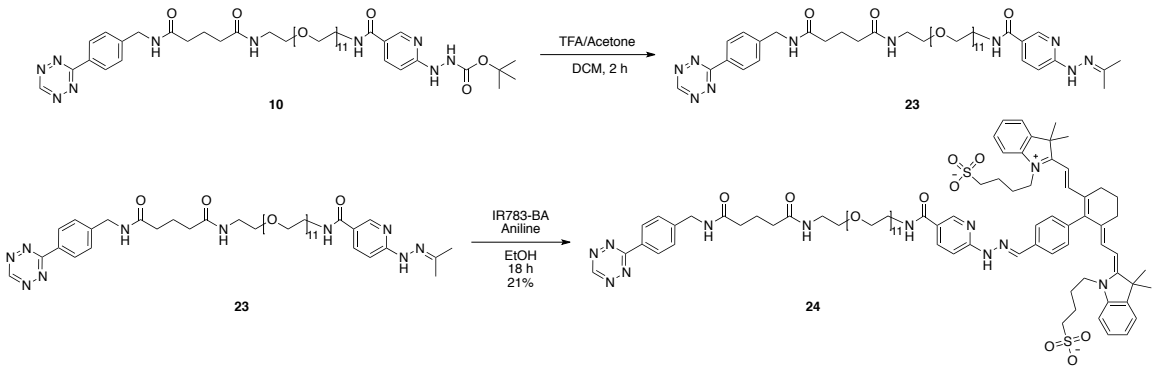

Scheme 11: Synthesis of $TzPEG_{11}HYNIC$-hydrazone **23** and IR783-$TzPEG_{11}HYNIC$ **24**

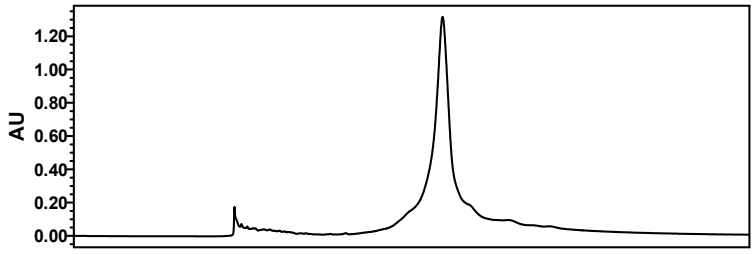

Figure 26: UV-HPLC trace of IR783-$TzPEG_{11}HYNIC$ **24** using Method C on a Waters 1525 Binary HPLC with a 2998 UV/Vis (λ = 350 nm) detector with Empower 2 software. A semi-preparative Synergi 4 μM Polar-RP 80 Å LC Column 250 x 10 mm was used, where Method C used HPLC grade water with 0.1% TFA (solvent A) and acetonitrile with 0.1% TFA (solvent B) as eluents using a gradient mobile phase from 10% to 90% A from 0-20 min, followed by 90% to 10%A from 20-21 min at a flow rate of 4 ml/min

The absorbance and emission of **24** was measured in 10% EtOH/PBS at 50 μM at room temperature, where the maximum absorbance observed was at 764 nm, and the associated emission maxima was at 788 nm (Figure 27). The two absorbance peaks (690 and 764 nm) could be due to solvent used, protonation of the species, or individual vibrational energy states.[61] While the absorbance at 690 nm was more intense, it was decided to use the absorbance value closest to the near-infrared region and that of which closely resembled the other IR783-derivitives for the following *in vitro* bacterial assays. The stability of the hydrazone bond was assessed in PBS at 37˚C over 48h, using the same procedure for **22**. HPLC analysis of the solution (2 mg/ml, 575 μM) at select time points, demonstrated that **24** remained stable and showed no sign of hydrolysis to

precursors **23** and IR783-BA (Figure 28). Similarly to that of **22**, the peak was broad, which could potentially be attributed to the negative charges of the two sulphonate groups and the overall low concentration of the compound in solution. Further optimization of the HPLC method is needed. In comparison, the stability of **22** was superior to **24**, in that at 48 h compound **22** remained in tact whereas the latter showed multiple peaks as early as 12 hours.

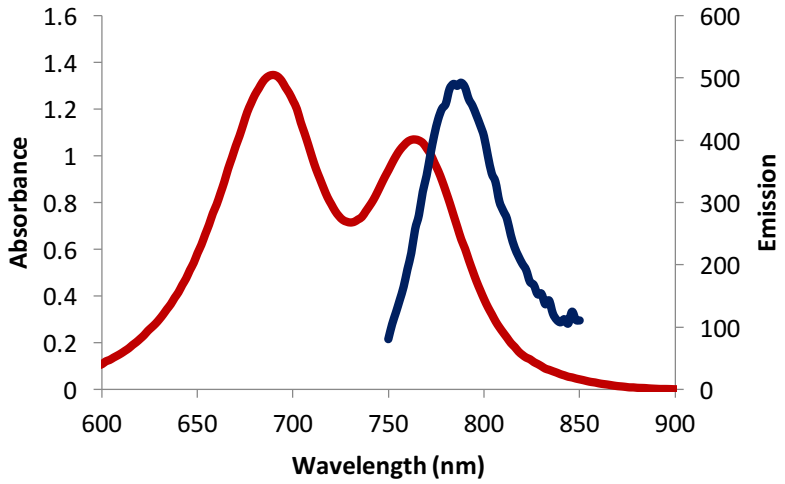

Figure 27: Absorbance (red) and emission (blue) of **24** measured at room temperature in 10% EtOH/PBS (50μM) using a TECAN 96-well plate reader

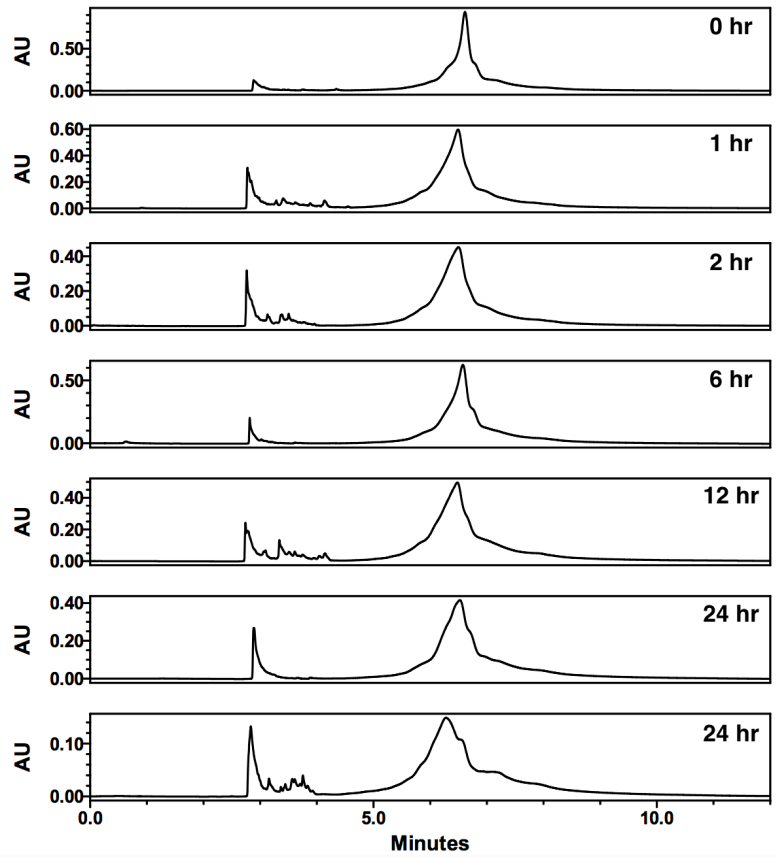

Figure 28: Stability of **24** in 10%EtOH/PBS at 37˚C as determined by UV HPLC using Method C on a Waters 1525 Binary HPLC with a 2998 UV/Vis (λ = 350 nm) detector with Empower 2 software. A semi-preparative Synergi 4 µM Polar-RP 80 Å LC Column 250 x 10 mm was used, where Method C used HPLC grade water with 0.1% TFA (solvent A) and acetonitrile with 0.1% TFA (solvent B) as eluents using a gradient mobile phase from 10% to 90% A from 0-20 min, followed by 90% to 10%A from 20-21 min at a flow rate of 4 ml/min.

The reactivity of **24** towards TCO was also assessed by mass spectrometry (Figure 29). TCO-OH was used in place of TCO-vancomycin because of its lower molecular weight and greater likelihood of ionizing once conjugated. An excess of TCO-OH was added to **24** in methanol. After a 10 minute incubation, the electrospray spectrum (negative ion mode) showed a peak corresponding to the conjugated complex (Figure 29, m/z of 1838.3).

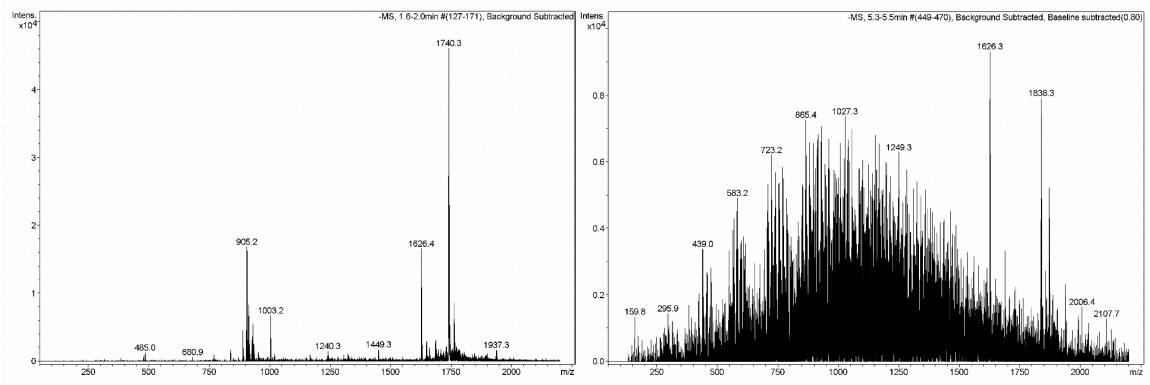

Figure 29: ES^- mass spectra of **24** (left) showing the $[M+H]^-$ ion (m/z = 1740) and ES^- mass spectra (right) following the addition of TCO-OH to a solution of **24** ($[M+H]^-$, m/z = 1838)

3.4 *In vitro* bacterial binding assay

With compounds **22** and **24** in hand, their utility as fluorophores for *in vitro* studies were evaluated. The focus was to assess the extent of binding of the tetrazines to *Staphylococcus aureus* treated with TCO-vancomycin (experiments performed in collaboration with Nancy Janzen). Figure 30 shows the general scheme of the bacterial assay. *S. aureus* bacteria (ATCC, 25923, approximately $5x10^8$ CFU/mL) were incubated with 20 μM TCO-vancomycin for 30 min at room temperature. The bacteria were washed with PBS-F (phosphate buffered saline supplemented with fetal bovine serum) to remove excess unbound TCO-vancomycin, and subsequently incubated with **22** or **24** for an additional 30 minutes at room temperature. A vancomycin blocking study was also completed to determine binding specificity, which involved the use of a mixture containing 20 μM TCO-vancomycin and 200 μM vancomycin. An additional control was run where the bacteria were treated with only **22** or **24** and no TCO-vancomycin, to account for non-specific binding of the tetrazines to the bacteria.

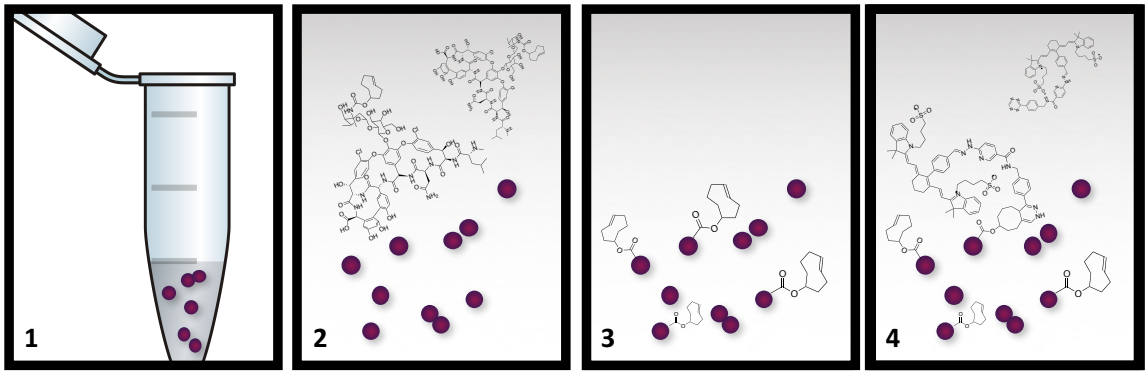

Figure 30: Schematic of an *in vitro* bacterial cell assay (**1**) using TCO-Vancomycin and IR783-TzHYNIC **22**. In **2**, *S. aureus* cells are incubated with TCO-vancomycin for 30 minutes, after which excess TCO-vancomycin is washed off the cells. Cells which displayed uptake of TCO-vancomycin will have TCO-residues available to undergo ligation with tetrazines (**3**). Cells are then incubated with **22** for 30 minutes, allowing to time to undergo ligation and then are subsequently washed and subjected to a plate reader to quantify fluorescence using a TECAN reader (**4**).

Initially, various amounts of **22** were used to determine the optimal loading concentration for the bacterial binding assay. The concentration must be high enough to elicit a signal, but low enough to not promote quenching and non-linear responses. Figure 31 shows the relative fluorescent intensity (expressed as %RFU) at 50 nM, 500 nM and 5 μM concentrations (calculated as 100 x $(I_{target}\text{-}I_{non\text{-}target})/I_{non\text{-}target}$ where I is intensity values of the sample).[47] The 50 nM concentration was determined to have had the best difference between the targeted and blocked samples (16.2-fold increase).

While the *in vitro* studies were successful, corresponding fluorescence microscopy images could not be generated at the 50 nM concentration. Images at 500 nM were obtained, however only aggregates of *S. aureus* were observed under these conditions (Figure 32). At 5 μM, both the targeted and non-target images showed fluorescent cells. A second experiment was performed using 1 μM **22** for imaging purposes, however the dye was prone to photobleaching/quenching. While high absorption values were recorded using a TECAN plate reader, optimization of imaging

concentrations still needs to be investigated. IR775 (a similar dye without the solubilizing sulphonate chains) was reported to exhibit quenching at concentrations >1 μM in solution, indicating that evaluations should be carried out in the current concentration range.[77]

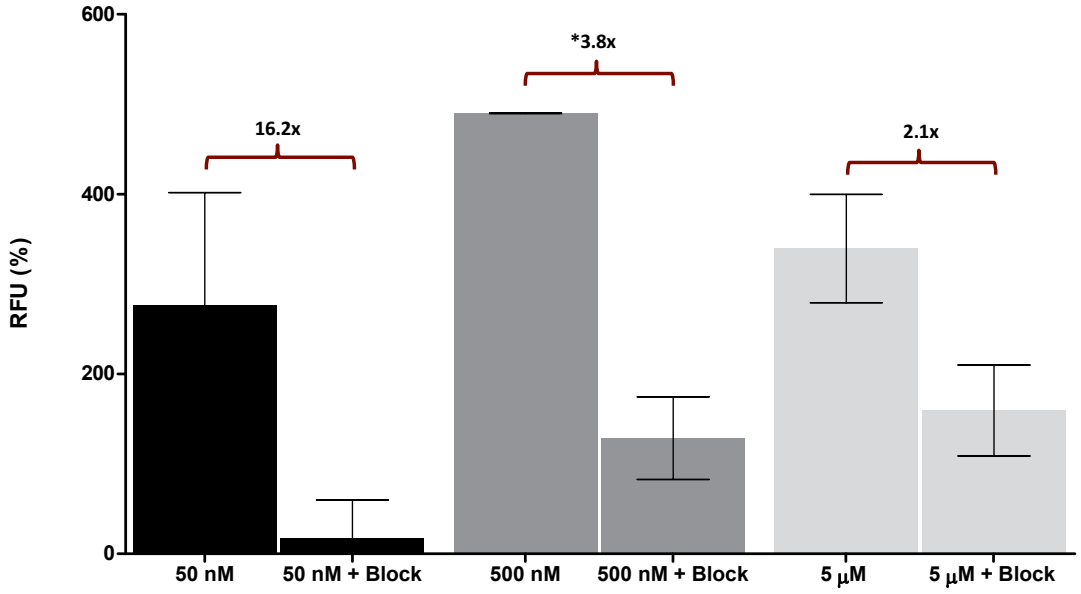

Figure 31: IR783-TzHYNIC **22** binding to *S. aureus* treated with TCO-vancomycin. Cells were incubated with 20 μM TCO-vancomycin, washed, and then treated with 50 nM, 500 nM or 5 μM of **22**. Blocking solution contained 20 μM TCO-vancomycin and 200 μM vancomycin. %RFU was calculated as 100 x $(I_{target}-I_{non\text{-}target})/I_{non\text{-}target}$ where I is the intensity values of the samples as read by a TECAN plate reader. * indicates significant difference using a Student's t-test where $p < 0.5$.

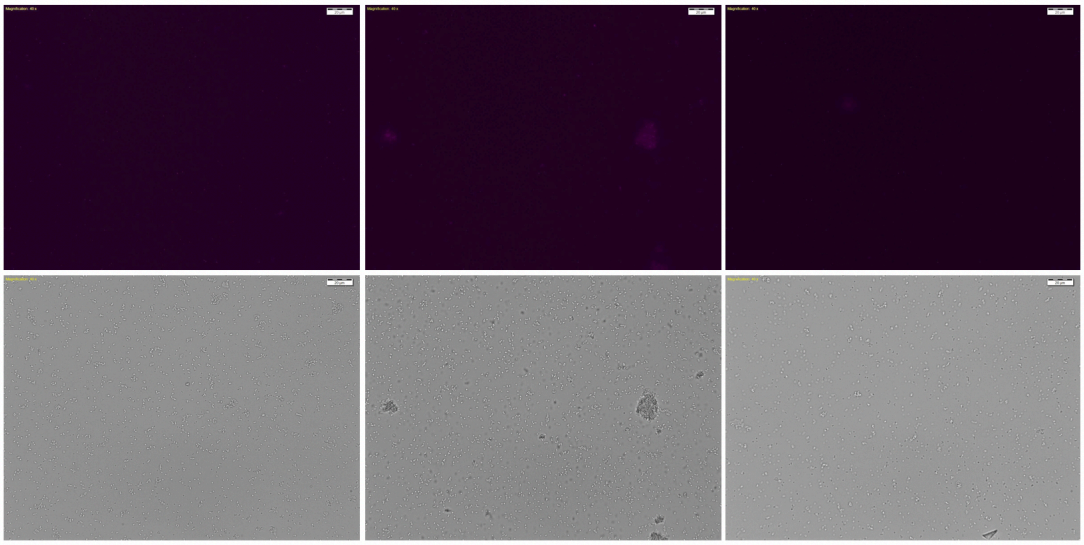

Figure 32: Fluorescent microscopy images (top) and the corresponding bright field images (bottom) of *S. aureus* incubated with 500 nM of **22** at 40x magnification. Left images correspond to the non-targeted **22** (without TCO-vancomycin), middle images are the pretargeted images using 20 µM TCO-vancomycin and the right images are cells incubated with 20µM TCO-vancomycin and 200 µM of the vancomycin block.

The binding of compound **24** (IR783-TzPEG$_{11}$HYNIC) was also tested *in vitro* using the same assay and a tetrazine concentration of 500 nM. As seen in Figure 33, the relative fluorescent intensity of the targeted to the vancomycin block was 8.6-fold higher (compared to 3.8-fold with **22** at the same concentration (Figure 31). The robustness of the assay was validated by repeating the assay a total of 5 times, along with samples done in duplicate and triplicate. While 100% blocking was not achieved, this is likely due to the fact that the target is not saturable and that higher vancomycin concentrations cause cell death. Nevertheless, it was demonstrated that the new fluorescent-Tz probes **22** and **24** bind to TCO-vancomycin, which in turn binds specifically and competitively, where the target is reported to be the D-Ala-D-Ala residues found in the cell wall.[47]

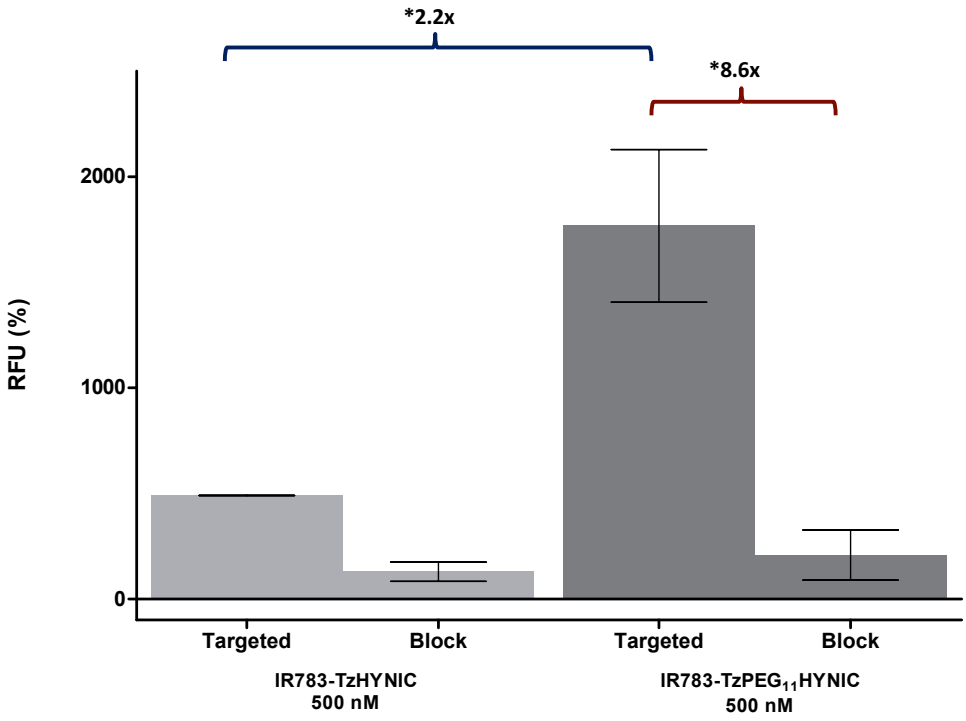

Figure 33: A plot of relative fluorescent intensity units (%RFU) of IR783-TzPEG$_{11}$HYNIC **24** binding to *S. aureus* treated with TCO-vancomycin, along with a comparison to IR783-TzHYNIC **22**. %RFU was calculated as 100 x $(I_{target}-I_{non\text{-}target})/I_{non\text{-}target}$ where I is the intensity values of the samples as read by a TECAN plate reader. * indicates significant difference using a Student's t-test where $p < 0.5$

3.5 Conclusions

By exploiting hydrazone chemistry, a new class of tetrazine derived fluorescent probes were synthesized for molecular imaging applications that employ pretargeting and bioorthogonal chemistry. Derivatizing a commercially available near-IR dye and coupling the corresponding aldehyde with HYNIC derived tetrazines resulted in the synthesis of **22** and **24**. These are fluorescent analogs of the ^{99m}Tc-HYNIC derivatives **6** and **12** reported in Chapter 2. The compounds were tested *in vitro* with *S. aureus* and demonstrated specific binding when used with TCO-vancomycin. Previously published work on **6** reported binding of the ^{99m}Tc-probe to *S. aureus* bacteria (~40% at 6h),

however direct comparison of the nuclear and optical probes is difficult.[42] The most effective method to compare binding would be through flow cytometry/fluorescence-activated cell sorting (FACS), followed by radioactive counting. Between the compounds reported here, **24** showed a 2.2-fold increase in fluorescence signal when compared to **22** (at the same concentration) and is a promising new probe for optical imaging applications.

3.5.1 Future Work

The immediate future work should focus on optimizing the reaction conditions between IR783-BA and **20/23** to achieve better yields of **22/24**. In addition, determining the optimal concentration to obtain images using fluorescent microscopy is required. Following this, *in vivo* studies should be explored where the biodistribution of **22** and **24** can be assessed using various TCO-derivatives. These studies would validate the probes for both fluorescence microscopy and for *in vivo* applications.

The hydrazine chemistry and HYNIC tetrazines developed here can be further exploited by changing the fluorescent moiety. This can include the use of a broader array of organic dyes and inorganic quantum dots, all using the same TzHYNIC core.[78,79] By building a library of TzHYNIC optical probes, it would be possible to select the most appropriate derivative for specific applications. Lastly, the optical probe could also be administered with the corresponding ^{99m}Tc complex and multimodal imaging used to detect TCO-tagged biomarkers. As an example, after using the radionuclide to identify and localize tumors using tomographic wholebody imaging, intraoperative imaging/resection can be completed to delineate the margins for tumor resection using a single TCO-derivitive.[25]

4 Summary and Final Thoughts

This thesis focused on investigating, synthesizing, and evaluating nuclear and optical TzHYNIC probes for molecular imaging. The distribution of a previously reported radiolabelled TzHYNIC derivative was repeated, and it was determined that HPLC-purification was not required, thus facilitating the development of a kit-like method for producing a radiolabelled tetrazine. Furthermore, a more polar pegylated benzylamino tetrazine derivative was prepared, which had a decrease in non-target uptake in most organs compared to the previously reported construct. The investigation using the more reactive bispyridyl tetrazine was also undertaken, however the newly synthesized ligand could not be labelled with ^{99m}Tc. Future work for the nuclear probes should entail the screening co-ligands in order to tune the pharmacokinetics for optimal target uptake using a variety of different TCO-biomolecule derivatives.

Work on the development of fluorescent probes for optical imaging was also undertaken. The investigation and synthesis of TzHYNIC-hydrazone derivatives was completed, along with the conjugation to an aromatic aldehyde functionalized near-IR dye. The reactivity of the resulting near-IR compounds were tested *in vitro* using TCO-vancomycin with *S. aureus*. The assays were successful in demonstrating specific binding to the Gram-positive bacteria, with an overall increase in fluorescent signal compared to various controls. The *in vitro* assays validated the chemistry, and future work will entail the evaluation of the probes *in vivo* using relevant animal models for optical imaging applications.

By developing a platform that can incorporate complementary pairs of radionuclides and fluorophores, imaging of biomarkers using multimodal imaging

technologies can be accomplished. The pretargeting and bioorthogonal chemical approach used should allow for higher target-to-background signals, with less dose burden (for radionuclides), for a system that employs the most widely used nuclear isotope and a highly effective optical dye platform that absorbs and emits in the near-IR. The platform reported here was used to create SPECT and optical imaging agents. However, the TzHYNIC core can be used more broadly. Future work should include the incorporation of ^{18}F prosthetic groups for PET applications, and ^{188}Re for potential therapeutic treatments.

5 Experimental

General

Unless otherwise stated, all reagents were received from Sigma-Aldrich without further purification. Solvents were purchased from Caledon and all anhydrous solvents were dried using the Pure Solv solvent system. ((4-Tetrazine-3-yl)phenyl)methanamine hydrochloride (Tetrazine) was obtained from Conju-Probe LLC., NH_2-CH_2-CH_2PEG_{11}-NHBoc obtained from ChemPep Inc, TCO-NHS obtained from Click Chemistry Tools LLC., and benzotriazol-1-yl-oxytripyrrolidinophosphonium hexafluorophosphate (PyBOP) was purchased from Chem-Impex International Inc. Unless otherwise stated, compound purification was done using silica gel 60 (particle size 0.040-0.063 mm) purchased from EMD chemicals.

^{1}H and ^{13}C NMR were recorded on Bruker AV600 MHz spectrometer at ambient temperature. Deuterated solvents were obtained from Cambridge Isotope Laboratories with the proton and carbon shifts reported in ppm relative to the residual solvent signals. High resolution mass spectra (HRMS) were provided by the McMaster Regional Centre for Mass Spectrometry using a Waters/Micromass Q-ToF Global Ultima spectrometer. $^{99m}TcO_4^-$ was obtained from a $^{99}Mo/^{99m}Tc$ generator (Lantheus Medical Imaging) in 0.9% saline.

High performance liquid chromatography (HPLC) of selected compounds were performed on a Varian Prostar 230 monitored with a Prostar 335 PDA detector or Waters 1525 Binary HPLC with a 2998 UV/Vis (λ = 254 nm) detector and Bioscan Glow count gamma detector with Empower 2 software. An analytical Gemini 5 μm NX-C18 110 Å LC Column 250 x 4.6 mm, semi-preparative Gemini 5 μm NX-C18 110 Å LC Column

250 x 10 mm or a semi-preparative Synergi 4 μM Polar-RP 80 Å LC Column 250 x 10 mm was used. Method A used HPLC grade water (solvent A) and acetonitrile (solvent B) as eluents using a gradient mobile phase from 95% 5% A over 30 minutes. Method B used HPLC grade water (solvent A) and acetonitrile (solvent B) as eluents using a gradient mobile phase from 95% to 40% A from 0-10 min, followed by 40% to 20 %A from 10-16 min, followed by 20% A to 95% from 16- 18 min. Method C used HPLC grade water with 0.1% TFA (solvent A) and acetonitrile with 0.1% TFA (solvent B) as eluents using a gradient mobile phase from 10% to 90% A from 0-20 min, followed by 90% to 10%A from 20-21 min at a flow rate of 4 ml/min. Method D used HPLC grade water containing 4 g/L ammonium formate and acetonitrile as eluents. The method had a flow water of 4 mL/min following a gradient mobile phase from 98% A to 85% A from 0–8 min, followed by 85% to 5% A from 8–12 min, ending with 5% A to 98% A from 12-16 min.

5.1 Synthesis of HYNIC Compounds

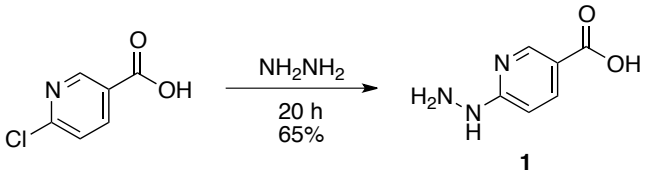

1

Scheme 12: Synthesis of HYNIC **1**

6-Hydrazinylnicotinic acid (HYNIC) 1: The procedure was adapted from Abrams *et al*. where 65% hydrazine monohydrate (23 ml, 456.0 mmol, 24 equiv.) was added to a 50 ml oven-dried round bottom flask containing 6-chloronicotinic acid (3.0 g, 19.04 mmol).[11] The reaction mixture was heated to reflux at 100˚C for 18 hours, thereafter it was concentrated under reduced pressure. The white solid was redissolved in

20 ml distilled water in an Erlenmeyer flask and then acidified to pH 5.5 using concentrated HCl while cooled on ice. The resulting white precipitate was collected by filtration and washed with cold ethanol and ether to afford a white fluffy solid **1** (1.90 g, 65%). ^{1}H NMR (600MHz, DMSO-d_6): δ 8.52 (d, 1H, J = 6 Hz), 8.26 (s, 1H), 7.86 (dd, 2H, J = 6, 6 Hz), 6.69 (d, 1H, J = 6 Hz), 3.17 (s, 1H).

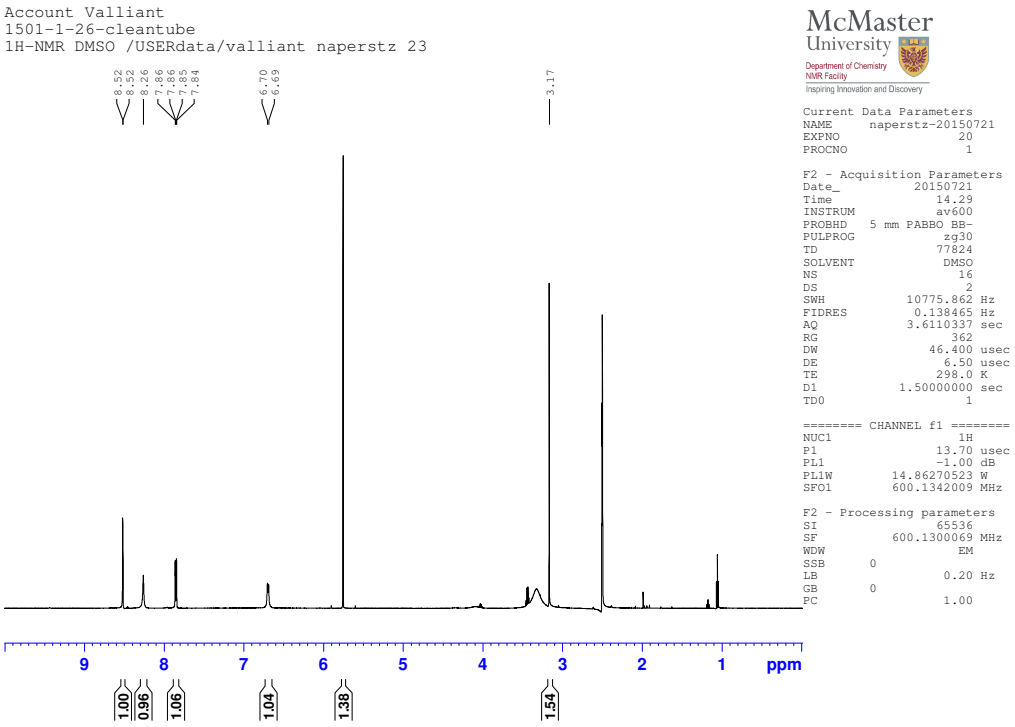

Figure 34: ^{1}H NMR (600 MHz, DMSO-d_6) of HYNIC **1**

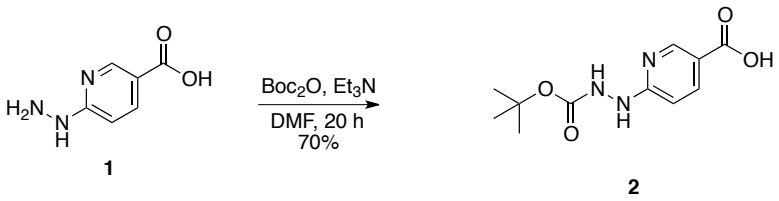

Scheme 13: Synthesis of Boc-HYNIC **2**

6-(2-(*tert*-Butoxycarbonyl)hydrazinyl)nicotinic acid (Boc-HYNIC) 2: A 25 ml oven-dried round bottom flask was charged with HYNIC **1** (1.90 g, 0.0124 mol), di-tert-butyl dicarbonate (2.90 ml, 0.0132 mol), anhydrous DMF (13 ml) and triethylamine (1.25 ml, 0.0124 mol). The reaction mixture was stirred under N_2 gas overnight (18 hours) at room temperature, and then concentrated under reduced pressure. The resulting solid was purified by column chromatography with 100% ethyl acetate, then concentrated *in vacuo* to obtain the final product **2** as an off-white powder (2.20 g, 70%). ^{1}H NMR (600 MHz, DMSO-d_6): δ 8.99 (s, 1H), 8.90 (s, 1H), 8.58 (d, 1H, J = 6 Hz), 7.96 (d, 1H, J = 12 Hz), 6.53 (d, 1H J = 12 Hz), 1.42 (s, 9H).

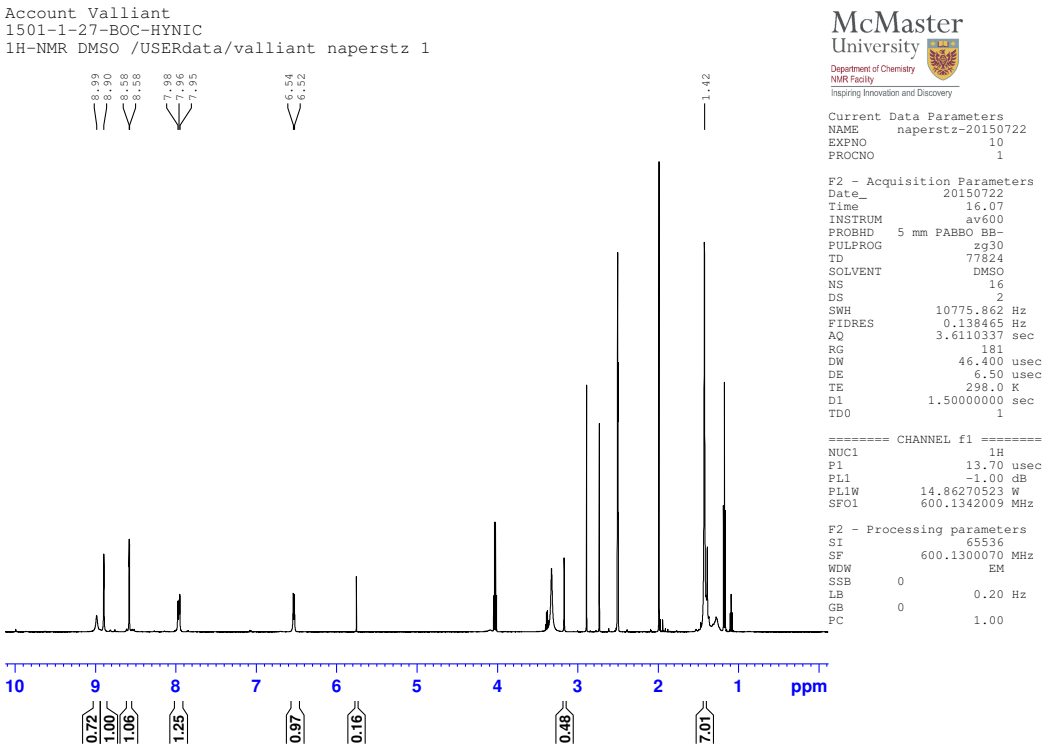

Figure 35: ^{1}H NMR (600 MHz, DMSO--d_6) of Boc-HYNIC **2**

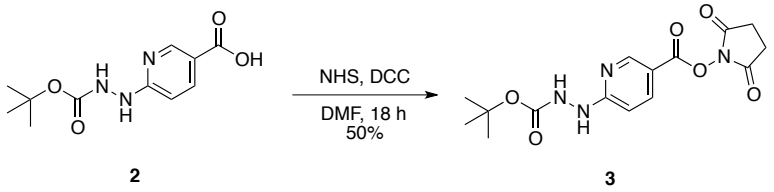

2 3

Scheme 14: Synthesis of Boc-HYNIC-NHS **3**

2,5-dioxopyrrolidin-1-yl 6-(2-(*tert*-butoxycarbonyl)hydrazinyl)nicotinate (Boc-HYNIC-NHS) 3: Boc-HYNIC **2** (500 mg, 1.97 mmol), *N*-Hydroxysuccinimide (272 mg, 2.36 mmol) and *N*,*N*'-Dicyclohexylcarbodiimide (DCC) (447 mg, 2.17 mmol) were added to a 25 ml round bottom flask and dissolved in anhydrous DMF (8 ml). The reaction mixture was stirred overnight (18 hours) at room temperature under N_2 gas. Upon completion (monitored by TLC), the reaction was filtered to remove dicyclohexyl urea and then concentrated under reduced pressure to obtain a brown oil. The oil was purified by column chromatography with 100% ethyl acetate, to obtain a colorless oil. The oil was recrystallized in DCM and concentrated to afford a white powder **3** (361 mg, 52%). ^{1}H NMR (600 MHz, CD_2Cl_2): δ 8.81 (s, 1H), 8.10 (d, 1H, J = 12 Hz), 7.98 (s, 1H), 7.38 (s, 1H), 6.73 (d, 1H, J = 12 Hz), 2.85 (s, 4H), 1.43 (s, 9H).

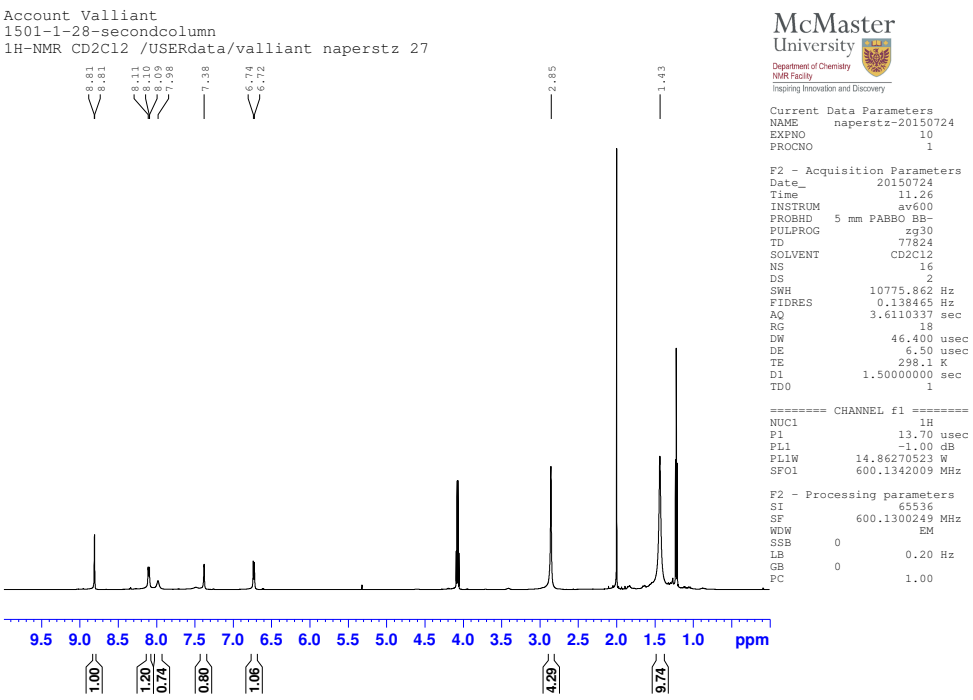

Figure 36: ^{1}H NMR (600 MHz, CD_2Cl_2) of Boc-HYNIC-NHS **3**

5.2 Synthesis of Benzylamino Tetrazine Compounds

Compounds **4** through **6** were synthesized and radiolabelled according to the procedures published by Vito *et al*.[42] In brief, **4** was synthesized through an amide-coupling reaction using benzylamino tetrazine and Boc-HYNIC **2** with PyBOP in a 72% yield; deprotected in a 1:2 v/v TFA/DCM solution to afford **5a/b**; and radiolabelled using TcO_4^-, stannous chloride and tricine to obtain **6** in a 28% RCY and 91% RCP.

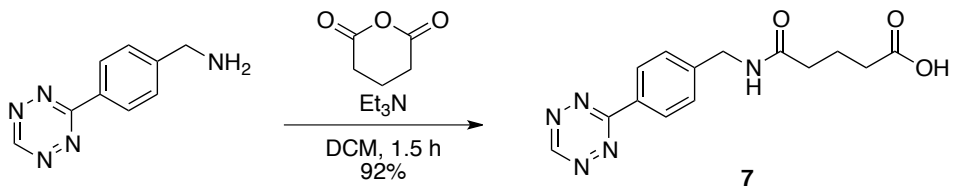

Scheme 15: Synthesis of TzCOOH

5-((4-(1,2,4,5-tetrazin-3-yl)benzyl)amino)-5-oxopentanoic acid (TzCOOH)

7: ((4-Tetrazine-3-yl)phenyl)methanamine hydrochloride (10 mg, 0.045 mmol) was dissolved in 2.5 ml DCM with triethylamine (13.6 µl, 0.134 mmol) and the mixture stirred for 5 min. Glutaric anhydride (5.1 mg, 0.045 mmol) was added and the reaction mixture stirred under N_2. After the reaction was deemed complete as determined by TLC (approximately 1.5 hours), the mixture was evaporated to dryness and resuspended in 6 ml distilled water. The resulting suspension was acidified to pH 3 with 0.1 M HCl and then extracted with ethyl acetate (4 x 10 ml). The organic layers were combined and washed with 15 ml brine, and dried over sodium sulfate. The organic layer was concentrated *in vacuo* to obtain **7** as a vivid pink powder (12 mg, 92%). ^{1}H NMR (600 MHz, CD_3OD): δ 10.34 (s, 1H), 8.57 (d, 2H, J = 6 Hz), 7.57 (d, 2H, J = 6 Hz), 4.52 (s, 2H), 2.38 (td, 4H, J = 6, 6 Hz), 1.97 (q, 2H, J = 6, 6, 18 Hz). ^{13}C NMR (150 MHz, CD_3OD): δ 176.9, 175.5, 159.2, 145.6, 132.3, 129.4, 43.8, 36.0, 34.1, 33.9, 22.3, 21.3. HRMS (ES^+) m/z calculated for $C_{14}H_{15}N_5O_3$ [M+H$^+$] 301.1267, found 301.1263.

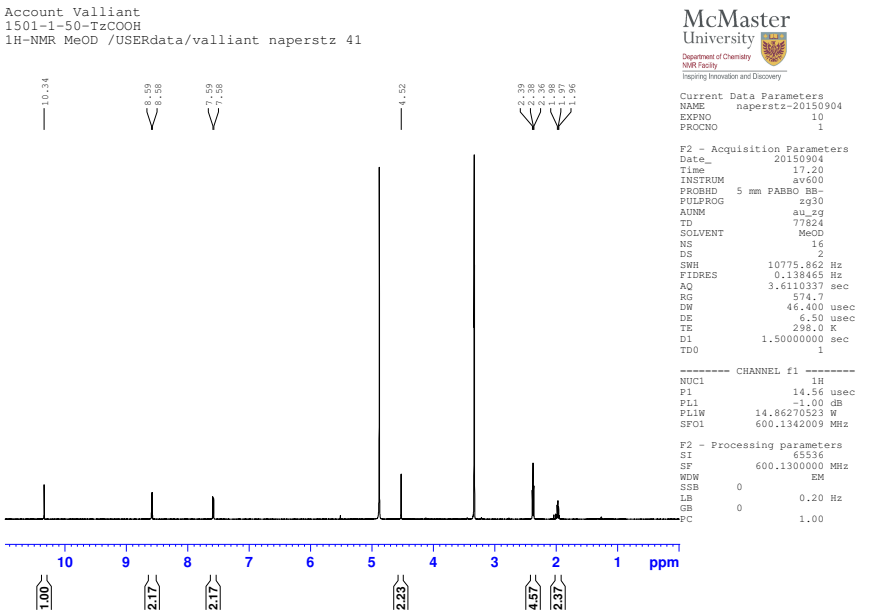

Figure 37: ^{1}H NMR (600 MHz, CD_3OD) of TzCOOH **7**

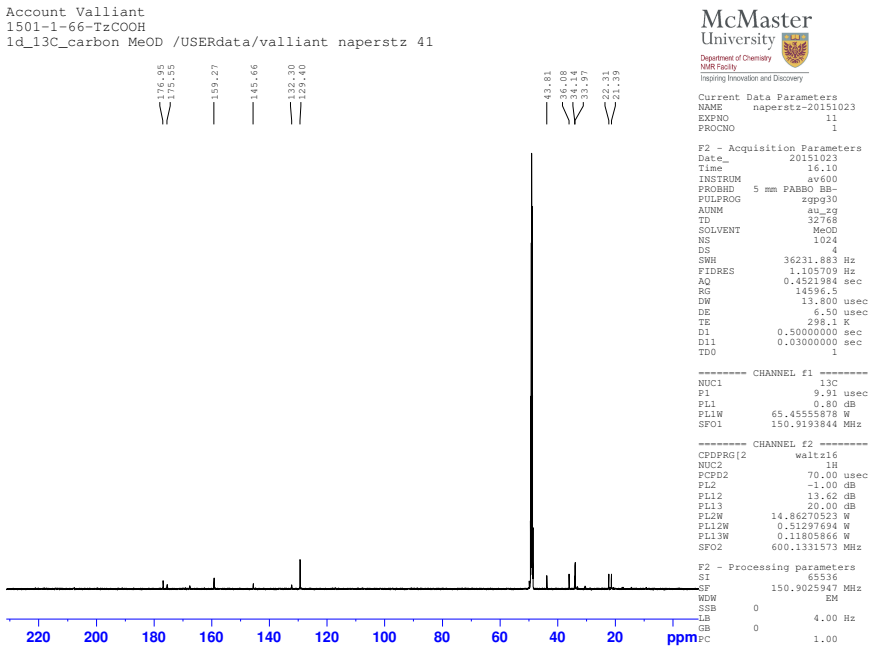

Figure 38: ^{13}C (150 MHz, CD_3OD) of TzCOOH **7**

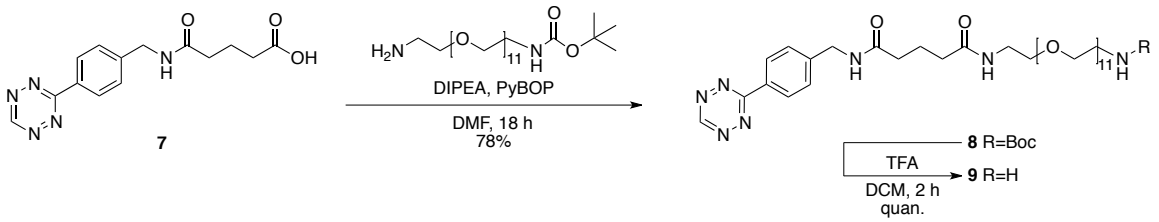

Scheme 16: Synthesis of $TzPEG_{11}$-Boc

***tert*-Butyl-(2-(2-(5-((4-(1,2,4,5-tetrazin-3-yl)benzyl)amino)-5-oxopentanamido)ethoxy$_{11}$)ethyl)carbamate ($TzPEG_{11}$-Boc) 8:** Compound **7** (44.6 mg, 0.15 mmol), NH_2-CH_2-CH_2PEG_{11}-NHBoc (105 mg, 0.16 mmol) and PyBOP (81 mg, 0.155 mmol) were combined and the reaction vial capped and purged with argon gas for 5 min. DMF (4.5 ml) and DIPEA (257 µl, 1.48 mmol) were then added and the reaction mixture stirred overnight (18 hours). DMF was evaporated *in vacuo* and the crude material was purified via Biotage SP1 system with a SNAP-ultra 25 cartridge using a 5-20% gradient of MeOH/DCM to obtain a bright pink oil (62 mg, 45%). ^{1}H NMR (600 MHz, CD_3OD): δ 10.33 (s, 1H), 8.56 (d, 2H, J = 6 Hz), 7.57 (d, 2H, J = 12 Hz), 4.51 (s, 2H), 3.65 (PEG multiplet, 44H), 3.57 (2H, J = 6, 12 Hz), 3.53 (2H, J = 6, 12 Hz) 2.33 (t, 2H, J = 12, 18 Hz), 2.27 (t, 2H, J = 6, 12 Hz), 1.96 (q, 2H, J = 6, 6, 18 Hz), 1.43 (s, 9H). ^{13}C NMR (150 MHz, CD_3OD): δ 175.3, 167.5, 159.2, 145.6, 132.3, 129.4, 71.4 (PEG), 70.5, 43.7, 41.3, 40.3, 36.1, 28.7, 23.1, 18.7, 17.2. HRMS (ES+) m/z calculated for $C_{43}H_{73}N_7O_{15}$ [M+H$^+$] 928.5243, found 928.5245.

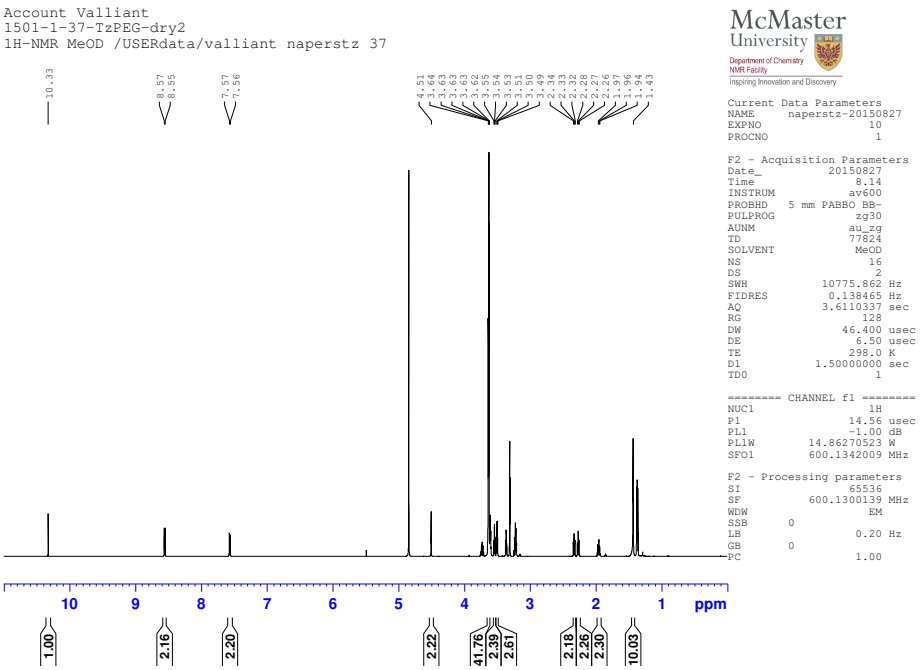

Figure 39: ^{1}H NMR (600 MHz, CD_3OD) of $TzPEG_{11}$-Boc **8**

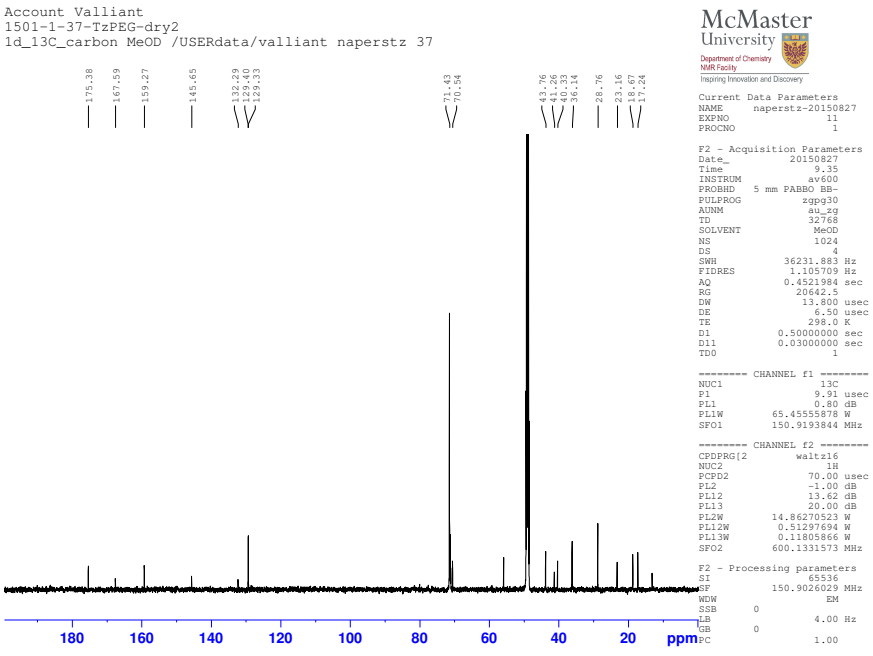

Figure 40: ^{13}C NMR (150 MHz, CD_3OD) of $TzPEG_{11}$-Boc **8**

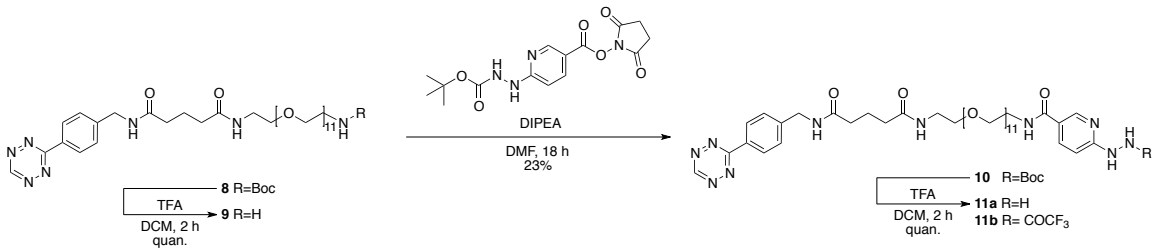

Scheme 17: Synthesis of $TzPEG_{11}HYNIC$-Boc **10** and $TzPEG_{11}HYNIC$ **11**

***tert*-Butyl-2-(5-((2-(2-(5-((4-(1,2,4,5-tetrazin-3-yl)benzyl)amino)-5-oxopentanamido)ethoxy$_{11}$)ethyl)carbamoyl)pyridin-2-yl)hydrazinecarboxylate ($TzPEG_{11}HYNIC$-Boc) 10:** Compound **8** (50 mg, 0.053 mmol) was initially dissolved in DCM (8 ml), whereafter TFA (3 ml) was added. The reaction was monitored by TLC and electrospray MS^+ until complete (approximately 2 h). The reaction mixture was concentrated under reduced pressure, where it was neutralized using a Water Sep-Pak (C18 cartridge) conditioned with 10 ml MeOH, washed with distilled water (30 ml or until pH 5-6) and eluted using 10 ml acetonitrile. Once dried, the intermediate **9** was redissolved in anhydrous DMF (8 ml). DIPEA (84.3 µl, 0.484 mmol) was added and the reaction mixture was stirred for 5 min whereupon 2,5-dioxopyrrolidin-1-yl 6-(2-(*tert*-butoxycarbonyl)hydrazinyl)nicotinate (Boc-HYNIC-NHS **3**) (17.9 mg, 0.511 mmol) was added, and the solution allowed to stir overnight (18 hours). The next day the reaction mixture was concentrated *in vacuo*, and the product isolated by flash column chromatography using 20:4:1 v/v/v to 16:1:3 v/v/v DCM, EtOAc, MeOH, as a vivid pink oil **10** (19 mg, 23%).^{1}H NMR (600 MHz, CD_3OD): δ 10.33 (s, 1H), 8.55 (d, 3H, J = 6 Hz), 8.00 (dd, 1H, J = 6, 12 Hz), 7.56 (d, 2H, J = 6 Hz), 6.70 (d, 1H, J = 6 Hz), 4.50 (s, 2H), 3.61 (PEG multiplet, 44H), 3.54 (multiplet, 5H), 2.33 (t, 2H, J = 6, 12 Hz), 2.27 (t, 2H, J = 6, 18 Hz), 1.95 (q, 2H, J = 6, 6, 18 Hz), 1.49 (s, 9H). ^{13}C NMR (150 MHz, CD_3OD): δ 175.4, 168.4, 167.6, 163.3, 159.3, 158.3, 149.0, 145.7, 138.3, 132.3, 129.4,

129.3, 122.4, 106.7, 81.82, 71.3 (PEG), 70.6, 43.8, 40.8, 40.3, 36.2, 28.6, 23.2. HRMS (ES^+) m/z calculated for $C_{49}H_{78}N_{10}O_{16}$ [M+H^++Na^+] 1085.5509, found 1085.5495

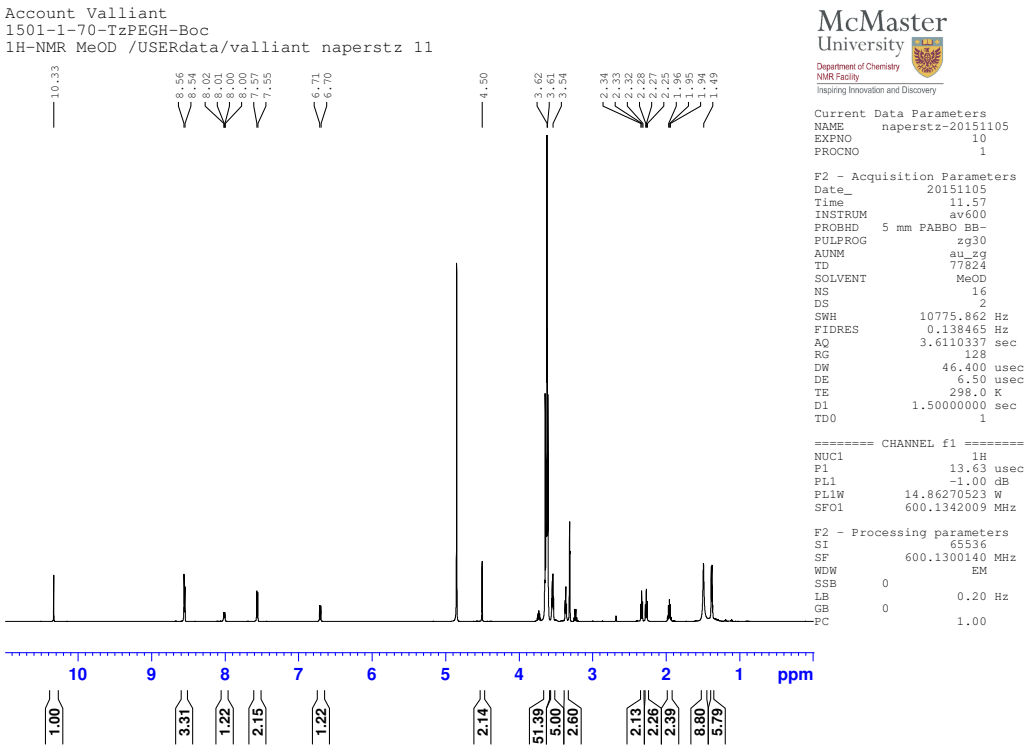

Figure 41: ^{1}H NMR (600 MHz, CD_3OD) of $TzPEG_{11}$HYNIC **10**

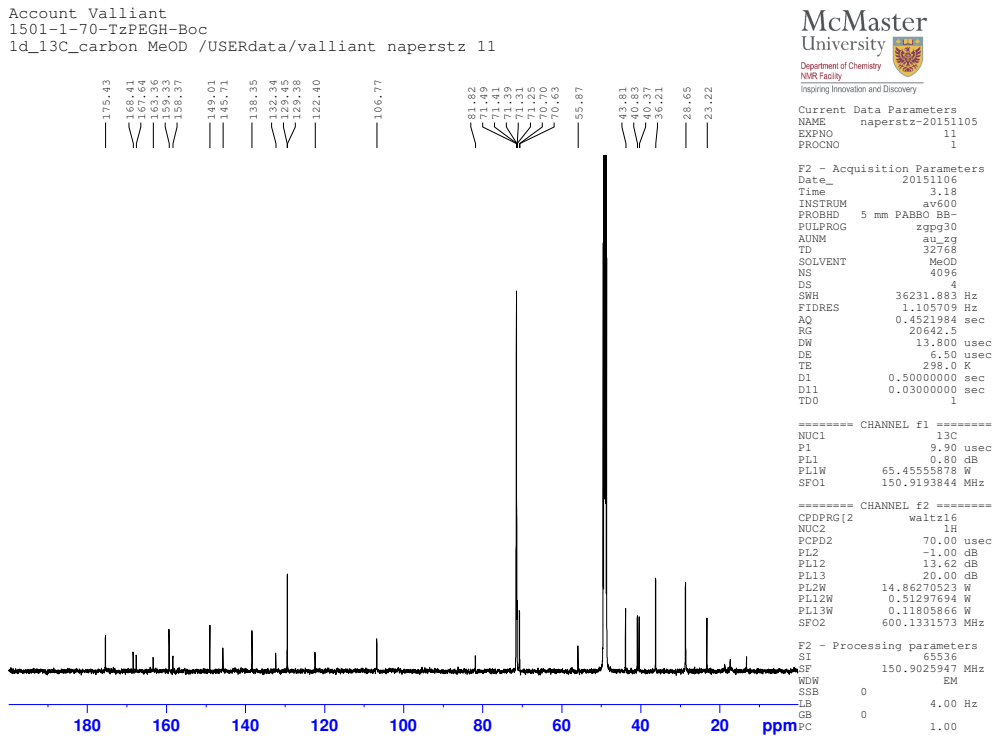

Figure 42: ^{13}C NMR (150 MHz, CD_3OD) of $TzPEG_{11}HYNIC$-Boc **10**

***N*^{1}-(4-(1,2,4,5-Tetrazin-3-yl)benzyl)-*N*^{5}-(2-(2-(6-hydrazinylnicotinamido)ethoxy y$_{11}$)ethyl)glutaramide (TzPEG$_{11}$HYNIC) 11:** Compound **10** (6 mg) was dissolved in 800 µl of DCM. Upon addition of 400 µl TFA, the vivid pink color immediately changed to a pale pink and the reaction mixture was stirred until deemed complete by TLC/MS (approximately 30 minutes). The resulting mixture was then neutralized using a Waters Sep-Pak C18 cartridge conditioned with 10 ml MeOH, washed with 50 ml dH_2O, eluted using 10 ml methanol and dried under reduced pressure *in vacuo* to obtain a pink oil containing **11a** and the TFA-derivative side product **11b** (3.4 mg, 62%) ^{1}H NMR (600 MHz, d_4-MeOD): δ 10.33 (s, 1H), 8.55 (d, 3H, J = 6 Hz), 8.21 (d, 1H, J = 6 Hz), 7.57 (d,

2H, J = 6 Hz), 7.01 (d, 1H, J = 6 Hz), 4.50 (s, 2H), 3.62 (PEG multiplet, 44H), 2.33 (t, 2H, J = 6, 12 Hz), 2.27 (t, 2H, J = 6, 18 Hz), 1.96 (q, 2H, J = 6, 6, 18 Hz).

HRMS (ES$^+$) m/z calculated for $C_{44}H_{70}N_{10}O_{14}$ [M+H$^+$] 963.5151, found 963.5160

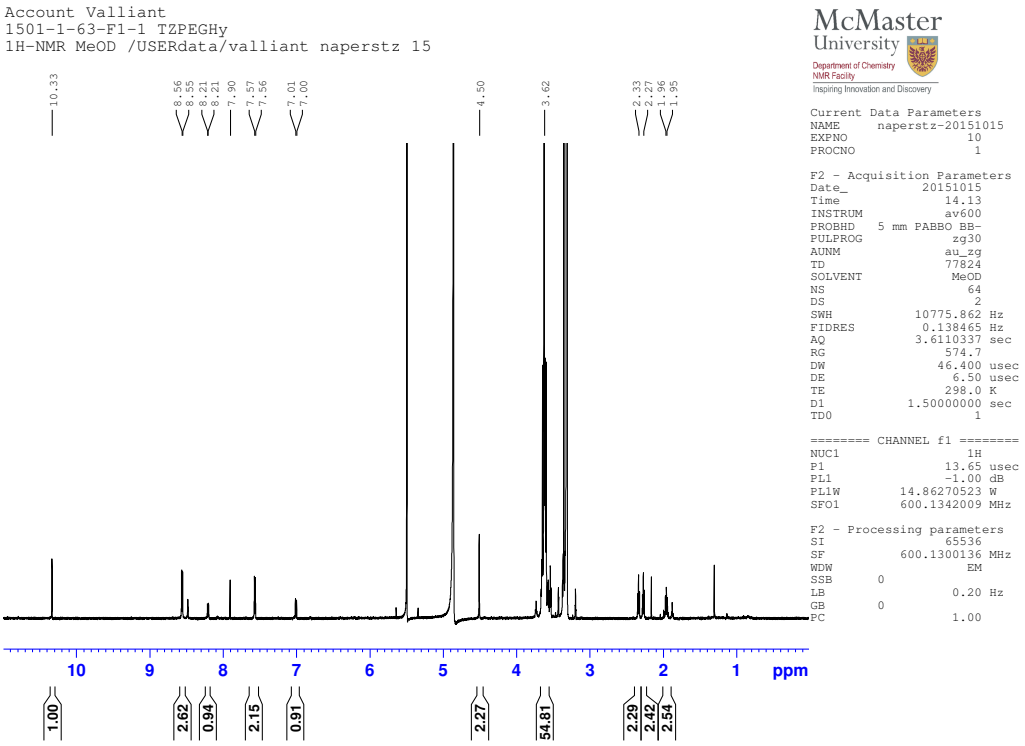

Figure 43: ^{1}H NMR (600 MHz, CD_3OD) of $TzPEG_{11}HYNIC$ **11**

5.2.1 ^{99m}Tc Radiolabelling of TzPEG$_{11}$HYNIC

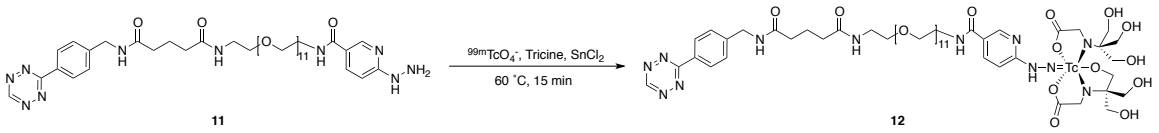

Scheme 18: Radiolabelling of ^{99m}Tc-TzPEG$_{11}$HYNIC **12**

Compound **11a/b** (100 μg, 104 nmol) was dissolved in saline (100 μl) in an Eppendorf tube. 500 μL of a tricine solution (100 mg/ml saline), 500 μl ^{99m}TcO4$^-$ and 10 μl stannous chloride dihydrate solution (3 mg/ml ethanol) were added. The solution was vortexed for 10 seconds and heated to 60˚C for 15 minutes. The desired product was confirmed by HPLC using Method B and radio-TLC using acetone as the elution solvent to quantify the amount of ^{99m}TcO$_4^-$ present.

5.3 Biological Studies

5.3.1 ^{99m}Tc-TzHYNIC HPLC-Purified and Reaction Mixture

Biodistribution studies of **6** were performed using 10-11 week old female CD1 mice (Charles River Laboratories, Montreal, PQ). A 5 mg/ml solution of TCO-bisphosphonate (TCO-BP) in saline (100 μl) was administered via tail-vein injection to 6 mice 1 h prior to injection of the radiolabeled purified and crude **6**. Three mice were injected with approximately 20 μCi (100 μl) of HPLC-purified **6** and the other three with non-HPLC purifed **6** (20 μCi in 100μl). At 6 h post-injection of the ^{99m}Tc-labelled compounds, the animals with anesthetized with 3% isoflurane and cervical dislocation. Blood, bone (knee, shoulder) and select tissues were collected, weighed and counted in a gamma counter and expressed as percent injected dose per gram (%ID/g). Decay correction was used to normalize the activity measurements to time of dose preparation for data calculations.

5.3.2 ^{99m}Tc-TzPEG$_{11}$HYNIC

Biodistribution studies of **12** were performed using 7-8 week old female CD1 mice (Charles River Laboratories, Montreal, PQ). A 5 mg/ml solution of TCO-bisphosphonate (TCO-BP) in saline (100 µl) was administered via tail-vein injection to 3 mice 1 h prior to injection of the radiolabeled compound **12** (20 µCi in 100µl). At 6 h post-injection of the ^{99m}Tc-labelled compounds, the animals with anesthetized with 3% isoflurane and cervical dislocation. Blood, bone (knee, shoulder) and select tissues were collected, weighed and counted in a gamma counter and expressed as percent injected dose per gram (%ID/g). Decay correction was used to normalize the activity measurements to time of dose preparation for data calculations.

5.3.3 Blood Clearance Study using ^{99m}Tc-TzPEGHYNIC

^{99m}Tc-TzPEGHYNIC **12** was formulated in saline to a concentration of 1.75 mCi/ml. Healthy CD1 mice were injected with 200 µl of the formulation at 0, 5, 15, 30 and 60 minutes (n=3). The mice were placed under anesthesia and blood removed via cardiac puncture followed by cervical dislocation. The ~1ml of blood was split in half between a pre-weighed gamma tube and a heparinized Eppendorf tube. The mice tails were removed and placed in a pre-weighed gamma tube to calculate the injected dose. The gamma tubes were left to decay overnight and counted to determine %ID/g in the blood.

5.4 Statistical Analysis

Biodistribution studies and *in vitro* assays were reported using standard error of the mean (SEM). Standard deviation, which was not used, is a measurement of variability (dispersion) within the population (the mean) whereas SEM, which is commonly

employed for biodistribution studies of the types reported, is used to quantify uncertainty in the estimate of the mean.[80]

To analyze two sets of independent data, an unpaired, two-tailed Student's t-test was performed with a 95% confidence threshold ($p < 0.5$). These were performed after biodistribution studies and bacterial assays to determine if there was a significant difference between compounds and their respective uptake/binding profiles.

5.5 Synthesis of Bispyridyl Tetrazine Compounds

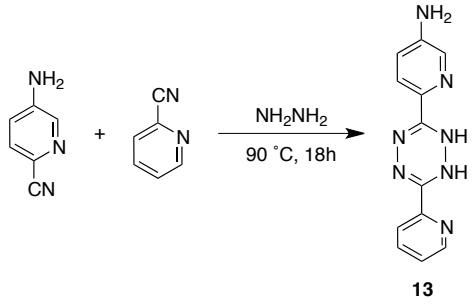

Scheme 19: Synthesis of BPTz **13**

6-(6-(pyridin-2-yl)-1,2-dihydro-1,2,4,5-tetrazin-3-yl)pyridin-3-amine (BPTz) 13:

Behind a blast shield, a 100 ml oven dried round bottom flask was charged with 5-amino-2-pyridine (3.00 g, 25.25 mmol), 2-cyanopyridine (4.94 g, 47.45 mmol) and hydrazine monohydrate (6 ml). The reaction was refluxed overnight at 90˚C. Once cooled

40 ml of distilled H_2O was added to resuspend the resulting solid. The solid was filtered and washed with water until the filtrate was pale yellow/clear. The solid was dried and purified using 2% MeOH/DCM to afford an orange powder with minimal side product (symmetrical reduced-BPTz). ^{1}H NMR (600 MHz, DMSO-d_6): δ 8.90 (dq, 1H, J = 4.7 Hz), 8.52 (d, 1H, J = 8 Hz), 8.36 (d, 1H, J = 8.5 Hz), 8.24 (d, 1H, J = 2.5 Hz), 8.12 (td, 1H, J = 1, 4.7 Hz), 7.69 (dd, 1H, J = 2.5, 8.3), 6.36 (s, 2H), 2.54 (s, 1H)

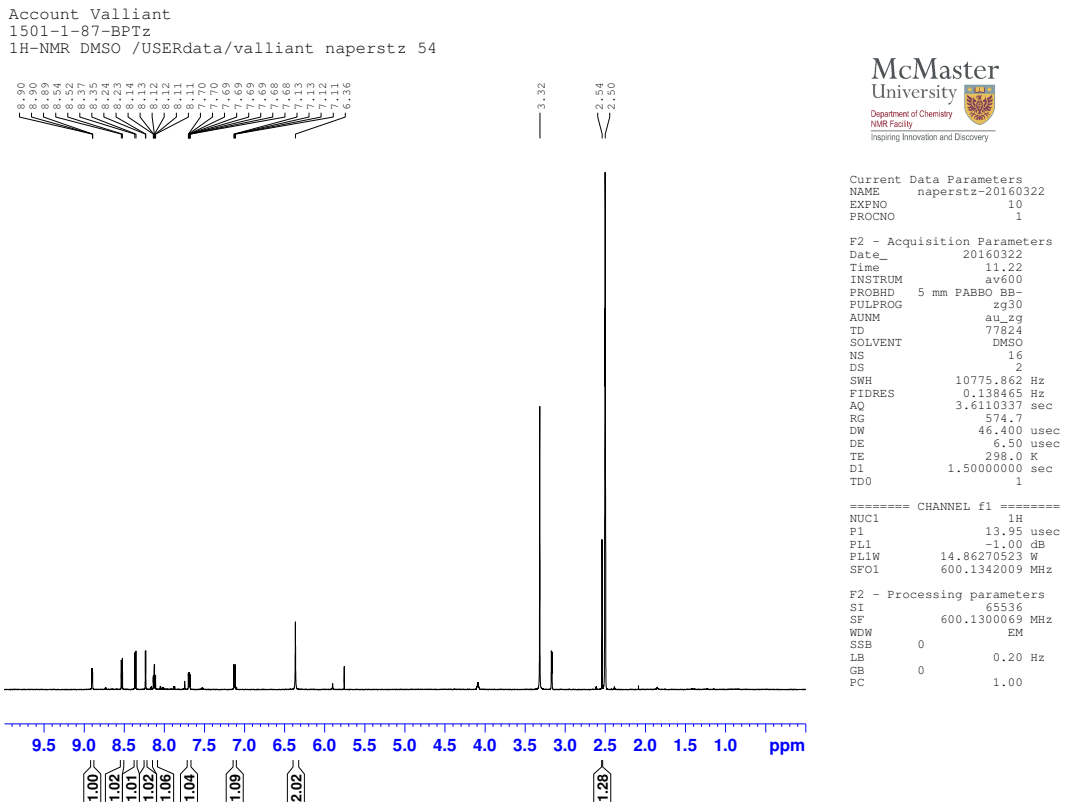

Figure 44: ^{1}H NMR (600 MHz, DMSO-d_6) of BPTz **13**

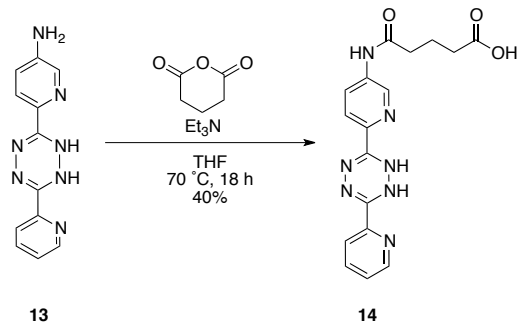

13 14

Scheme 20: Synthesis of reduced-BPTzCOOH **14**

5-oxo-5-((6-(6-(pyridin-2-yl)-1,2-dihydro-1,2,4,5-tetrazin-3-yl)pyridin-3-yl)amino)pentanoic acid 14: Bispyridyl tetrazine **13** (100 mg, 0.395 mmol) and glutaric anhydride (60 mg, 0.525 mmol) were added to a 25 ml oven dried 2-neck round bottom flask and fitted with a reflux condenser. The flask was purged with N_2 gas prior to addition of anhydrous THF (3 ml) and triethylamine (40 µl, 0.395 mmol). The reaction was heated to 70˚C overnight under N_2 gas. The following morning, the resulting orange solid was resuspended in THF and filtered over a Buchner funnel, and subsequently washed with DCM and EtOAc to afford **14** in 40% yield as an orange solid (59 mg) with minimal side product (symmetrical reduced-BPTz) as determined by TLC. The identity of the compound was determined by ESI-MS^+ before oxidation.

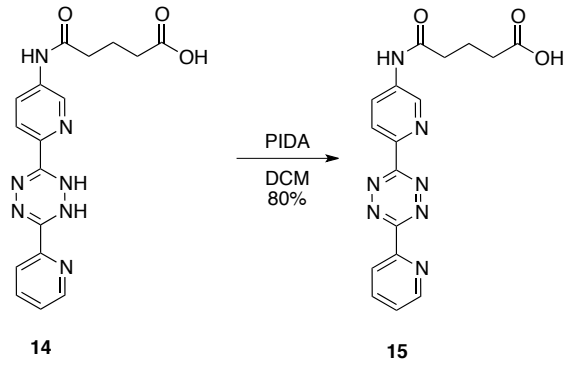

Scheme 21: Synthesis of BPTzCOOH **15**

5-oxo-5-((6-(6-(pyridin-2-yl)-1,2,4,5-tetrazin-3-yl)pyridin-3-yl)amino)pentanoic acid (BPTzCOOH) 15: Compound **14** (59 mg, 0.160) was dissolved in 2 ml DCM and 0.6 ml MeOH in a 10 ml round bottom flask. Phenyliodine(III) diacetate (77.6 mg, 0.241) was added and the reaction stirred for 2 hours. The resulting bright purple solution was evaporated and then washed with DCM to afford a fine purple powder **15** (BPTzCOOH) (46 mg, 80% yield). ^{1}H NMR (600 MHz, DMSO-d_6): δ 10.59 (s, 1H), 9.05 (d, 1H, J = 2.2Hz), 8.94 (d, 1H, J = 4Hz), 8.62 (d, 1H, J = 8.8Hz), 8.59 (d, 1H, J = 8Hz), 8.43 (dd, 1H, J = 2, 4, 9.2Hz), 8.15 (td, 1H, J = 2, 8Hz), 7.73 (ddd, 1H, J = 1, 4, 7Hz), 2.48 (t, 2H, J = 7.5Hz), 2.32 (t, 2H, J = 7.5Hz), 1.87 (m, 2H)

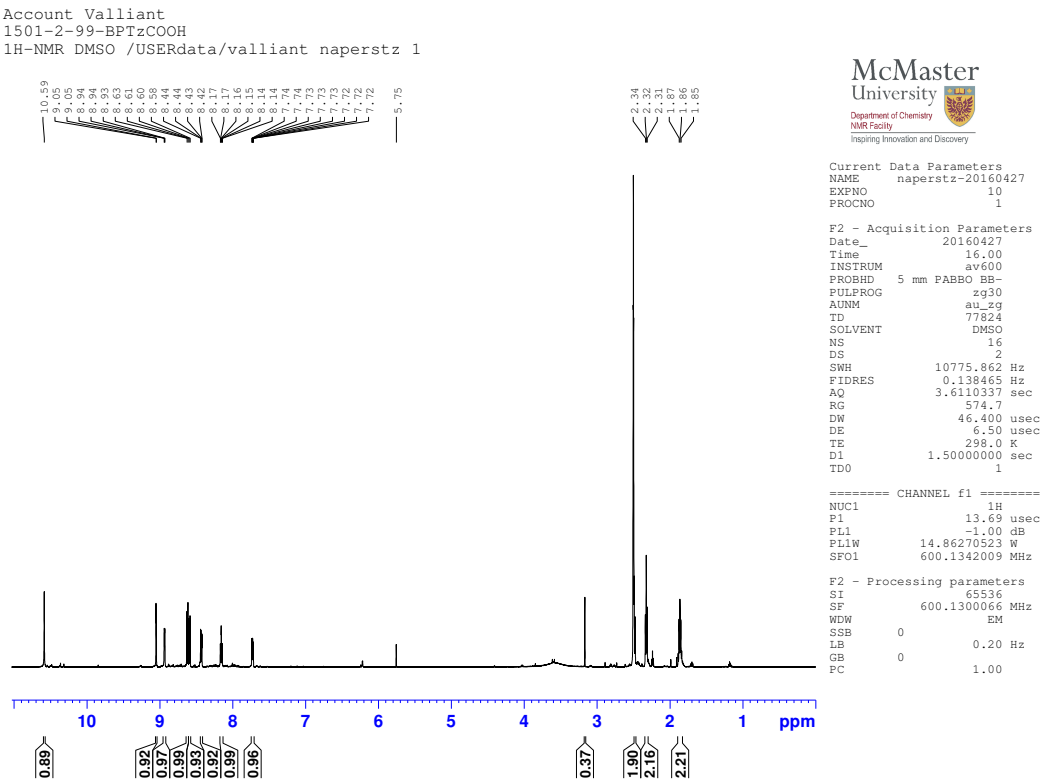

Figure 45: ^{1}H NMR (600 MHz, DMSO-d_6) of BPTzCOOH **15**

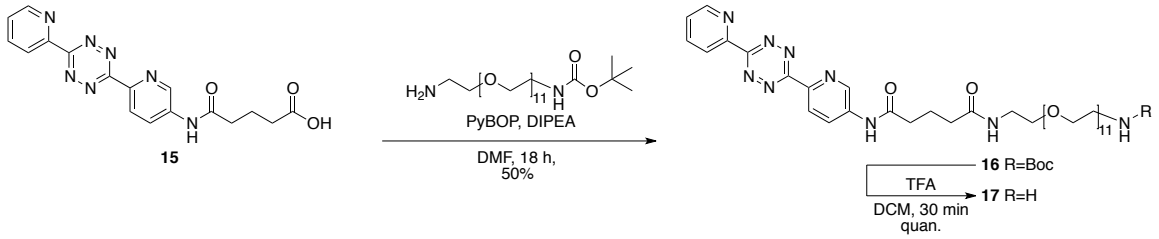

Scheme 22: Synthesis of $BPTzPEG_{11}$-Boc **16**

***tert*-butyl-(2-(2-(5-oxo-5-((6-(6-(pyridin-2-yl)-1,2,4,5-tetrazin-3-yl)pyridin-3-yl)amino)pentanamido)ethoxy$_{11}$)ethyl)carbamate ($BPTzPEG_{11}$-Boc) 16:** In a 5 ml vial, BPTzCOOH **15** (40 mg, 0.109 mmol), NH_2-CH_2-CH_2-PEG_{11}-NHBoc (78 mg, 0.120), PyBOP (60 mg, 0.115) and DIPEA (160 µl, 0.926 mmol) were added and purged with N_2. Anhydrous DMF (2.8 ml) was added and the reaction stirred overnight at room temperature. The solution was concentrated *in vacuo* and purified using a Biotage SP1 system with a SNAP-ultra 25 cartridge using a 2-20% gradient of MeOH/DCM to obtain **16** as a bright purple oil (55 mg, 50%). ^{1}H NMR (600 MHz, CD_3OD): δ, 9.05 (d, 1H, J = 2.4Hz), 8.88 (d, 1H, J = 4Hz), 8.76 (d, 1H, J = 8.84z), 8.74 (d, 1H, J = 8.2Hz), 8.47 (dd, 1H, J = 2, 7, 8.7Hz), 8.17 (td, 1H, J = 1.6, 7.6Hz), 7.73 (ddd, 1H, J = 1, 4, 7Hz), 3.64 (m, 41H (PEG)), 3.51 (t, 2H, J = 5.5Hz), 3.40 (t, 2H, J = 6Hz), 2.54 (t, 2H, J = 7.4), 2.34 (t, 2H, J = 7.7Hz), 2.03 (q, 2H), 1.43 (s, 9H)

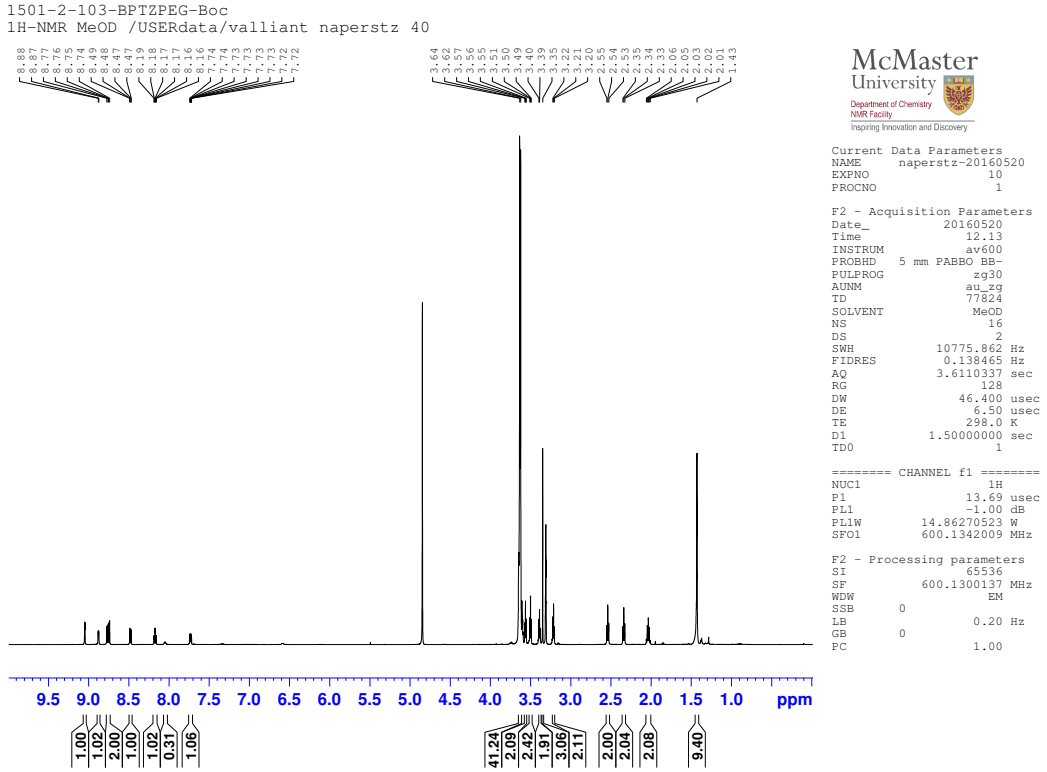

Figure 46: ^{1}H NMR (600 MHz, CD_3OD) of BPTzPEG$_{11}$-Boc **16**

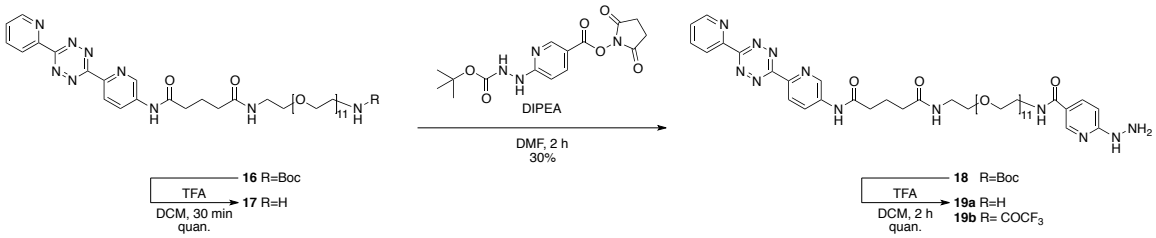

Scheme 23: Synthesis of BPTzPEG$_{11}$HYNIC-Boc **18**

***tert*-butyl-2-(5-((2-(2-(5-oxo-5-((6-(6-(pyridin-2-yl)-1,2,4,5-tetrazin-3-yl)pyridin-3-yl)amino)pentanamido)ethoxy$_{11}$)ethyl)carbamoyl)pyridin-2-yl)hydrazinecarboxylate (BPTzPEG$_{11}$HYNIC-Boc) 18**: In a scintillation vial, BPTzPEG$_{11}$-Boc **16** (43 mg, 0.043 mmol) was deprotected in a 1:3 v/v TFA:DCM and stirred for 30 minutes. The

mixture was concentrated and neutralized using a Water Sep-Pak (C18 cartridge) conditioned with 10 ml ACN, washed with distilled water (30 ml or until pH 5-6) and eluted using 10 ml acetonitrile. Once dried, the intermediate **17** was redissolved in anhydrous DMF (5 ml). DIPEA (69.9 µl, 0.391 mmol) was added and the reaction mixture stirred for 5 min whereupon 2,5-dioxopyrrolidin-1-yl 6-(2-(*tert*-butoxycarbonyl)hydrazinyl)nicotinate (Boc-HYNIC-NHS **3**) (16.7 mg, 0.047 mmol) was added and the solution allowed to stir overnight (18 hours). The next day the reaction mixture was concentrated *in vacuo*, and the product isolated by flash column chromatography using 20:4:1 v/v/v to 16:1:3 v/v/v DCM, EtOAc, MeOH, to obtain **18** as vivid purple oil (18 mg, 36%). ^{1}H NMR (600 MHz, CD_3OD): δ 9.05 (d, 1H, J = 3Hz), 8.88 (d, 1H, J = 4.7Hz), 8.77 (d, 1H, J = 8Hz), 8.75 (d, 1H, J = 9Hz), 8.55 (d, 1H, J = 2Hz) 8.48 (dd, 1H, J = 2, 5, 9Hz), 8.17 (td, 1H, J = 2, 8Hz), 8.00 (dd, 1H, J = 1 ,7, 9Hz), 7.73 (m, 2H), 7.62 (m, 1H), 6.70 (d, 1H, J= 8.5Hz), 4.28 (m, 1H) 3.64 (m, 44H (PEG)), 3.60 (m, 4H), 3.35 (m, 2H), 2.54 (t, 2H, J = 7.5), 2.34 (t, 2H, J = 7.2Hz), 2.04 (q, 2H), 1.49 (s, 9H). ^{13}C NMR (150 MHz, CD_3OD): δ 158.3, 151.5, 151.3, 149.0, 145.3, 142.7, 140.4, 139.5, 138.3, 132.3, 129.8, 128.3, 128.7, 126.2, 125.6, 106.7, 71.3 (PEG), 40.7, 40.4, 36.9, 36.0, 40.7, 40.3, 36.9, 36.0, 28.6, 22.6

HRMS (ES^+) m/z calculated for $C_{52}H_{78}N_{12}O_{16}$ [$M+H^+$] 1127.5732, found 1127.5727

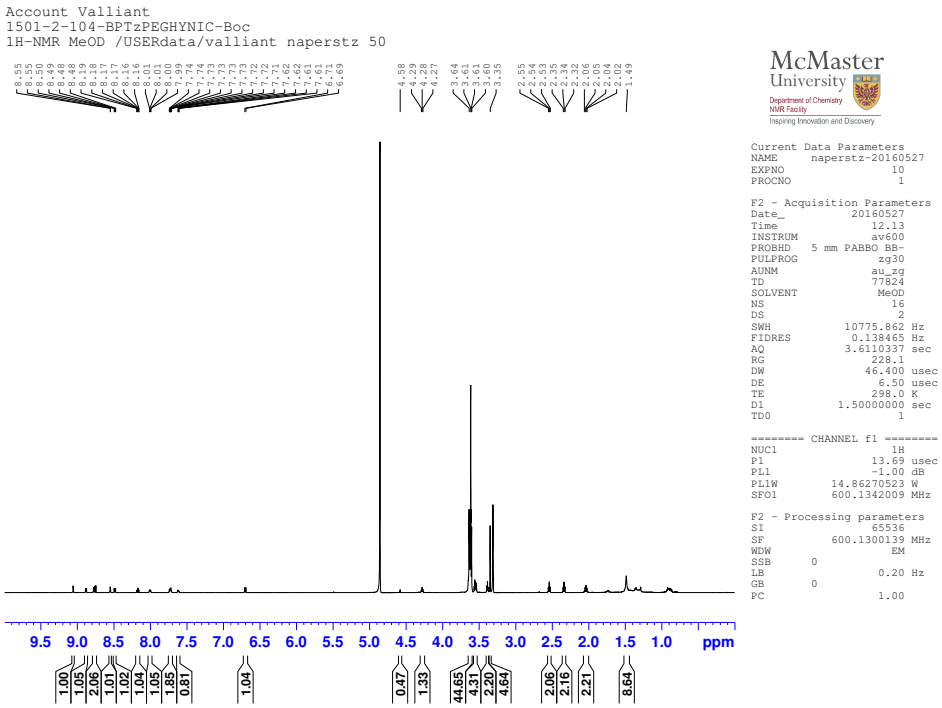

Figure 47: ^{1}H NMR (600 MHz, CD_3OD) of BPTzPEG$_{11}$HYNIC-Boc **18**

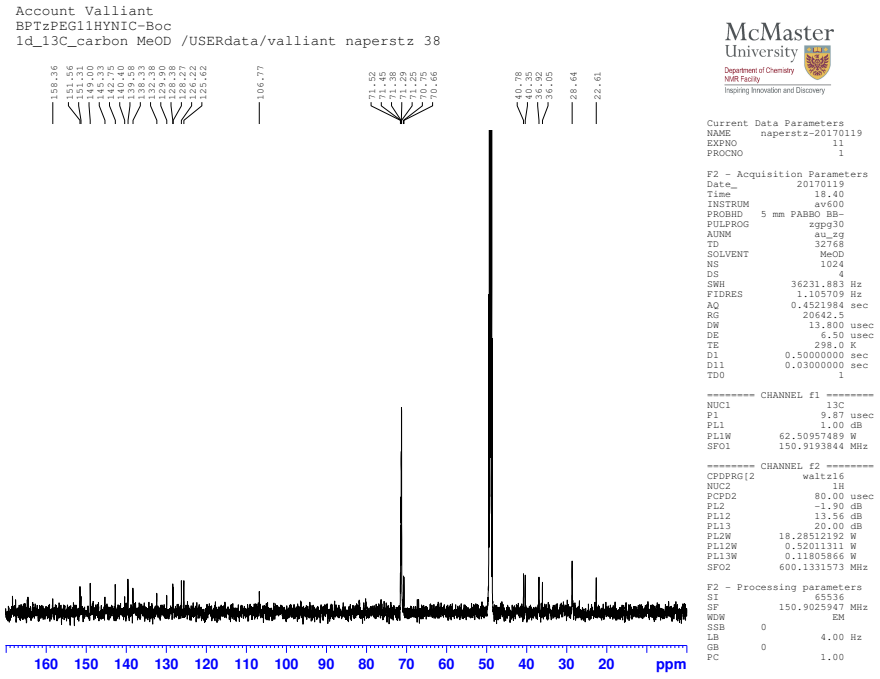

Figure 48: ^{13}C NMR (150 MHz, CD_3OD) of BPTzPEG$_{11}$HYNIC-Boc **18**

***N*^{1}-(2-(2-(6-hydrazinylnicotinamido)ethoxy$_{111}$)ethyl)-*N*^{5}-(6-(6-(pyridin-2-yl)-1,2,4,5-tetrazin-3-yl)pyridin-3-yl)glutaramide 19**: Prior to radiolabelling, compound **18** (2 mg) was dissolved in 800 µl of DCM and placed on ice. Upon addition of 400 µL TFA, the vivid purple color immediately changed and the reaction mixture was stirred until deemed complete by TLC/MS (approximately 2 hours). The resulting compound **19** was dried under a steady stream of nitrogen, reconstituted in DCM and aliquoted into Eppendorf tubes (100 µg per tube).

5.6 Synthesis of Fluorescent Derivatives

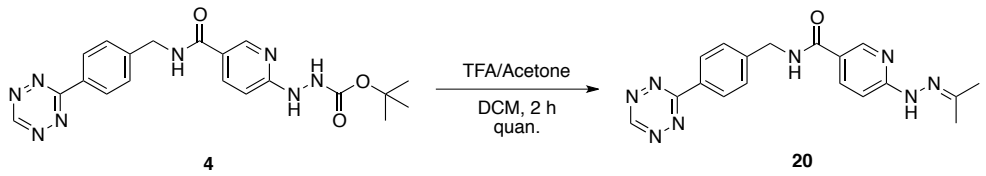

Scheme 24: Synthesis of TzHYNIC-hydrazone **20**

***N*-(4-(1,2,4,5-tetrazin-3-yl)benzyl)-6-(2-(propan-2-ylidene)hydrazinyl)nicotinamide (TzHYNIC-hydrazone) 20:** Compound **4** (2 mg) was dissolved in 800 µl of DCM. Upon addition of 400 µl TFA and 10-20% total volume acetone, the vivid pink colour immediately changed to a pale pink and the reaction mixture was stirred until deemed complete by TLC/MS (approximately 2 hours). Varying the initial concentration of **4** (2-50 mg) resulted in adjusting the amount of TFA and/or acetone until deemed complete via ESI-MS$^+$). The resulting mixture was initially dried by rotary evaporation and then again under N_2 gas to remove any excess TFA vapors, obtaining a pink oil in a quantitative yield.

^{1}H NMR (600 MHz, $CDCl_3$): δ 10.21 (s, 1H), 8.62 (d, 1H, J = 8.2Hz), 8.58 (d, 1H, J = 2.2Hz), 8.05 (dd, 1H, J = 2.3, 8.9Hz), 7.60 (d, 2H, J = 8.3), 7.31 (d, 1H J = 8.6Hz), 6.53 (2, 1H), 4.77 (d, 2H, J = 6.2), 2.07 (s, 3H), 1.95 (s, 3H).^{13}C NMR (150 MHz, $CDCl_3$): δ 157.8, 145.3, 137.5, 128.7, 107.1, 43.7, 25.5, 16.1

HRMS (ES^+) m/z calculated for $C_{18}H_{18}N_8O$ [$M+H^+$] 363.1676, found 363.1674

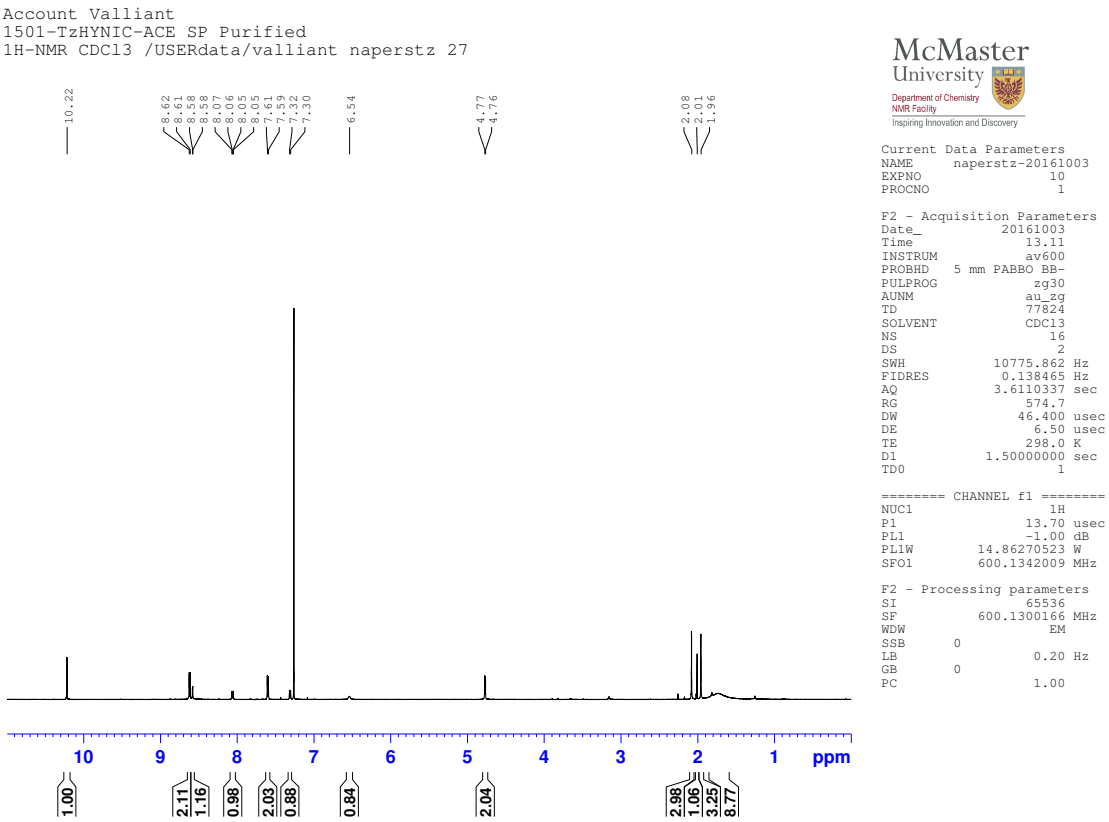

Figure 49: ^{1}H NMR (600 MHz, $CDCl_3$) of TzHYNIC-hydrazone **20**

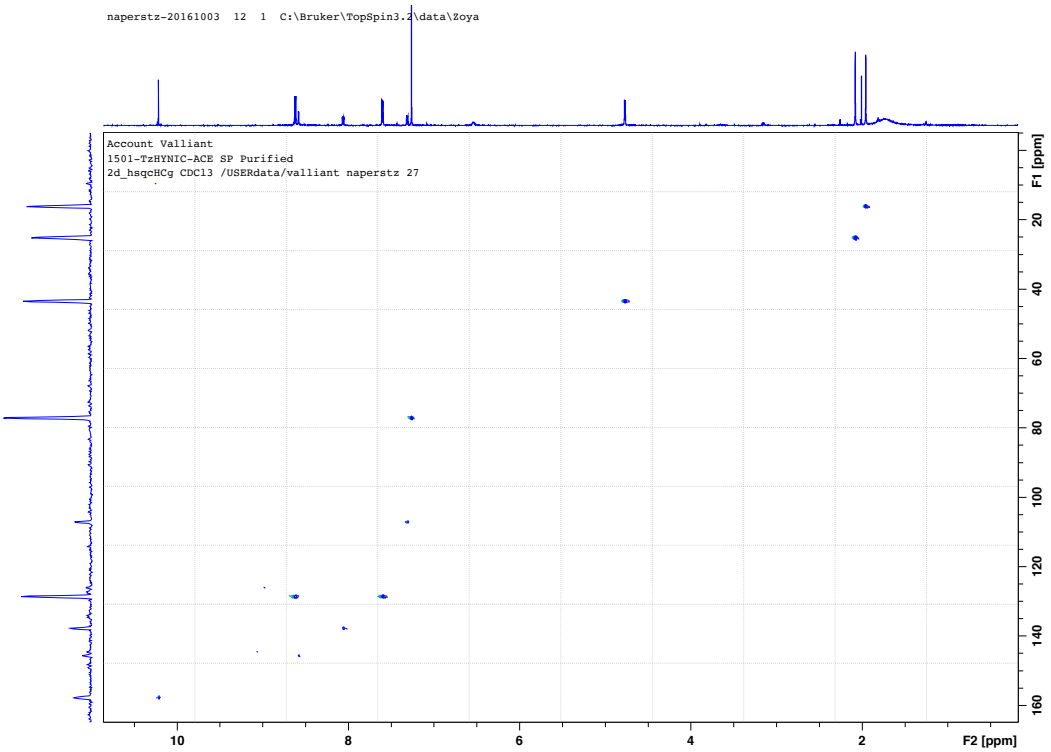

Figure 50: HSQC of TzHYNIC-hydrazone **20** in $CDCl_3$

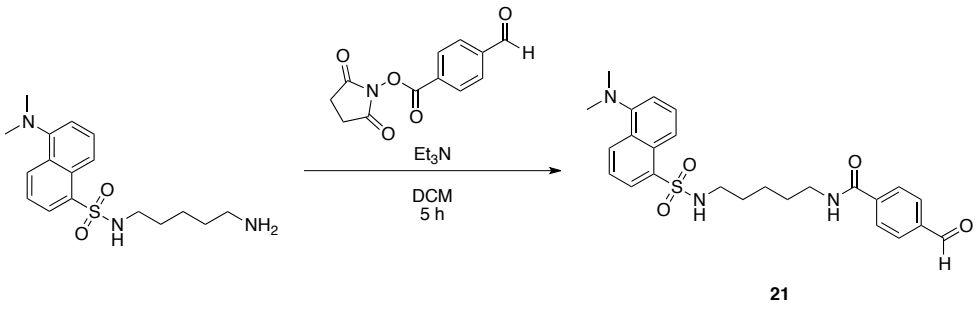

Scheme 25: Attempted synthesis of **21** (DC-4FB)

***N*-(5-(5-(dimethylamino)naphthalene-1-sulfonamido)pentyl)-4-formylbenzamide (DC-4FB) 21:** Dansylcadaverine (25 mg, 0.0745 mmol) and N-succinimidyl-4-formylbenzamide (S-4FB) (18.4 mg, 0.0745 mmol) were dissolved in 4 ml anhydrous DCM with Et_3N (32 µl, 0.223 mmol). The reaction mixture was stirred for 4 hours after which one extra equivalent of dansylcadaverine was added and stirred for an additional

hour. The crude mixture was concentrated to dryness and semi-purified using 50/50 v/v EtOAC/Hex column chromatography to afford **21**. ^{1}H NMR (600 MHz, $CDCl_3$): δ 10.05 (s, 1H), 8.54 (d, 1H, J = 7.3Hz), 8.29 (d, 1H, J = 9.5Hz), 8.21 (dd, 1H, J = 1.1, 7.2Hz), 7.93 (q, 4H, J = 13.4), 7.52 (m, 2H), 7.17 (d, 1H, J = 7.4Hz), 6.42 (s, 1H), 4.92 (s, 1H), 3.33 (q, 2H, J = 13.4Hz), 2.89 (m, 8H), 1.48 (m, 5H), 1.34 (m, 2H)

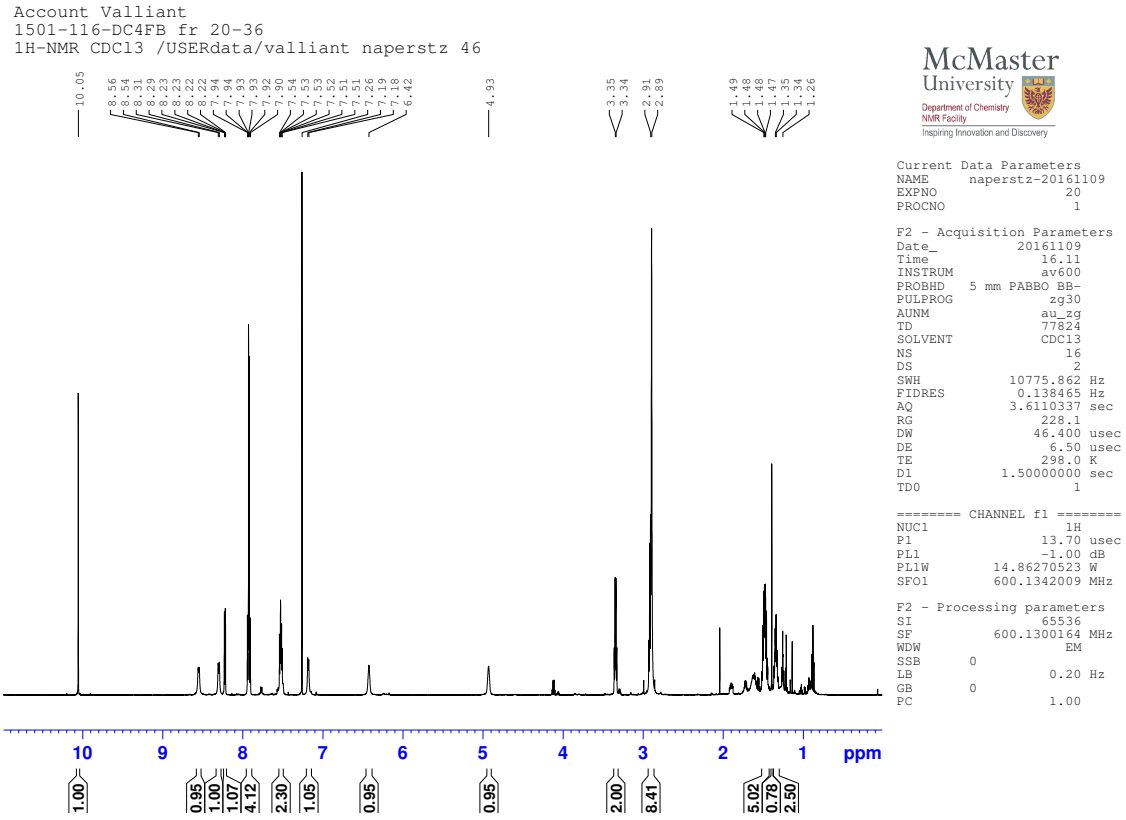

Figure 51: ^{1}H NMR (600 MHz, $CDCl_3$) of DC-4FB **21**

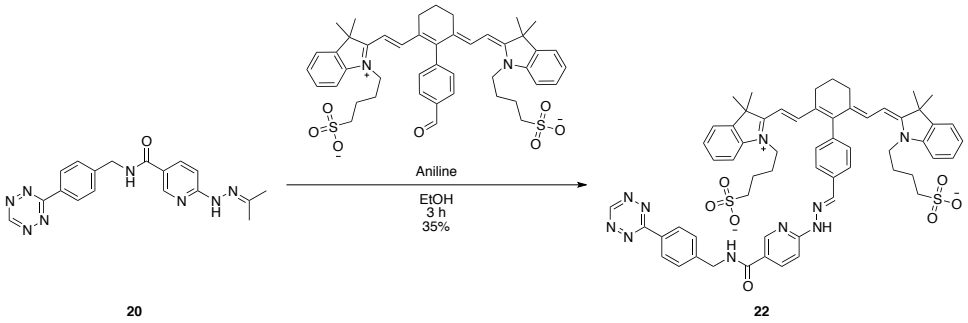

20 22

Scheme 26: Synthesis of IR783-TzHYNIC **22**

4-((*Z*)-2-((*E*)-2-(4'-((*E*)-(2-(5-((4-(1,2,4,5-tetrazin-3-yl)benzyl)carbamoyl)pyridin-2-yl)hydrazono)methyl)-6-((*E*)-2-(3,3-dimethyl-1-(4-sulfonatobutyl)-3*H*-indol-1-ium-2-yl)vinyl)-4,5-dihydro-[1,1'-biphenyl]-2(3*H*)-ylidene)ethylidene)-3,3-dimethylindolin-1-yl)butane-1-sulfonate (IR783-TzHYNIC) 22: IR783-BA (7.27 mg, 0.0091 mmol) and **20** (3.25 mg, 0.0100 mmol) were dissolve in 2.25 ml of ethanol with aniline (5.11 μl, 0.0548 mmol) and stirred for 3 h. The reaction mixture was diluted with ethanol and subjected to HPLC purification using Method C to afford **22** as a green oil in a 34% yield (characterized by Samantha Slikboer). ^{1}H NMR (600 MHz, CD_3OD) δ 10.33 (s, 1H), 8.67 (d, 1H J = 1.9 Hz,), 8.59 (d, 2H, J = 8.3 Hz), 8.54 (d, 1H, J = 9.6 Hz), 8.45 (s, 1H), 8.23 (d, 2H J = 7.7 Hz), 7.66 (d, 2H, J = 8.3 Hz), 7.43 (d, 2H, J = 7.9 Hz,), 7.34 (t, 4H, J = 7.6 Hz), 7.29 (d, 2H, J = 7.5 Hz), 7.26 (d, 3H, J = 8.4 Hz), 7.23 (s, 3H), 7.15 (t, 2H, J = 7.5 Hz,), 6.23 (d, 2H, J = 13.9 Hz,), 4.74 (s, 1H), 4.09 (s, 5H), 3.23 – 3.17 (m, 3H), 2.85 (t, 6H, J = 7.2 Hz), 2.76 (s, 5H), 2.08 (dd, 2H, J = 13.0, 6.9 Hz,), 2.03 (s, 1H), 1.94 (s, 2H), 1.86 (dd, J = 19.4, 11.1 Hz, 11H). HRMS (ES^-) m/z calculated for $C_{60}H_{63}N_{10}O_7S_2^-$ [$M+H^-$] 1099.4328, found 1099.4289

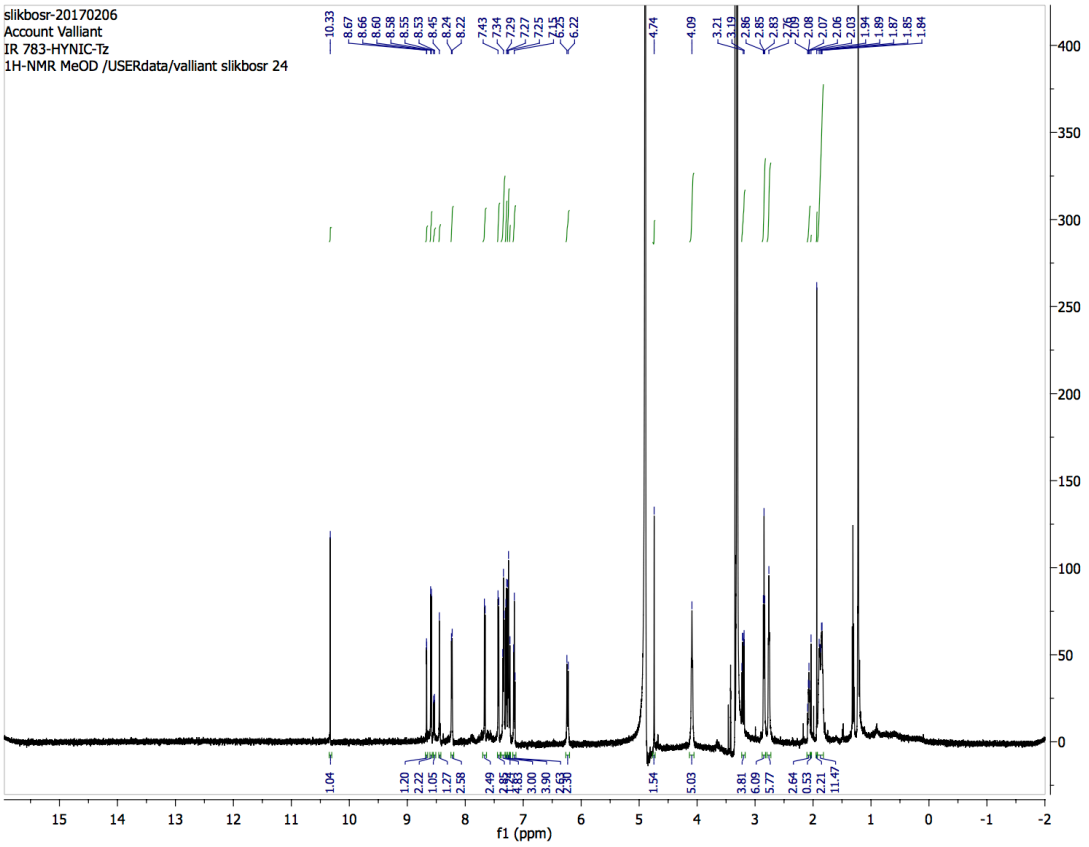

Figure 52: ^{1}H NMR (600 MHz, CD_3OD) of IR783-TzHYNIC **22** (provided by Samantha Slikboer)

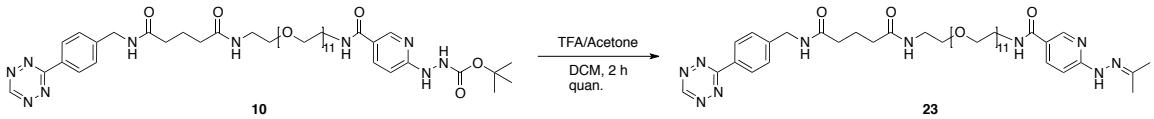

Scheme 27: Synthesis of $TzPEG_{11}$HYNIC-hydrazone **23**

N^1-(4-(1,2,4,5-tetrazin-3-yl)benzyl)-N^5-(2-(2-(6-(2-(propan-2 ylidene)hydrazinyl)nicotinamido)ethoxy)$_{11}$ethyl)glutaramide ($TzPEG_{11}$HYNIC-hydrazone) 23: Compound **16** (16 mg) was dissolved in 1000 µl of DCM. Upon addition of 500 µl TFA and 10-20% total volume acetone, the vivid pink color immediately changed to a pale pink and the reaction mixture was stirred until deemed complete by TLC/MS (approximately 45 min). After 45 min, the solution was adjusted to increase the formation of the hydrazone by addition of excess acetone in solution, and monitored

every 30 min via electrospray MS^+ (m/z 963). The resulting mixture was initally dried by rotary evaporation and then dried again under N_2 gas to remove any excess TFA vapors, obtaining a pink oil in a quantitative yield. ^{1}H NMR (600 MHz, CD_3OD): δ 10.32 (s, 1H), 8.55 (d, 2H, J = 8.6Hz), 8.45 (d, 1H, J = 1.8Hz), 8.38 (dd, 1H, J = 2.4, 9.3Hz), 7.56 (d, 2H, J = 8.4), 7.28 (d, 1H J = 9.5Hz), 4.50 (2, 2H), 3.64 (m, 52H, (PEG)), 3.61 (t, 2H, J = 6Hz), 3.34 (t, 2H, J = 5.4Hz), 2.33 (t, 2H, J = 7.8Hz), 2.26 (t, 2H, J = 7.2Hz), 2.18 (s, 3H), 2.12 (s, 3H), 1.95 (q).

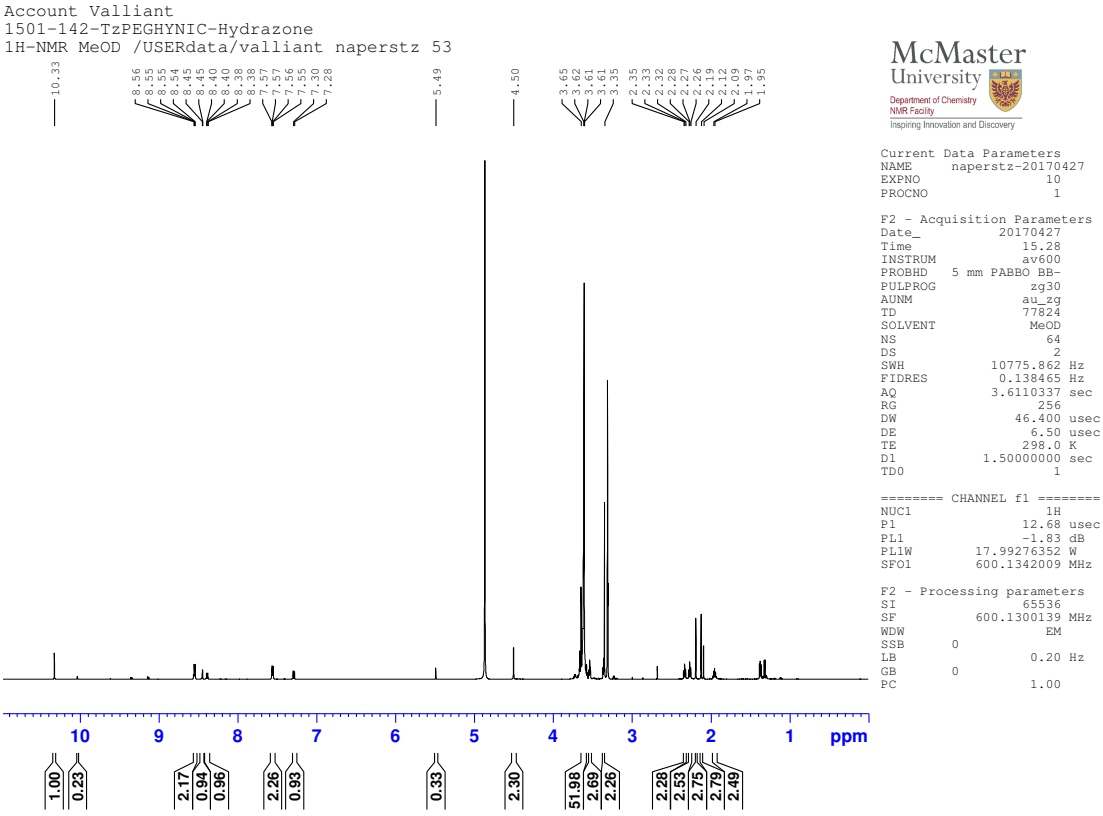

Figure 53: ^{1}H NMR (600 MHz, CD_3OD) of $TzPEG_{11}$HYNIC-hydrazone **23**

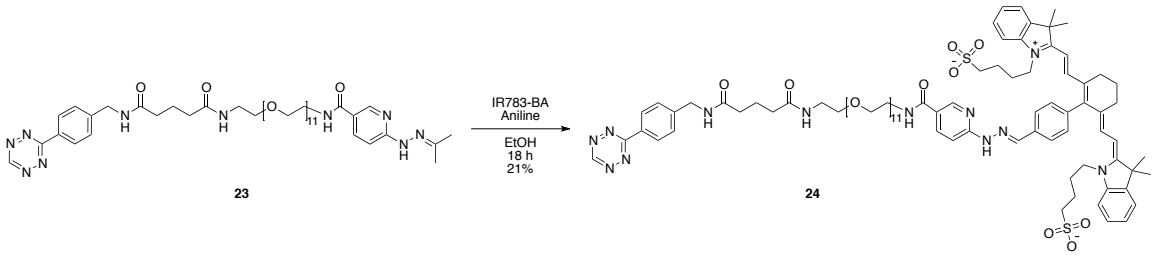

Scheme 28: Synthesis of IR783-TzPEG$_{11}$HYNIC **24**

4-((*Z*)-2-((*E*)-2-(4'-((*E*)-(2-(5-((2-(2-(5-((4-(1,2,4,5-tetrazin-3-yl)benzyl)amino)-5-oxopentanamido)ethoxy)$_{11}$ethyl)carbamoyl)pyridin-2-yl)hydrazono)methyl)-6-((*E*)-2-(3,3-dimethyl-1-(4-sulfonatobutyl)-3*H*-indol-1-ium-2-yl)vinyl)-4,5-dihydro-[1,1'-biphenyl]-2(3*H*)-ylidene)ethylidene)-3,3-dimethylindolin-1-yl)butane-1-sulfonate (IR783-TzPEG$_{11}$HYNIC) 24: IR783-BA (12 mg, 0.0151 mmol) and **23** (16 mg, 0.0166 mmol) were dissolve in 2 ml of ethanol containing aniline (8.25 µl, 0.0548 mmol) and stirred overnight. The reaction mixture was diluted with ethanol and subjected to HPLC purification using Method C to afford **24** as a green oil in a 21% yield.

HRMS (ES$^-$) m/z calculated for $C_{89}H_{120}N_{12}O_{20}S_2^-$ [M+H$^-$] 1740.8189, found 1740.8145

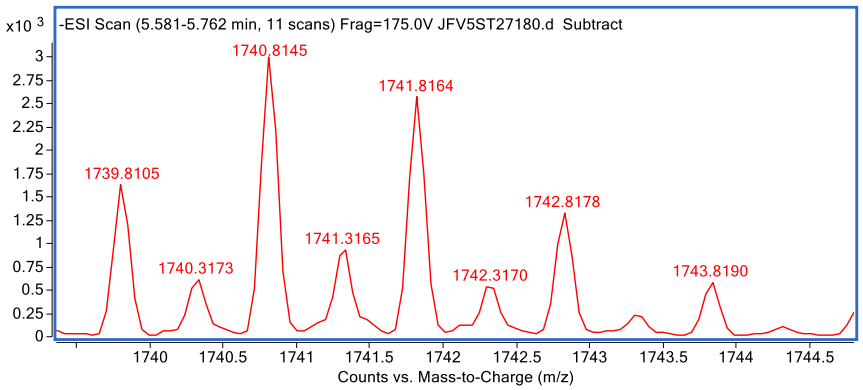

Figure 54: HRMS of IR783-TzPEG$_{11}$HYNIC **24**

5.6.1 Bacteria Studies

S. aureus bacteria (ATCC, 25923) were grown in TSB using a shaking incubator at 37˚C and 300 rpm for 16-24 hr. The following morning, cell samples in duplicate or

triplicate (approximately 5×10^8 CFU/mL) were washed twice with PBS-F (PBS + 2% FBS + 1mg/mL BSA) by centrifuging cells at 10,000 × g, aspirating off the supernatant, then resuspending the cells in PBS-F. Following the wash, the cells were then incubated for 30 minutes with either TCO-vancomycin vehicle (20%DMSO/PBS), 20 μM TCO-vancomycin, or a blocking solution of 20 μM TCO-vancomycin with 200 μM Vancomycin in PBS-F, and subsequently washed 2× with PBS-F. After washing, bacteria cells were incubated with **22** (50 nM, 500 nM, 1 μM or 5μM), **24** (500 nM) or fluorescence test article vehicle (10% EtOH/PBS), in PBS-F for 30 minutes. Unbound substrate was washed off twice with PBS-F. For fluorescence absorbance readings and microscopy, the cells were fixed in 10% paraformaldehyde for 30 minutes and then exchanged into PBS. Fluorescent measurement readings were recorded on a TECAN plate reader (abs. 762/ ex. 790 nm for **22**, abs. 764/ex. 788 nm for **24)**, where fluorescence intensity (%RFU) values were calculated as $100x(I_{target}-I_{non})/I_{non}$, where I_{target} and I_{non} are intensity values of targeted and non-targeted bacteria. For microscopy images, cells were imaged using an Olympus upright BX53 microscope fitted with a digital QImaging Retiga 2000R camera in monochromatic greyscale and processed using Olympus cellSens Dimension™ software.

5.7 Synthesis of TCO-Vancomycin (TCO-vanc.)

The synthesis was loosely adapted from literature, where(*E*)-Cyclooct-4-enyl 2,5-dioxo-1-pyrrolidinyl carbonate (TCO-NHS) (5 mg, 0.0187 mmol and vancomycin hydrochloride (63.9 mg, 0.0430 mmol) were dissolved in DMSO (1 mL) with DIPEA (42.3 μL, 0.243 mmol).[47] The reaction mixture was stirred for 48 hours under N_2 gas in

the dark. The solution was diluted with 4 mL dH_2O and purified by semi-preparative HPLC using Method D to afford a while film.

HRMS (ES^+) m/z calculated for $C_{75}H_{88}N_9O_{26}Cl_2$ [$M+H^+$] 1600.5218, found 1600.5220

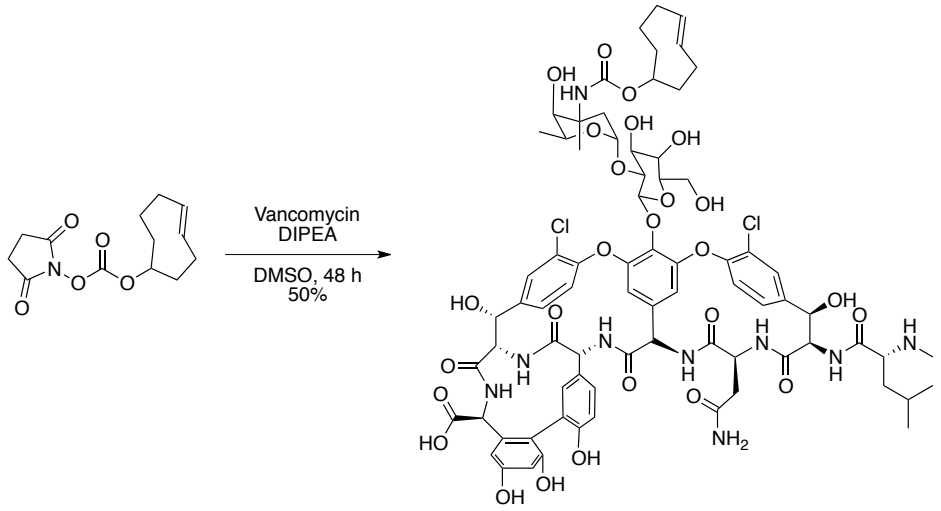

Scheme 29: Synthesis of TCO-vancomycin

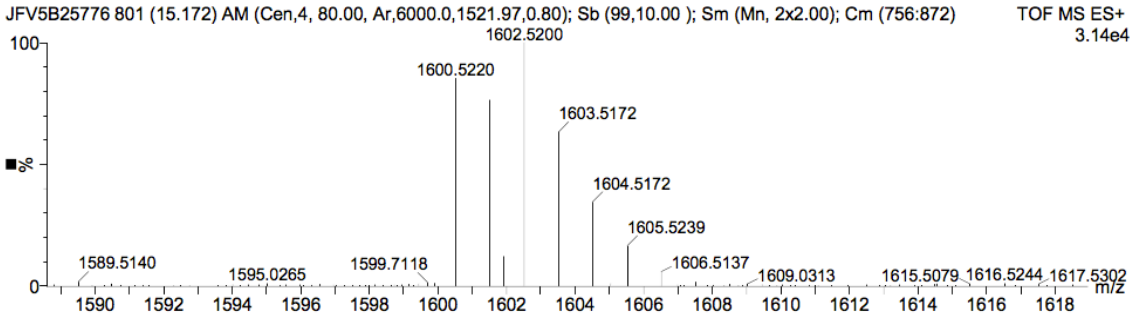

Figure 55: $HRMS^+$ of TCO-vancomycin

References

(1) James, M. L.; Gambhir, S. S. *Physiol. Rev.* **2012**, *92* (2), 897.

(2) Karlberg, A. M.; Saether, O.; Eikenes, L.; Goa, P. E. *EJNMMI Phys.* **2016**, *3* (5), 1.

(3) *Positron Emission Tomography*; Granov, A., Tuitin, L., Schwarz, T., Eds.; Springer: London, 2013.

(4) Miller, P. W.; Long, N. J.; Vilar, R.; Gee, A. D. *Angew. Chemie - Int. Ed.* **2008**,

47, 8998.

(5) *Molecular Anatomic Imaging: PET-CT and SPECT-CT Integrated Modality Imaging*, 2nd ed.; Gustav K. Von Schultes, Ed.; Lippincott Williams & Wilkens: Philadelphia, 2007.

(6) *Technetium-99m Pharmaceuticals: Preparation and Quality Control in Nuclear Medicine*; Zolle, I., Ed.; Springer: Berlin, 2007.

(7) Akbar, M. U.; Ahmad, M. R.; Shaheen, A.; Mushtaq, S. *J. Radioanal. Nucl. Chem.* **2016**, *310* (2), 477.

(8) Liu, S. *Chem. Soc. Rev.* **2004**, *33* (7), 445.

(9) Fritzberg, A. R. *Nuklearmedizin.* **1987**, *26* (1), 7.

(10) Lambrecht, F. Y. *Ann. Nucl. Med.* **2011**, *25*, 1.

(11) Abrams, M. J.; Juweid, M.; Caroline, I.; Schwartz, D. A.; Hauser, M. M.; Gaul, F. E.; Fuccello, A. J.; Rubin, R. H.; Strauss, H. W.; Fischman, A. J. *J. Nucl. Med.* **1990**, *31* (12), 2022.

(12) Meszaros, L. K.; Dose, A.; Biagini, S. C. G.; Blower, P. J. *Inorganica Chim. Acta* **2010**, *363* (6), 1059.

(13) Blankenberg, F.; Katsikis, P. D.; Tait, J. F.; Davis, R. E.; Ohtsuki, K.; Kopiwoda, S.; Abrams, M. J.; Darkes, M.; Robbins, R. C.; Maecker, H. T.; Strauss, H. W.; Tait, H. A. N. F.; Davis, R. E.; Naumovskiii, L.; Blankenberg, F. G.; Katsikist, P. D.; Darkes, M.; Robbinstt, R. C.; Ohtsukit, K.; Kopiwodat, S. *PNAS* **1998**, *95*, 6349.

(14) Gabriel, M.; Decristoforo, C.; Donnemiller, E.; Ulmer, H.; Rychlinski, C. W.; Mather, S. J.; Moncayo, R. *J Nucl Med* **2003**, *44* (5), 708.

(15) Welling, M. M.; Visentin, R.; Feitsma, H. I. J.; Lupetti, A.; Pauwels, E. K. J.; Nibbering, P. H. *Nucl. Med. Biol.* **2004**, *31* (4), 503.

(16) Yeh, S. H.-H.; Kong, F.-L.; Lin, M.-H. In *Personalized Pathway-Activated Systems Imaging in Oncology*; Springer Singapore: Singapore, 2017; pp 233–243.

(17) Li, L.; Wu, Y.; Wang, Z.; Jia, B.; Hu, Z.; Dong, C.; Wang, F. *J. Nucl. Med.* **2017**, jnumed.116.183863.

(18) Rennen, H. J. J. M.; Laverman, P.; van Eerd, J. E. M.; Oyen, W. J. G.; Corstens, F. H. M.; Boerman, O. C. *Nucl. Med. Biol.* **2007**, *34* (6), 691.

(19) Chang, Y. S.; Jeong, J. M.; Lee, Y. S.; Kim, H. W.; Rai, G. B.; Lee, S. J.; Lee, D. S.; Chung, J. K.; Lee, M. C. *Bioconjugate Chem.* **2005**, *16* (5), 1329.

(20) Lee, Y. S.; Jeong, J. M.; Kim, H. W.; Chang, Y. S.; Kim, Y. J.; Hong, M. K.; Rai, G. B.; Chi, D. Y.; Kang, W. J.; Kang, J. H.; Lee, D. S.; Chung, J. K.; Lee, M. C.; Suh, Y. G. *Nucl. Med. Biol.* **2006**, *33* (5), 677.

(21) Khoshbakht, S.; Kobarfard, F.; Beiki, D.; Sabzevari, O.; Amini, M.; Mehrnejad, F.; Tabib, K.; Shahhosseini, S. *J. Radioanal. Nucl. Chem.* **2016**, *307* (2), 1125.

(22) Luo, T.-Y.; Cheng, P.-C.; Chiang, P.-F.; Chuang, T.-W.; Yeh, C.-H.; Lin, W.-J. *Ann. Nucl. Med.* **2015**, *29* (1), 52.

(23) Norain, A.; Dadachova, E. *Semin. Nucl. Med.* **2016**, *46* (3), 250.

(24) Chen, K.; Chen, X. *Curr. Top. Med. Chem.* **2010**, *10* (12), 1227.

(25) Seibold, U.; Wängler, B.; Schirrmacher, R.; Wängler, C. *Biomed Res. Int.* **2014**, *2014*.

(26) Louie, A. *Chem. Rev.* **2010**, *110* (5), 3146.

(27) Li, J.; Chen, P. R. *Nat. Chem. Biol.* **2016**, *12* (3), 129.

(28) Carboni, R. A.; Lindsey, R. V. *J. Am. Chem. Soc.* **1959**, *81* (16), 4342.

(29) Karver, M. R.; Weissleder, R.; Hilderbrand, S. A. *Bioconjugate Chem.* **2011**, *22*, 2263.

(30) Knall, A.-C.; Slugovc, C. *Chem. Soc. Rev.* **2013**, *42* (12), 5131.

(31) Thalhammer, F.; Wallfahrer, U.; Sauer, J. *Tetrahedron Lett.* **1990**, *31* (47), 6851.

(32) Royzen, M.; Yap, G. P. A.; Fox, J. M. *J. Am. Chem. Soc.* **2008**, *130* (12), 3760.

(33) Goldenberg, D. M. *J. Nucl. Med.* **2002**, *43* (5), 693.

(34) Rossin, R.; Verkerk, P. R.; Bosch, S. M. Van Den; Vulders, R. C. M.; Verel, I.; Lub, J.; Robillard, M. S. *Angew. Chem. Int. Ed. Engl.* **2010**, *49*, 3375.

(35) Zeglis, B. M.; Brand, C.; Abdel-Atti, D.; Carnazza, K. E.; Cook, B. E.; Carlin, S.; Reiner, T.; Lewis, J. S. *Mol. Pharm.* **2015**, *12* (10), 3575.

(36) Denk, C.; Svatunek, D.; Filip, T.; Wanek, T.; Lumpi, D.; Frçhlich, J.; Kuntner, C.; Mikula, H. *Angew. Chemie - Int. Ed.* **2014**, *53*, 9655.

(37) Albu, S. A.; Al-Karmi, S. A.; Vito, A.; Dzandzi, J. P. K.; Zlitni, A.; Beckford-Vera, D.; Blacker, M.; Janzen, N.; Patel, R. M.; Capretta, A.; Valliant, J. F. *Bioconjugate Chem.* **2016**, *27* (1), 207.

(38) Denk, C.; Svatunek, D.; Mairinger, S.; Stanek, J.; Filip, T.; Matscheko, D.; Kuntner, C.; Wanek, T.; Mikula, H. *Bioconjugate Chem*. **2016**, *27*, 1707.

(39) Nichols, B.; Qin, Z.; Yang, J.; Vera, D. R.; Devaraj, N. K. *Chem. Commun*. **2014**, *50*, 5215.

(40) García, M. F.; Zhang, X.; Shah, M.; Newton-Northup, J.; Cabral, P.; Cerecetto, H.; Quinn, T. *Bioorg. Med. Chem*. **2016**, *24* (6), 1209.

(41) Yazdani, A.; Bilton, H.; Vito, A.; Genady, A. R.; Rathmann, S. M.; Ahmad, Z.; Janzen, N.; Czorny, S.; Zeglis, B. M.; Francesconi, L. C.; Valliant, J. F. *J. Med. Chem*. **2016**, *59* (20), 9381.

(42) Vito, A.; Alarabi, H.; Czorny, S.; Beiraghi, O.; Kent, J.; Janzen, N.; Genady, A. R.; Alkarmi, S. A.; Rathmann, S.; Naperstkow, Z.; Blacker, M.; Llano, L.; Berti, P. J.; Valliant, J. F. *PLoS One* **2016**, *11* (12), 1.

(43) Vito, A. R.; Alarabi, H.; Kent, J.; Valliant, J. *J. Labelled Comp. Radiopharm*. **2015**, *58*, S18.

(44) Walsh, J.; Zeglis, B.; Sanders, V.; Lewis, J. S.; Francesconi, L. C. *J. Labelled Comp. Radiopharm*. **2015**, *58*, S60.

(45) Bilton, H.; Ahmad, Z.; Valliant, J. *J. Labelled Comp. Radiopharm*. **2015**, *58*, S61.

(46) Garcia, M. F.; Shah, M.; Newton, J.; Cabral, P.; Deutscher, S. L.; Cerecetto, H.; Quinn, T. P. *J. Labelled Comp. Radiopharm*. **2015**, *58*, S111.

(47) Chung, H. J.; Reiner, T.; Budin, G.; Min, C.; Liong, M.; Issadore, D.; Lee, H.; Weissleder, R. *ACS Nano* **2011**, *5* (11), 8834.

(48) Perkins, H. R.; Hill, M. **1971**, *143*, 789.

(49) Dörwald, F. Z. *Lead optimization for medicinal chemists*; Wiley: Weinham, 2012.

(50) Surfraz, M. B.; Biagini, C. G.; Blower, P. J. *Dalt. Trans*. **2008**, 2920.

(51) Liu, S.; Edwards, D. S.; Looby, R. J.; Harris, A. R.; Poirier, M. J.; Barrett, J. a; Heminway, S. J.; Carroll, T. R. *Bioconjugate Chem* **1996**, *7*, 63.

(52) Kyung, M. S.; Se, E. K.; Moon, C.; Kim, S. H.; Bae, C. S.; Ho, J. H.; Seong, S. K. *In Vivo (Brooklyn)*. **2009**, *23* (4), 551.

(53) Haun, J. B.; Devaraj, N. K.; Hilderbrand, S. A.; Lee, H.; Weissleder, R. *Nat. Nanotechnol*. **2010**, *5* (9), 660.

(54) Han, H.-S.; Hilderbrand, S. A. .; Devaraj, N. K. .; Weissleder, R.; Bawendi, M. G.

Compositions and methods for bioconjugation of organic compounds to quantum dots. WO 2011/112970 A3, 2011.

(55) Alge, D. L.; Donohue, D. F.; Anseth, K. S. *Tetrahedron Lett*. **2013**, *54* (41).

(56) Shitara, Y.; Maeda, K.; Ikejiri, K.; Yoshida, K.; Horie, T.; Sugiyama, Y. *Biopharm. Drug Dispos*. **2013**, *34* (1), 45.

(57) Kimura, T.; Sudo, K.; Kanzaki, Y.; Miki, K.; Takeichi, Y.; Kurosaki, Y.; Nakayama, T. *Biol. Pharm. Bull* **1994**, *17* (2), 327.

(58) Selvaraj, R.; Fox, J. M. *Tetrahedron Lett*. **2014**, *55* (34), 4795.

(59) Barrera, J.; Burrell, A. K.; Bryan, J. C. *Inorg. Chem*. **1996**, *35* (2), 335.

(60) Decristoforo, C.; Mather, S. J. *Nucl. Med. Biol*. **1999**, *26* (98), 389.

(61) Lakowicz, J. R. *Principles of Fluorescence Spectroscopy Principles of Fluorescence Spectroscopy*; 2006.

(62) Kobayashi, H.; Ogawa, M.; Alford, R.; Choyke, P. L.; Urano, Y. *Chem. Rev*. **2010**, *110* (5), 2620.

(63) Hilderbrand, S. A.; Weissleder, R. *Curr. Opin. Chem. Biol*. **2010**, *14* (1), 71.

(64) Vahrmeijer, A. L.; Hutteman, M.; van der Vorst, J. R.; van de Velde, C. J. H.; Frangioni, J. V. *Nat. Rev. Clin. Oncol*. **2013**, *10* (9), 507.

(65) Devaraj, N. K.; Hilderbrand, S.; Upadhyay, R.; Mazitschek, R.; Weissleder, R. *Angew. Chemie - Int. Ed*. **2010**, *49* (16), 2869.

(66) Wu, H.; Yang, J.; Seckute, J.; Devaraj, N. K. *Angew. Chemie - Int. Ed*. **2014**, *53* (23), 5805.

(67) Erdmann, R. S.; Takakura, H.; Thompson, A. D.; Rivera-Molina, F.; Allgeyer, E. S.; Bewersdorf, J.; Toomre, D.; Schepartz, A. *Angew. Chemie - Int. Ed*. **2014**, *53* (38), 10242.

(68) Agarwal, P.; Beahm, B. J.; Shieh, P.; Bertozzi, C. R. *Angew. Chemie - Int. Ed*. **2015**, *54* (39), 11504.

(69) Lukinavičius, G.; Umezawa, K.; Olivier, N.; Honigmann, A.; Yang, G.; Plass, T.; Mueller, V.; Reymond, L.; Corrêa Jr, I. R.; Luo, Z.-G.; Schultz, C.; Lemke, E. A.; Heppenstall, P.; Eggeling, C.; Manley, S.; Johnsson, K. *Nat. Chem*. **2013**, *5* (2), 132.

(70) Ni, Z.; Zhou, L.; Li, X.; Zhang, J.; Dong, S. *PLoS One* **2015**, *10* (11), 2.

(71) Koo, H.; Lee, J. H.; Bao, K.; Wu, Y.; El Fakhri, G.; Henary, M.; Yun, S. H.; Choi, H. S. *Adv. Healthc. Mater.* **2016**, *5* (19), 2510.

(72) Dirksen, A.; Dawson, P. E. *Bioconjugate Chem.* **2008**, *19* (12), 2543.

(73) Dirksen, A.; Hackeng, T. M.; Dawson, P. E. *Angew. Chemie - Int. Ed.* **2006**, *45*, 7581.

(74) Solulink Bioconjugation Primer http://www.solulink.com/white_papers/Why_Solulink.pdf (accessed Jan 16, 2017).

(75) Bradshaw, C. W.; Eltepu, L.; Kabakibi, A.; Lam, S.; Liu, B.; Liu, D.; Meade, B. R.; Sakamuri, S. POLYNUCLEOTIDE CONSTRUCTS HAVING DISULFIDE GROUPS. US 20160257961A1, 2016.

(76) Slikboer, S.; Valliant, J. F. *J. Labelled Comp. Radiopharm.* **2017**, *60* (S1), S605.

(77) Mann, A.; Semenenko, I.; Meir, M.; Eyal, S. *AAPS J.* **2015**, *17* (4), 788.

(78) Iyer, G.; Pinaud, F.; Xu, J.; Ebenstein, Y.; Li, J.; Chang, J.; Dahan, M.; Weiss, S. *Bioconjugate Chem.* **2011**, *22* (6), 1006.

(79) Blanco-Canosa, J. B.; Medintz, I. L.; Farrel, D.; Mattoussi, H.; Dawson, P. E. *J. Am. Chem. Soc.* **2010**, *132* (29), 10027.

(80) Barde, M. P.; Barde, P. J. *Perspect. Clin. Res.* **2012**, *3* (3), 113.